AGU PUBLICATIONS

Reviews of Geophysics

REVIEW ARTICLE
10.1002/2014RG000478

**Key Points:**
- Tropical cloudiness and wind variations on 30–70 day timescales impact the upper ocean
- The upper ocean response modulates heat and moisture fluxes to the atmosphere
- Understanding the 30–70 day ocean-atmosphere feedbacks remains challenging

**Correspondence to:**
C. A. DeMott,
demott@atmos.colostate.edu

**Citation:**
DeMott, C. A., N. P. Klingaman, and S. J. Woolnough (2015), Atmosphere-ocean coupled processes in the Madden-Julian oscillation, *Rev. Geophys.*, *53*, 1099–1154, doi:10.1002/2014RG000478.

Received 19 NOV 2014
Accepted 30 SEP 2015
Accepted article online 5 OCT 2015
Published online 26 NOV 2015



# Atmosphere-ocean coupled processes in the Madden-Julian oscillation

**Charlotte A. DeMott[1], Nicholas P. Klingaman[2], and Steven J. Woolnough[2]**

[1]Department of Atmospheric Science, Colorado State University, Fort Collins, Colorado, USA, [2]National Centre for Atmospheric Science-Climate and Department of Meteorology, University of Reading, Reading, UK

**Abstract** The Madden-Julian oscillation (MJO) is a convectively coupled 30–70 day (intraseasonal) tropical atmospheric mode that drives variations in global weather but which is poorly simulated in most atmospheric general circulation models. Over the past two decades, field campaigns and modeling experiments have suggested that tropical atmosphere-ocean interactions may sustain or amplify the pattern of enhanced and suppressed atmospheric convection that defines the MJO and encourage its eastward propagation through the Indian and Pacific Oceans. New observations collected during the past decade have advanced our understanding of the ocean response to atmospheric MJO forcing and the resulting intraseasonal sea surface temperature fluctuations. Numerous modeling studies have revealed a considerable impact of the mean state on MJO ocean-atmosphere coupled processes, as well as the importance of resolving the diurnal cycle of atmosphere-upper ocean interactions. New diagnostic methods provide insight to atmospheric variability and physical processes associated with the MJO but offer limited insight on the role of ocean feedbacks. Consequently, uncertainty remains concerning the role of the ocean in MJO theory. Our understanding of how atmosphere-ocean coupled processes affect the MJO can be improved by collecting observations in poorly sampled regions of MJO activity, assessing oceanic and atmospheric drivers of surface fluxes, improving the representation of upper ocean mixing in coupled model simulations, designing model experiments that minimize mean state differences, and developing diagnostic tools to evaluate the nature and role of coupled ocean-atmosphere processes over the MJO cycle.

## 1. Introduction

The Madden-Julian oscillation (MJO) is a large-scale ($O$(10,000 km)), zonally oriented tropical convective disturbance that propagates east at about 5 m $s^{-1}$ with a period of 30–70 days or an "intraseasonal" time scale [*Madden and Julian*, 1972]. The circulation anomalies are most prominent in zonal wind, where low-level anomalies are out of phase with those at upper levels. Maximum rainfall associated with the MJO is observed over the tropical Indian and West Pacific Oceans, where sea surface temperatures (SSTs) are warmest, but the MJO's upper level circulation anomalies may circumnavigate the Earth. These fundamental features of the MJO are illustrated schematically in Figure 1.

In the tropical Indian and western Pacific Oceans, where low-level mean state winds are generally westerly, the MJO propagates east with a suppressed phase of light winds, reduced surface fluxes, and reduced cloudiness east of the convective anomaly. The convectively active phase of the MJO is marked by deep clouds, heavier rainfall, and westerly wind anomalies. During the active phase, surface fluxes are enhanced because the mean and anomalous low-level winds are of the same sign and because the westerly anomalies are generally stronger than the suppressed phase easterly anomalies.

In the tropics, the MJO is known to regulate wet and dry conditions [*Jones et al.*, 2004a; *Carvalho et al.*, 2004; *Zhang et al.*, 2009], modulate tropical cyclone activity in all ocean basins [e.g., *Liebmann et al.*, 1994; *Maloney and Hartmann*, 2000; *Camargo et al.*, 2008; *Klotzbach*, 2010], influence the North and South American, African, Indian, and Asian-Australian monsoons [*Kayano and Kousky*, 1999; *Higgins and Shi*, 2001; *Wheeler and Hendon*, 2004; *Lorenz and Hartmann*, 2006] and impact El Niño–Southern Oscillation (ENSO) cycles through oceanic Kelvin waves [*Kessler*, 2001; *Zhang and Gottschalck*, 2002]. When MJO convection propagates from the Indian Ocean, across the Maritime Continent, and into the West Pacific, the response of the local circulation to the MJO's convective heating anomaly is exported to higher latitudes through teleconnections [*Donald et al.*, 2006]. Extratropical influences of the MJO include the formation of "atmospheric rivers"

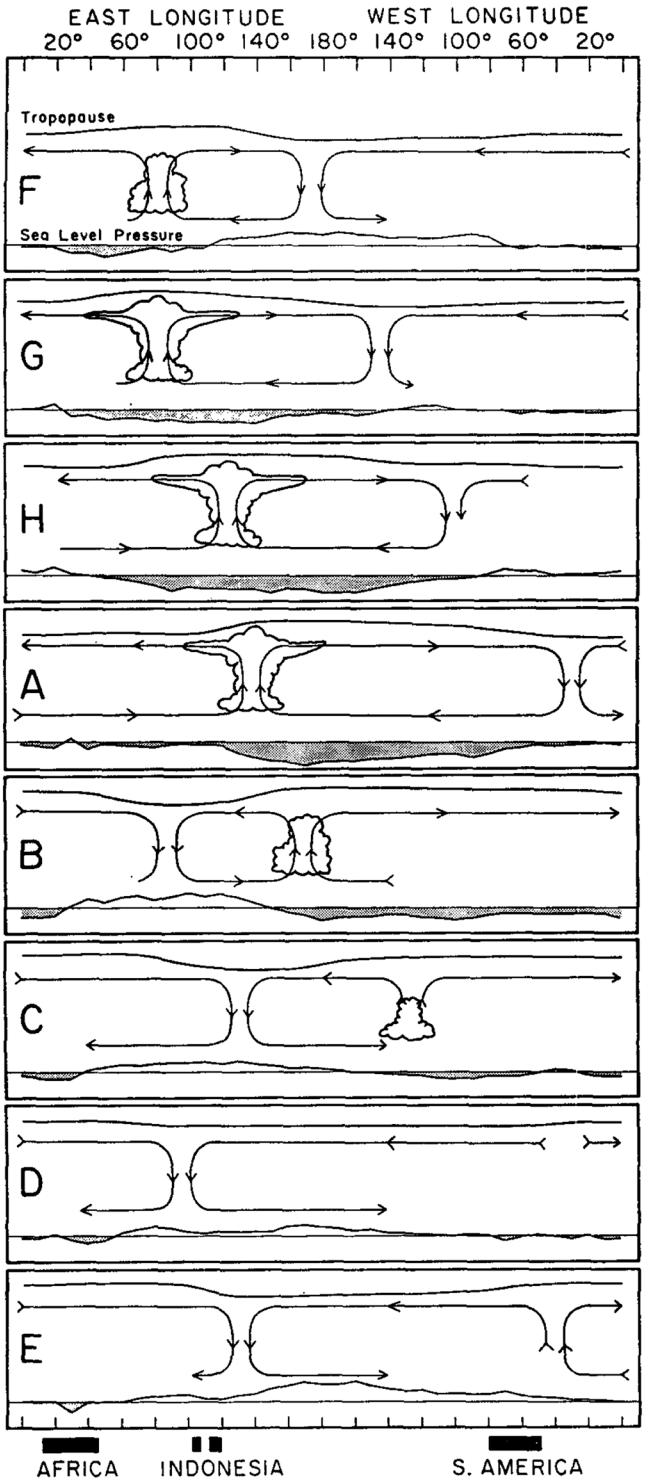


**Figure 1.** Schematic illustration of the equatorial time and space evolution of MJO convection, circulation, and surface pressure anomalies. Time increases downward, with panels spaced roughly 5 days apart. Major land masses are indicated at the bottom (reprinted from *Madden and Julian* [1972], copyright 1972, with permission from American Meteorological Society).

[e.g., *Higgins et al.*, 2000], which play an important role in western North American water supplies but are also linked to floods and landslides; interactions with the polar Southern [*Matthews and Meredith*, 2004] and Northern Annular Modes and cold air outbreaks over Europe [*Zhou and Miller*, 2005; *Cassou*, 2008; *Lin et al.*, 2009; *Vitart and Molteni*, 2010]; and Arctic sea ice extent [*Henderson et al.*, 2014]. These large-scale perturbations may influence many other phenomena, including flooding, wildfires, lightning, cold air outbreaks and heat waves, stratospheric water vapor, and aerosols [*Zhang*, 2013, and references therein].

Because of its longer-than-synoptic time scale and interactions with numerous global weather systems, successful forecasts of MJO initiation and its propagation may improve weather prediction over large parts of the globe and short-term climate prediction of interannual phenomena such as ENSO and the Indian Ocean Dipole. However, most state-of-the-art general circulation models (GCMs) struggle to simulate the MJO structure and frequency [*Hung et al.*, 2013] and its propagation beyond the Maritime Continent [*Jiang et al.*, 2015]. Many studies have noted improved MJO simulation when an atmosphere-only GCM (AGCM) is coupled to an ocean model [e.g., *Kemball-Cook et al.*, 2002; *Zhang et al.*, 2006; *Pegion and Kirtman*, 2008a; *Kim et al.*, 2008], suggesting a role for ocean feedbacks in the MJO life cycle.

The ocean and atmosphere communicate through exchanges of heat, moisture, and momentum, which regulate intraseasonal SST variations. On intraseasonal time scales, the atmosphere senses these SST variations via their impact on surface fluxes. How these SST-modulated fluxes affect MJO convection is still not clear [e.g., *Zhang*, 2005; *Sobel et al.*, 2010], although the topic has been addressed in many studies during the past decade.

This review summarizes and assesses the literature concerning the role of ocean feedbacks onto the MJO. In order to understand these feedbacks, two questions must be answered: "How does the ocean SST modulate surface fluxes throughout the MJO life cycle?" and "How do SST-modulated fluxes impact MJO convection?" The first question requires an understanding of the ocean response to intraseasonal atmospheric forcing; significant progress has been made on this front in the past decade. The second question seeks an understanding of the processes through which surface fluxes impact MJO initiation, maintenance, and propagation. Our review focuses on feedbacks associated with intraseasonal SST variations. Direct assessment of ocean feedbacks on intraseasonal time scales is difficult because observations cannot provide information on MJO behavior in the absence of MJO-modulated SSTs. When GCMs are used to study the problem, long-standing deficiencies in MJO simulation hamper efforts to understand the MJO response to ocean feedbacks, including the processes for which those fluxes are important.

Modeling studies have shown that ocean feedbacks can improve poleward and eastward propagating intraseasonal disturbances. The former are associated with the Asian-Australian summer monsoons [e.g., *Yasunari*, 1979; *Krishnamurti and Subrahmanyam*, 1982] and are sometimes linked to the latter. Together, the poleward and eastward propagating systems are referred to as the "intraseasonal oscillation (ISO)"; the eastward propagating component of the ISO is the MJO. Although the two types of ISOs are closely linked, we focus here on the less complicated boreal winter MJO. Several of the papers included in this review examine both northward and eastward propagation, but we limit our discussion to results pertaining to the boreal winter eastward propagating MJO.

The outline of our review follows. In section 2, we provide an overview of MJO research, briefly introduce some theories to explain the MJO, and review recent progress in simulating the MJO in models. Section 3 summarizes observations of the coupled ocean-atmosphere system relevant to the MJO, while section 4 presents theories of how ocean feedbacks may impact the MJO. Section 5 provides a detailed, comparative assessment of the many modeling studies focused on ocean feedbacks in the MJO. Recommendations for possible future observational campaigns, modeling experiments, and diagnostic methods are given in section 6. We summarize our review in section 7.

## 2. Overview

In this section, we provide a synopsis of the progression of MJO research: section 2.1 describes observations of the MJO since its discovery in 1970; section 2.2 discusses theories for the maintenance and eastward propagation of the MJO; and section 2.3 introduces efforts to improve the representation of the MJO in GCMs. Each of these brief, general subsections provides context for a larger section of the manuscript that focuses on air-sea interactions in the MJO.

### 2.1. Observations of the MJO

The MJO was discovered by accident. In 1970, Roland Madden and Paul Julian analyzed a 10 year record of daily sounding data from Canton Island in the central Pacific. Madden and Julian wanted to document a class of upper air 5 day waves by applying the recently developed fast Fourier transform (FFT) to surface pressure and upper level and lower level wind data. Their analysis resolved the 5 day wave but also revealed an unexpected—and much larger—spectral peak at 41–53 days [*Madden and Julian*, 2012]. Initial descriptions of the 40–50 day oscillation appeared in *Madden and Julian* [1971, 1972], which included the remarkably complete description of the horizontal and vertical structure of the MJO and its periodicity, propagation, and cloud characteristics (Figure 1).

The prominence of intraseasonal convective variability over the Indian and western Pacific Oceans was noted during the earliest stages of MJO research, but the possibility that air-sea interactions could provide an energy source to convective motions that are sustained for 30–50 day periods was not formally proposed until *Krishnamurti et al.* [1988]. In that paper, it was demonstrated that oceanic fluxes of latent and sensible heat were primarily controlled by wind speed fluctuations but that intraseasonal SST fluctuations of ~0.3°C could account for ~10–15% of the surface flux amplitude. This nonnegligible impact of intraseasonal SST variability on surface fluxes suggested that the ocean state could influence the MJO.

While the MJO was discovered by applying a basic analytic tool—the FFT—to one of the most fundamental measures of the atmospheric state—the daily sounding record—further advances in our understanding of the disturbance have relied heavily upon global outgoing longwave radiation (OLR) measurements from satellites and steadily evolving reanalysis data sets [e.g., *Kalnay et al.*, 1996; *Saha et al.*, 2006; *Onogi et al.*, 2007; *Dee et al.*, 2011; *Rienecker et al.*, 2011]. Analyses based on these products have led to progressively more detailed descriptions of the MJO, which have spawned theories for its existence and provided a basis for comparing these theories when they are tested in models. Limitations of these global data sets have been addressed with targeted, short-duration in situ field experiments, such as the Tropical Ocean-Global Atmosphere (TOGA) Coupled Ocean-Atmosphere Response Experiment (COARE) in the West Pacific Ocean in 1992–1993 [*Webster and Lukas*, 1992], the Mirai Indian Ocean cruise for the Study of the MJO-convection Onset (MISMO) [*Yoneyama et al.*, 2008], the Cirene field campaign in the Seychelles thermocline ridge region [*Vialard et al.*, 2009], and the recently completed Cooperative Indian Ocean Experiment on Intraseasonal Variability in the Year 2011/Dynamics of the MJO (CINDY/DYNAMO) [*Yoneyama et al.*, 2013] in the equatorial Indian Ocean from October 2011 to March 2012.

*Madden and Julian* [1994] published the first major review of observational studies of the MJO, summarizing papers written prior to TOGA COARE. Noted MJO impacts on the ocean were the excitation of sea surface height perturbations and oceanic Kelvin waves and their possible link to ENSO, and the effects on surface fluxes and currents by MJO winds. Ocean feedbacks onto the MJO were discussed only implicitly in regard to the "critical importance of moist processes" to the MJO. The rich data set collected during TOGA COARE offered new insights into atmospheric and oceanic processes associated with the MJO. A review article that incorporated these findings was written by *Zhang* [2005]. In the same year, *Lau and Waliser* [2005] published the first edition of their book *Intraseasonal Variability in the Atmosphere-Ocean Climate System* that included chapters on "Air-sea interaction" by *Hendon* [2005], "The oceans" by *Kessler* [2005], and "Modeling intraseasonal variability" by *Slingo et al.* [2005]. Improved understanding of the ocean response to MJO forcing and heightened awareness of the convection-humidity connection for the MJO were key results of TOGA COARE.

In the decade following the *Zhang* [2005], *Hendon* [2005], *Kessler* [2005], and *Slingo et al.* [2005] reviews, MJO research was bolstered by expanded or newly available global gridded data sets, such as the 0.25° resolution microwave measurements of tropical precipitation and SST from the Tropical Rainfall Measuring Mission (TRMM) [*Kummerow et al.*, 1998] and Advanced Microwave Scanning Radiometer–EOS (AMSR-E) [*Wentz et al.*, 2000], 0.25° resolution ocean surface wind stress from the QuikSCAT satellite [e.g., *Chelton and Freilich*, 2005], sea surface height data from the TOPEX/POSEIDON satellite [*Gaspar et al.*, 1994], surface salinity from the Aquarius satellite [*Lagerloef et al.*, 2008], remotely observed cloud structures from CloudSat [*Stephens et al.*, 2002], and improved reanalysis products. Additional in situ observing systems include new Tropical Atmosphere Ocean (TAO) Triangle Trans Ocean Buoy Network buoys in the West Pacific, Indian Ocean moorings of the Research Moored Array for African-Asian-Australian Monsoon Analysis and Prediction (RAMA) [*McPhaden et al.*, 2009], and the global array of Argo profiling drifters [*Roemmich et al.*, 2009].

Knowledge gleaned from these measurements was incorporated into the second edition of *Lau and Waliser* [2005], including a new chapter on the upper ocean response to MJO forcing [*Duvel*, 2012].

### 2.2. Theories for the MJO

In the years since its discovery, a number of theories and mechanisms for the maintenance and propagation of the MJO have been proposed. We summarize their essential features here; *Wang* [2012] provides a comprehensive review.

Early theories for the MJO focus on destabilization of the equatorial modes of the tropical atmosphere described by *Matsuno* [1966]. *Emanuel* [1987] and *Neelin et al.* [1987] propose a mechanism commonly known as WISHE (Wind-Induced Surface Heat Exchange), in which the eastward propagating equatorial-wave modes are destabilized by a wind-induced enhanced evaporation to the east of the existing convection. Since mean Indo-Pacific surface winds during boreal winter are weakly westerly, the easterly anomalies generate negative, rather than positive, surface fluxes immediately east of MJO convection. This incongruity has been used to argue against the validity of WISHE as a mechanism for the MJO [e.g., *Wang*, 1988a; *Zhang*, 1996], although it may be an important (but incorrect) mechanism for the MJO in some GCMs when biases result in mean easterly winds in the Indian Ocean or West Pacific. Some more recent studies have argued for nonlinear or modified WISHE mechanisms which do not depend on an easterly basic state wind [e.g., *Wang and Rui*, 1994; *Maloney and Sobel*, 2004]. It should be noted that while the title of *Emanuel* [1987] describes his theory as an air-sea interaction, this mechanism involves no coupling between the atmosphere and ocean.

*Lau and Peng* [1987] propose an instability related to the interaction between the convective heating and wave-induced moisture convergence known as wave-CISK (conditional instability of the second kind). Linear theory cannot explain the planetary scale for these wave modes, with phase speeds and growth rates that depend on the vertical structure of the heating profile. *Wang and Rui* [1990] consider the instability due to frictional convergence in the boundary layer (frictional wave-CISK). Their system is stable in the absence of frictional effects, but boundary layer moisture convergence to the east of the convection induced by frictional convergence drives the instability. This mechanism produces unstable modes with spatial scales and structures and propagation characteristics consistent with the observed MJO.

More recently, attention has focused on moisture modes, in which the critical component of the instability is the relationship between precipitation intensity and column saturation, which itself is regulated by convective activity [e.g., *Raymond and Fuchs*, 2009]. Net column moistening can also result from anomalous vertical and horizontal moisture advection [e.g., *Sobel and Maloney*, 2013], as well as surface latent heat fluxes [e.g., *Kiranmayi and Maloney*, 2011; *DeMott et al.*, 2014]. A number of studies have focused on the role of the vertical heating profile on convectively coupled equatorial waves and the MJO, both in terms of the energetics of the waves or moisture feedbacks [e.g., *Mapes*, 2000; *Wu*, 2003; *Kuang*, 2008; *Fuchs et al.*, 2012] and the role of cloud radiative feedbacks [e.g., *Raymond*, 2001].

A further branch of theories can be classified under the heading of multiscale interactions [e.g., *Biello and Majda*, 2005; *Majda and Stechmann*, 2009, 2012; *Liu and Wang*, 2012]. The key to these theories is the modulation of synoptic scale disturbances, and their associated heating and momentum transports, by the planetary scale MJO circulation.

There is considerable overlap between these theories and mechanisms: all depend to some degree on the relationship between convection and moisture, or moisture sources, and most rely on similar forms of the linearized equations of motion for the tropics. However, many of these proposed theories and mechanisms fail to predict key aspects of the MJO, e.g., spatial scale or preferred period. A more complete theory for the MJO would likely include many of these ideas.

Ocean feedbacks may influence the MJO through the modulation of surface fluxes and their influence on the evolution of the atmospheric boundary layer, and the subsequent impact of the boundary layer on the circulation and convection. Section 4 describes theoretical and idealized modeling approaches to understanding the role of these ocean feedbacks in the MJO.

### 2.3. Modeling the MJO

Interest in examining, and improving, the representation of the MJO in GCMs intensified after TOGA COARE. *Slingo et al.* [1996] found that most of the GCMs that participated in the Atmospheric Model Intercomparison Project (AMIP) failed to simulate one or more essential characteristics of the MJO: its period, amplitude,

and eastward propagation. Similar atmosphere-only and coupled model intercomparison efforts have been carried out periodically over the past two decades [*Lin et al.*, 2006; *Kim et al.*, 2009; *Hung et al.*, 2013], but models have shown limited progress in simulating the MJO despite intensive efforts to revise GCM physical parameterizations. In these studies, it is difficult to identify a single feature that links either the better or worse performing models beyond the presence or absence of an MJO. *Sperber et al.* [2012] reviews efforts to simulate the MJO and the boreal summer ISO in GCMs.

Numerous sensitivity experiments with one or several GCMs have explored how the simulated MJO responds to variations in physical parameters in GCM convective, boundary layer, and radiation schemes. Alterations to the subgrid-scale treatment of deep convection often have proved the most effective means of improving the representation of the MJO. Specifically, studies have found an enhanced MJO when introducing momentum mixing by convection to reduce vertical wind shear [e.g., *Neale et al.*, 2008; *Zhou et al.*, 2012]; by revising the triggering of convection to account for low-level horizontal moisture convergence [e.g., *Wang and Schlesinger*, 1999]; by altering the convective parameterization to enhance shallow-convective heating and moistening east of the MJO active phase [e.g., *Zhang and Mu*, 2005; *Li et al.*, 2009; *Zhang and Song*, 2009] or to produce more upper level heating from stratiform precipitation [*Fu and Wang*, 2009; *Seo and Wang*, 2010], which increases the covariance between convective heating and temperature anomalies and destabilizes convectively coupled waves [*Mapes*, 2000]; by artificially increasing the westward tilt of the GCM diabatic heating profile with height [*Lappen and Schumacher*, 2012, 2014]; and by increasing the sensitivity of an ascending convective parcel to environmental humidity, particularly in the middle troposphere [e.g., *Tokioka et al.*, 1988; *Bechtold et al.*, 2008; *Neale et al.*, 2008; *Chikira and Sugiyama*, 2010; *Hannah and Maloney*, 2011; *Subramanian et al.*, 2011; *Hirons et al.*, 2013; *Klingaman and Woolnough*, 2014a]. Most of these alterations, particularly the latter, center on sharpening the distinction between the MJO suppressed and active phases in models, by either reducing precipitation during the suppressed phase or increasing instability during the active phase. The transition from shallow to deep convection appears to be particularly critical [e.g., *Benedict et al.*, 2013]. Replacing the convective parameterization with a cloud-resolving model, a practice known as "superparameterization," has been shown to be an effective, if computationally expensive, means of producing an MJO in atmosphere-only [*Benedict and Randall*, 2009] and coupled GCMs [*Stan et al.*, 2010; *Benedict and Randall*, 2011]. The Nonhydrostatic Icosahedral Atmospheric Model, a global cloud-resolving model, has demonstrated higher prediction skill for the MJO than most parameterized convection models [e.g., *Miura et al.*, 2007; *Liu et al.*, 2009; *Miyakawa et al.*, 2014]. Regional models with explicit representations of deep convection have also shown improved skill over their parameterized counterparts [e.g., *Holloway et al.*, 2013]. The representation of the MJO in GCMs with parameterized convection has also been found to be sensitive to atmospheric horizontal [e.g., *Liess et al.*, 2004; *Jia et al.*, 2008; *Crueger et al.*, 2013] and vertical resolution [*Inness et al.*, 2001], as well as the presence of air-sea coupling, which we discuss further in section 5.

Nearly all of the above studies have examined parameter and resolution sensitivities in either the atmosphere-only or coupled configuration of a GCM but not both. Therefore, it is difficult to compare quantitatively the impact on MJO simulation of altering subgrid-scale parameterizations or horizontal resolution with the impact of including air-sea interactions. The relative importance of these factors almost certainly varies from one model to the next. Two recent studies have found that air-sea coupling improved the MJO only when the convection parameterization had first been modified to increase the amplitude of subseasonal variability in tropical precipitation [*Crueger et al.*, 2013; *Klingaman and Woolnough*, 2014b]. We discuss these studies further in section 5.6; in section 6.2, we recommend that future sensitivity studies be performed with coupled models in which the ocean mean state can be controlled. Based only on these studies and the authors' own experience, biases in the treatment of tropical convection are likely the primary factor limiting MJO simulation in most GCMs, with erroneous, poorly resolved, or missing atmosphere-ocean interactions a secondary factor.

Despite the wealth of sensitivity studies demonstrating an improved MJO, the representation of the MJO in the standard configurations of most atmosphere-only and coupled GCMs remains poor [e.g., *Hung et al.*, 2013]. One potential reason for this is an anticorrelation in GCMs between MJO fidelity and the accuracy of the tropical mean climate [e.g., *Kim et al.*, 2011]. Many of the parameter changes that improve the MJO worsen the GCM simulation in other respects [e.g., *Benedict et al.*, 2013]. For example, improving the sensitivity of convection to environmental humidity in the Met Office Unified Model (MetUM) GCM caused deep convection to terminate lower in the atmosphere, increasing upper level temperature and wind biases [*Klingaman and Woolnough*, 2014a] and altering the pattern of tropical precipitation biases [*Bush et al.*, 2015].

Yet the representation of the MJO is known to be sensitive to the fidelity of the tropical basic state, as we discuss in section 5.3. Achieving both an accurate simulation of the tropical mean state and a strong, eastward propagating MJO is a continuing challenge for GCM developers.

### 2.4. Outstanding Questions Since the 2005 Reviews

Answers to several questions surrounding the MJO in general and the role of air-sea interactions in particular were unknown when *Zhang* [2005], *Hendon* [2005], *Slingo et al.* [2005], and *Kessler* [2005] were published. For instance, there existed no formal framework for quantifying ocean feedbacks to the MJO and whether these feedbacks were most important to MJO initiation, maintenance, or propagation. Ocean feedbacks were (and often still are) assessed using qualitative comparisons of the MJO simulated in coupled and uncoupled GCMs, which often exhibited substantial biases in their tropical mean climates.

Processes responsible for MJO initiation, including the possible role of ocean feedbacks, were not directly observed, since MJO convection most often develops in the Indian Ocean. Also unresolved was the closely related question of what promotes the transition from isolated trade cumulus convection to large-scale organized cloud clusters on intraseasonal time scales and its potential connection to air-sea interactions. The unique climatology and geography of the Indian Ocean suggested potentially different ocean responses to intraseasonal forcing than seen in the West Pacific Ocean, but observations with sufficient spatial coverage and temporal resolution generally did not exist until after 2005. Finally, there was considerable uncertainty regarding the impact of the Maritime Continent and its surrounding waters on the MJO. The Maritime Continent was known as an MJO "propagation barrier" for many GCMs, but its role in supporting or hindering the MJO was not well understood. Maritime Continent effects on the MJO were summarized by *Neale and Slingo* [2003] and *Inness and Slingo* [2006] and may directly or indirectly involve air-sea interactions: a reduction of ocean area, disruption of low-level winds by island topography, land-sea differences in the vertical profile of heating, and land-sea breeze interactions with the pronounced diurnal cycle of island rainfall.

## 3. Observations

Air-sea interactions include fluxes of heat (radiation, latent heat, and sensible heat), fresh water (precipitation and evaporation), momentum (via wind stress and surface drag), and chemical and biological constituents (gases and aerosols). In the tropics, these fluxes influence and are influenced by the following: cloudiness, surface currents and deep-ocean waves [e.g., *McPhaden*, 2002; *Talley et al.*, 2011], surface waves, sea spray [*Janssen*, 1991; *Melville*, 1996], bubble and foam layer formation [*Jahne and Haussecker*, 1998; *Aziz et al.*, 2005; *Wanninkhof et al.*, 2009; *Fairall et al.*, 2011], biological reactions [e.g., phytoplankton, bacteria, chlorophyll; *Ragueneau et al.*, 2000; *Xie*, 2003; *Xie et al.*, 2005], and the injection of marine aerosols into the atmosphere [e.g., *de Leeuw et al.*, 2011; *Gantt and Meskhidze*, 2013]. Energy and freshwater transfer at the air-sea interface dominates MJO air-sea interaction literature; other interactions have received less attention. This bias arises from the decades-long quest to understand the energetics of the MJO and the role of surface energy fluxes in MJO maintenance and propagation. The surface turbulent fluxes are modulated by upper ocean heat content and stability, which are governed by temperature and salinity. Consequently, MJO air-sea interaction studies are primarily focused on SST—through which ocean heat content is communicated to latent and sensible heat fluxes—and salinity. For the remainder of this section, "air-sea interaction" refers to interactions among radiation, rainfall, wind, surface turbulent fluxes, SST, and salinity. Other air-sea interactions on intraseasonal time scales are discussed in section 3.6.

Intraseasonal air-sea interactions can be broadly organized as (1) MJO forcing to the ocean, (2) ocean response to MJO forcing, and (3) ocean feedbacks to the MJO. In the following subsections, we summarize these topics as revealed by observations and, occasionally, models forced by observed data. While descriptions of air-sea interactions herein include some overlap with the *Zhang* [2005], *Hendon* [2005], and *Kessler* [2005] reviews, we do not attempt to duplicate those reviews. Rather, we selectively cover topics included in those reviews to provide necessary background and focus on new observations and analyses carried out over the past decade.

### 3.1. Some Notes on Turbulent Flux Measurements

The ocean surface energy balance has been studied with data obtained from in situ measurements, satellite observations, and reanalysis products. In situ instrumentation on research vessels or buoys can measure downwelling solar (and sometimes infrared) radiation, wind speed and direction, SST, air temperature, relative humidity, and sometimes air pressure and the subsurface ocean state. Fluxes of latent and sensible heat can be directly calculated as the eddy covariance of near-surface temperature or specific humidity

with vertical velocity ($\overline{w'q'}$ and $\overline{w'T'}$, respectively) but require carefully controlled measurements at ~10 Hz [*Rebmann et al.*, 2012]. Over the oceans, these direct flux measurements are usually only collected by research vessels during short field campaigns, so their availability is limited in space and time. More typically, in situ surface turbulent fluxes are calculated using bulk flux parameterizations driven by buoy- or ship-based wind speed, SST, and air temperature and humidity measurements. The flux parameterizations are validated against eddy covariance fluxes. For buoys, surface net solar flux is calculated using the measured downwelling solar flux and an assumed surface albedo; upwelling infrared flux is estimated using the SST, while the downwelling flux is either measured or estimated using air temperature and a cloud cover index [e.g., *Cronin and McPhaden*, 1997]. All radiation components can be directly measured by ships.

The bulk flux algorithm developed specifically for TOGA COARE by *Fairall et al.* [1996a] is the basis of most in situ MJO surface energy budget studies and agrees with eddy covariance flux estimates to within ~5 W $m^{-2}$ (1~2 W $m^{-2}$) for latent (sensible) heat flux when driven with buoy input variables [*Fairall et al.*, 1996a; *Chang and Grossman*, 1999]. Routine collection of tropical flux measurements from buoys began in the late 1980s with the Tropical Atmosphere Ocean (TAO) array [*McPhaden et al.*, 1998] and now provide a long time series of surface flux data with coarse spatial resolution and limited geographic extent. In contrast, satellites provide global coverage and good temporal and spatial resolution of flux-related variables (winds from passive or active microwave sensors, SST, and air temperature and humidity from a variety of algorithms), which are incorporated into several satellite-based bulk flux products [*Chou et al.*, 1995; *Schulz et al.*, 1997; *Curry et al.*, 1999; *Kubota et al.*, 2002; *Bourras et al.*, 2002; *Chou et al.*, 2003; *Bentamy et al.*, 2003; *Curry et al.*, 2004; *Andersson et al.*, 2011]. The drawbacks to satellite flux data sets are their limited temporal record (~1987 onward) and the remaining challenge of retrieving near-surface air temperature and humidity [*Schulz et al.*, 1993; *Jin and Yu*, 2015], although progress is being made [e.g., *Jackson et al.*, 2006; *Jackson and Wick*, 2010; *Roberts et al.*, 2010]. Air temperature and humidity estimates are readily available from reanalysis products but often with systematic biases. *Brunke et al.* [2011] reports that uncertainties in daily mean turbulent flux estimates from satellite and reanalysis products range 30~40 W $m^{-2}$ (15~20 W $m^{-2}$) for latent (sensible) heat flux. Two optimally interpolated flux products—OAFlux [*Yu et al.*, 2008] and TropFlux [*Kumar et al.*, 2012]—combine bias- and amplitude-corrected (compared to buoys) reanalysis and satellite observations to produce surface fluxes. Compared to bulk flux estimates from buoys (which are incorporated into the merged products), the uncertainties are ~1 W $m^{-2}$, as would be expected. When less constrained by buoy corrections, the uncertainties are likely larger, but by how much is unknown.

The bulk flux algorithm depends on potentially erroneous SST measurements. Buoy-based SST measurements are made at ~1 m depth and are subject to random and systematic errors (i.e., biases) of 0.1~0.3 K and 0.1~0.2 K, respectively [*Abraham et al.*, 2013; *Kennedy*, 2014]. Satellite SST estimates are based on the radiative temperature of the ~1 mm depth SST "skin temperature" [*Katsaros*, 1980]. Skin temperature is typically several tenths of a degree colder than subsurface waters, but in very calm conditions can be warmer and exhibit large diurnal variations [e.g., *Kawai and Wada*, 2007]. TRMM Microwave Imager (TMI) SST uncertainty is estimated to be ~0.7 K [*Wentz et al.*, 2000]. Because ocean fluxes to the atmosphere are sensitive to the skin temperature, adjustments must be made to buoy-based SST measurements before fluxes are calculated [*Fairall et al.*, 1996b].

Uncertainties in SST and flux measurements should be considered when studying their variations throughout the MJO life cycle. This is particularly true for case studies and studies that contrast a few individual events, where peak-to-trough or event-to-event differences should significantly exceed measurement uncertainties and estimates by reanalyses and satellites. Composite studies of the MJO, in which characteristics of many events are averaged together, reduce the uncertainties of random errors. Furthermore, the effects of measurement bias are reduced when composites are based on anomaly, rather than total, fields. Such composite studies may mask potentially important event-to-event differences.

### 3.2. MJO Forcing to the Ocean

#### 3.2.1. The Surface Energy Balance

The MJO impacts upper ocean temperature and salinity via fluxes of radiation, latent and sensible heat, precipitation, and momentum. Time series of the net surface heat flux (radiative, latent heat, and sensible heat fluxes), precipitation, wind stress, and SST during DYNAMO and TOGA COARE are shown in Figures 2 and 3.

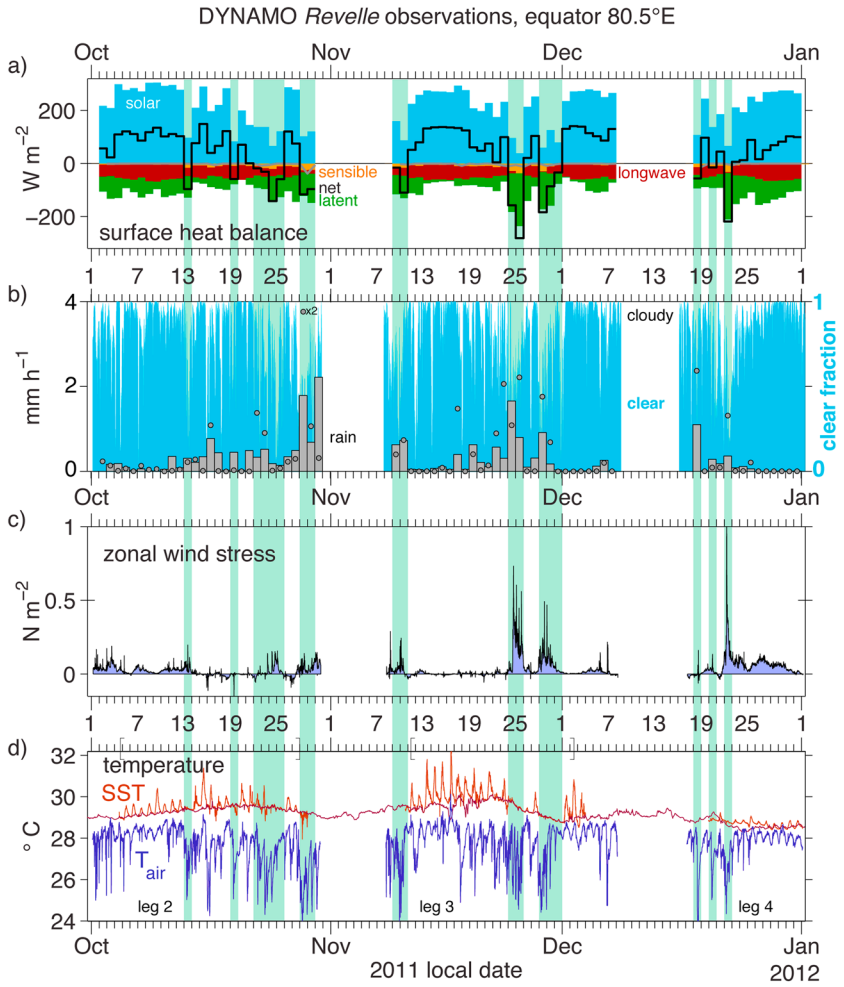


**Figure 2.** (a) Daily average surface heat fluxes incident on the ocean (positive warms the ocean) in DYNAMO, averaged over each local solar day at 0°, 80.5°E. Solar radiation (blue) is compensated by evaporation (green), longwave radiation (red), and sensible heat flux (orange), resulting in the net surface heat balance (black). (b) Variations in cloud fraction (clear fraction indicated as blue) and rain from the TOGA precipitation radar averaged within 20 km of the ship (bars) and ship optical rain gauge (circles). (c) Hourly running mean of 10min zonal wind stress. (d) The 10min 0.05 m depth sea surface temperature (from the *Revelle* when stationed at 0°N, 80.5°E, orange). Ocean temperature at 10 m depth from the Oregon State University Ocean Mixing Group Chameleon profiler (dark red) and the Applied Physics Lab buoy (0°N, 79°E) when the ship was off station. Surface air temperature (blue) measured on the ship in the DYNAMO experiment. Green shading behind all panels highlights days when negative net surface heat flux cooled the ocean (reprinted from *de Szoeke et al.* [2015], copyright 2014, with permission from American Meteorological Society).

A net heat flux into the ocean is observed during periods of light rainfall and winds, warming the sea surface. Such conditions also produce large diurnal SST amplitudes, in which daytime warming exceeds nighttime cooling and so enhances the warming trend [*Lau and Sui*, 1997]. The transition from dry to rainy conditions is marked by increasing cloudiness [*Myers and Waliser*, 2003; *Riley et al.*, 2011], midlevel moisture [*Lin and Johnson*, 1996; *Johnson et al.*, 2015], winds, and decreasing net solar radiation [*Weller and Anderson*, 1996; *Webster et al.*, 1996]. Rainy and windy periods are characterized by reduced diurnal SST amplitudes, net heat flux out of the ocean, and decreasing SST. Since the maximum d*SST*/d*t* coincides with maximum net surface heat flux, the SST response lags surface heating or cooling on intraseasonal time scales [*Zhang*, 1996; *Hendon and Glick*, 1997; *Jones et al.*, 1998; *Woolnough et al.*, 2000].

Indian and West Pacific Ocean net surface energy budget terms for the December–February mean state, plus convectively active and suppressed phases of the MJO, are summarized in Figure 4. The signs of the input terms (radiative + surface turbulent) are the same for both active and suppressed phases, and only their magnitudes vary. Net surface heating, however, is positive (negative) during suppressed (active) phases,

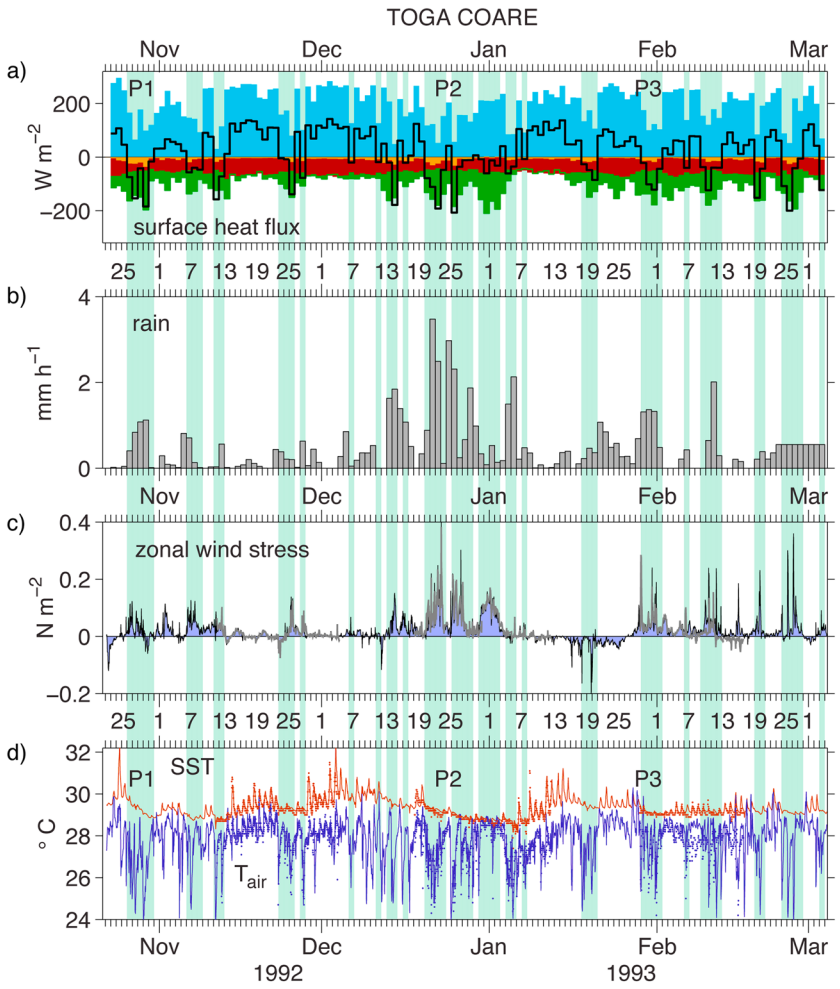


**Figure 3.** As in Figure 2 but for hourly data from the R/V *Moana Wave* and Improved Meteorology (IMET) buoy during TOGA COARE. Wind stress (gray, R/V *Moana Wave*; shaded, IMET), SST (red line, 0.45 m IMET; dots, *Moana Wave*), and air temperature (blue line, IMET; dots, *Moana Wave*) (reprinted from *de Szoeke et al.* [2015], copyright 2014, with permission from American Meteorological Society).

where it heats (cools) the upper ocean. Seasonal means and MJO active/suppressed phase means of rainfall, SST, zonal surface stress, and upper ocean mixed layer depth are also shown. Compared to the West Pacific, mean Indian Ocean latent heat fluxes are weaker (114 W $m^{-2}$ vs 127 W $m^{-2}$), and shortwave radiation has a stronger influence on the net surface energy budget [*Hendon and Glick*, 1997; *Shinoda et al.*, 1998; *Moum et al.*, 2013]. For all variables (except SST) shown in Figure 4, active phase anomalies (the difference between active phase mean and seasonal mean) are larger than suppressed phase anomalies (suppressed phase mean minus seasonal mean). Mean and anomalous fluxes of longwave radiation and sensible heat are much smaller than those of shortwave radiation and latent heat, respectively. $Q_{net}$ anomalies, to a close approximation, are the sum of the (opposite-signed) latent heat flux anomalies, which are mostly controlled by winds [*Weller and Anderson*, 1996], and anomalous net surface shortwave radiation fluxes, which are controlled by clouds [*Lau and Sui*, 1997].

The atmospheric control of the net surface energy balance on intraseasonal time scales has important consequences. First, it implies that intraseasonal air-sea interactions are primarily driven by the atmosphere. Second, it implies a central role for clouds and convection in modulating the surface exchanges of radiant and turbulent energy, respectively. Ocean warming by solar radiation is strongly modulated by cloud properties, such as cloud fraction, glaciation, thickness, organization, and lifetime. Intraseasonal variations in wind-dominated surface turbulent fluxes are driven by downdrafts and large-scale wind anomalies.

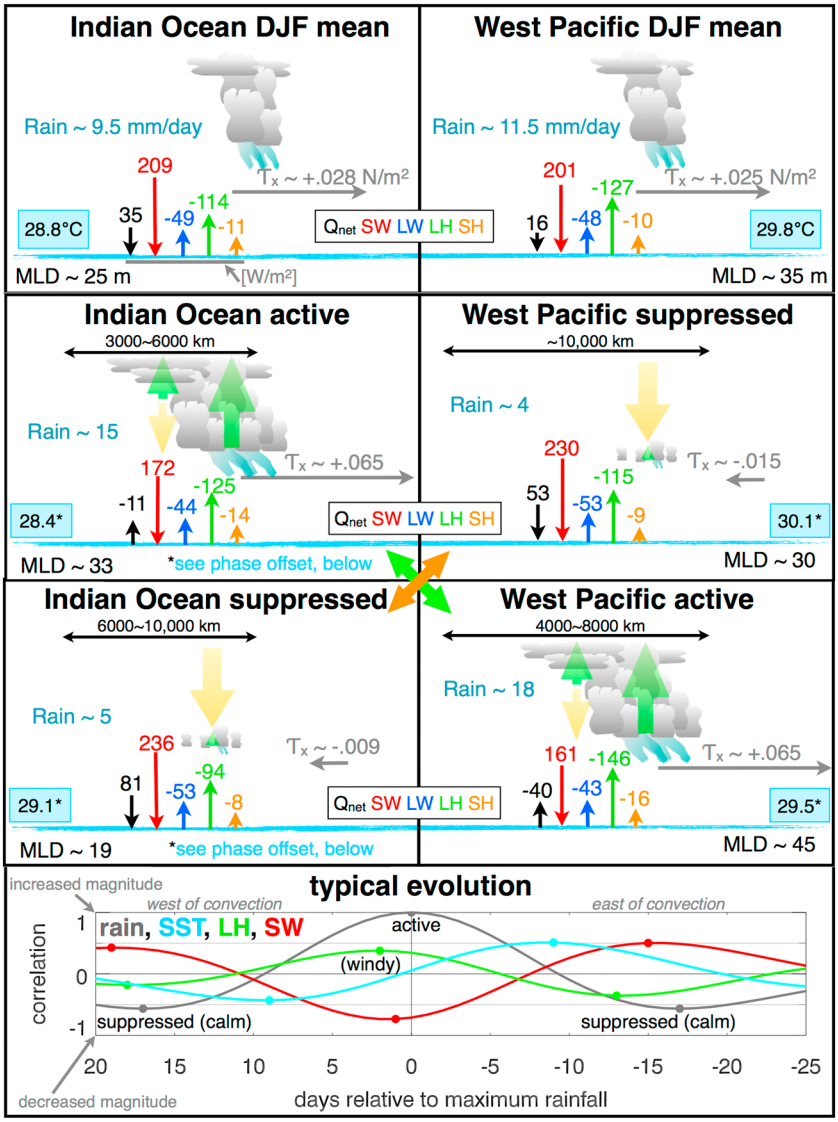


**Figure 4.** December–February (DJF) surface energy balance over the (left column) eastern Indian (0°–10°S, 80°–90°E) and (right column) West Pacific (0°–10°S, 155°–165°E) Oceans for (first row) DJF means and (second row) active and (third row) suppressed MJO (computed as the mean when local maximum (minimum) 20–100 day filtered rainfall is greater than (less than) one DJF standard deviation ($\sigma$)): net surface shortwave (red) and longwave (blue) radiation, latent (green) and sensible (orange) heat flux, and net heating (black) (all W m$^{-2}$). Fluxes from 2002–2012 ERA-Interim and 1998–2009 OAFlux are subjectively combined with guidance from *de Szoeke et al.* [2015]. Positive values are fluxes into the ocean. Flux uncertainties in Figure 4 (first row) are ≤5% (~10%) for component (net) fluxes. Active and suppressed phase interevent standard deviations are about 10%, 25%, and 150% for radiative, turbulent, and net fluxes, respectively. TMI rainfall and SST (blue boxes), zonal wind stress ($\tau_x$) [*de Szoeke et al.*, 2015], and ocean mixed layer depth [*de Boyer Montégut et al.*, 2004; *Drushka et al.*, 2012] are also shown. Clouds are overlaid with arrows for anomalous rising (green) and sinking (yellow) motion. (fourth row) Typical point lag correlations of rainfall (gray), SST (blue), surface shortwave (red), and latent (green) fluxes with rainfall; dots show local maxima and minima.

### 3.2.2. Factors Controlling Intraseasonal Surface Flux Variations

To a first order, intraseasonal surface latent (LH′) and sensible heat (SH′) flux anomalies depend on mean and anomalous wind speeds and near-surface vertical gradients of moisture and temperature:

$$\mathrm{LH}' \sim \Delta q' \overline{|V|} + \overline{\Delta q} |V|' \tag{1}$$

$$\mathrm{SH}' \sim \Delta T' \overline{|V|} + \overline{\Delta T} |V|' \tag{2}$$

where $\Delta q$ is the near-surface vertical moisture gradient ($q^*_{SST} - q_{air}$; where $q^*_{SST}$ is the saturation specific humidity at $T$ = SST), $\Delta T$ is the temperature gradient $(\mathrm{SST} - T_{air})$, and $|V|$ is wind speed. Overbars represent background mean quantities, and primed quantities (hereafter not retained) are time-varying departures from the background means. The nonlinear terms $\Delta q'|V|'$ and $\Delta T'|V|'$ are omitted, as they are negligibly small [e.g., *Riley Dellaripa and Maloney*, 2015]. Secondary dependencies on stability and ocean wave state (section 3.6) are not included. The wind speed variations are controlled by both the wind anomaly and the mean wind. Zonal wind anomalies of either sign may produce suppressed or enhanced fluxes, depending on the sign of the mean wind. To a first approximation, tropical oceanic surface fluxes are determined by wind speed fluctuations [*Krishnamurti et al.*, 1988; *Zhang*, 1996; *Weller and Anderson*, 1996; *Hendon and Glick*, 1997; *Shinoda et al.*, 1998; *Woolnough et al.*, 2000; *Inness and Slingo*, 2003; *Araligidad and Maloney*, 2008; *DeMott et al.*, 2014], but ~10–20% (~15–40%) of LH (SH) variations are controlled by $\Delta q$ ($\Delta T$) [*Krishnamurti et al.*, 1988; *Zhang*, 1996; *Araligidad and Maloney*, 2008; *Yokoi et al.*, 2014; *DeMott et al.*, 2014], depending on location. $\Delta q$ and, to a lesser degree, $\Delta T$ are more sensitive to $q_{air}$ and $T_{air}$ than SST [*Hendon and Glick*, 1997; *DeMott et al.*, 2014], particularly near convective downdrafts [*Saxen and Rutldge*, 1998; *Yokoi et al.*, 2014; *Ruppert and Johnson*, 2015]. *Weller and Anderson* [1996] found that $\Delta q$, and especially $q_{air}$, could strongly modulate latent heat fluxes for similar wind speeds during westerly wind events.

The strong dependence of flux variations on atmospheric variables should not be interpreted as a lack of sensitivity to SST. A given $|V|$ and $T_{air}$ ($q_{air}$) will produce a stronger sensible (latent) heat flux over a warmer patch of ocean than it will over a colder patch. At 30°C, a 1°C warming gives a 1.74 g kg$^{-1}$ increase in $q^*_{SST}$ [*Hendon and Glick*, 1997] and an ~18 W m$^{-2}$ increase in LH [*Webster et al.*, 1996]. The typical SST range over the MJO life cycle is 0.2~0.5°C (depending on event definition criteria [*Duvel and Vialard*, 2007; *Drushka et al.*, 2012]) but can exceed 1°C for individual events [e.g., *Duvel and Vialard*, 2007; *Vialard et al.*, 2008; *Moum et al.*, 2013]. For moderate to strong wind conditions, SST modulates the flux; during light-wind conditions, SST may directly induce a local wind response and flux as the atmospheric boundary layer adjusts to the warm surface anomaly (section 3.4).

#### 3.2.3. Relative Phasing of SST, Surface Fluxes, and Rainfall

The impact of SST on MJO surface fluxes varies with the magnitude of the SST anomaly and its phasing relative to the wind. The evolution of the surface energy budget terms has been studied using in situ measurements [*Zhang*, 1996; *Weller and Anderson*, 1996; *Lau and Sui*, 1997; *Hendon and Glick*, 1997; *Zhang and McPhaden*, 2000; *Vialard et al.*, 2008; *Araligidad and Maloney*, 2008; *Drushka et al.*, 2012; *Moum et al.*, 2013] and gridded satellite and reanalysis data [*Krishnamurti et al.*, 1988; *Jones and Weare*, 1996; *Hendon and Glick*, 1997; *Jones et al.*, 1998; *Shinoda et al.*, 1998; *Woolnough et al.*, 2000; *Inness and Slingo*, 2003; *Benedict and Randall*, 2007; *Duvel and Vialard*, 2007; *Araligidad and Maloney*, 2008]. Figure 4 (fourth row) illustrates the evolution. The MJO suppressed phase is driven by the compensating subsidence forced by MJO convection (Figure 1). Individual MJO events may be separated by an intervening period of generally suppressed convection, or large-scale active convection in different forms, such as the Intertropical Convergence Zone (ITCZ) [*Yoneyama et al.*, 2013], neither of which is part of the MJO life cycle. For "successive" events (those that immediately follow a prior MJO), development of MJO convection follows the suppressed phase; "primary" events (those not preceded by another MJO) appear to initiate locally [*Matthews*, 2008], although they, too, may be preceded by atmospheric wind anomalies [*Straub*, 2013; *Ling et al.*, 2013; *Haertel et al.*, 2015].

The arrival of the MJO suppressed phase is marked by a decrease in cloudiness, winds, and surface fluxes and an increase in surface radiation and lasts for 10~20 days. Transition to (initiation of) the active phase for successive (primary) MJO events begins with increasing cloudiness and reduced surface shortwave radiation, followed by an increase in wind speed and surface fluxes out of the ocean and decreasing SSTs. In the active phase, MJO convection roughly coincides with maximum winds and surface fluxes. Strong westerly anomalies can persist for several days, where they perturb the upper ocean [e.g., *Harrison and Vecchi*, 2001; *Moum et al.*, 2013]. This sequence of events is robust across the Indian Ocean, Maritime Continent, and West Pacific, although the relative timing [*Woolnough et al.*, 2000] or magnitude [*Matthews*, 2008] of each step varies for individual MJO events.

The representation of this sequence in data can be sensitive to temporal filtering. Temporal composites based on unfiltered data [e.g., *Zhang and McPhaden*, 2000; *Benedict and Randall*, 2007] show maximum winds and latent and sensible heat fluxes coincident with maximum convection, while those based on filtered data often suggest that winds and surface fluxes lag convection [e.g., *Hendon and Glick*, 1997; *Jones et al.*, 1998;

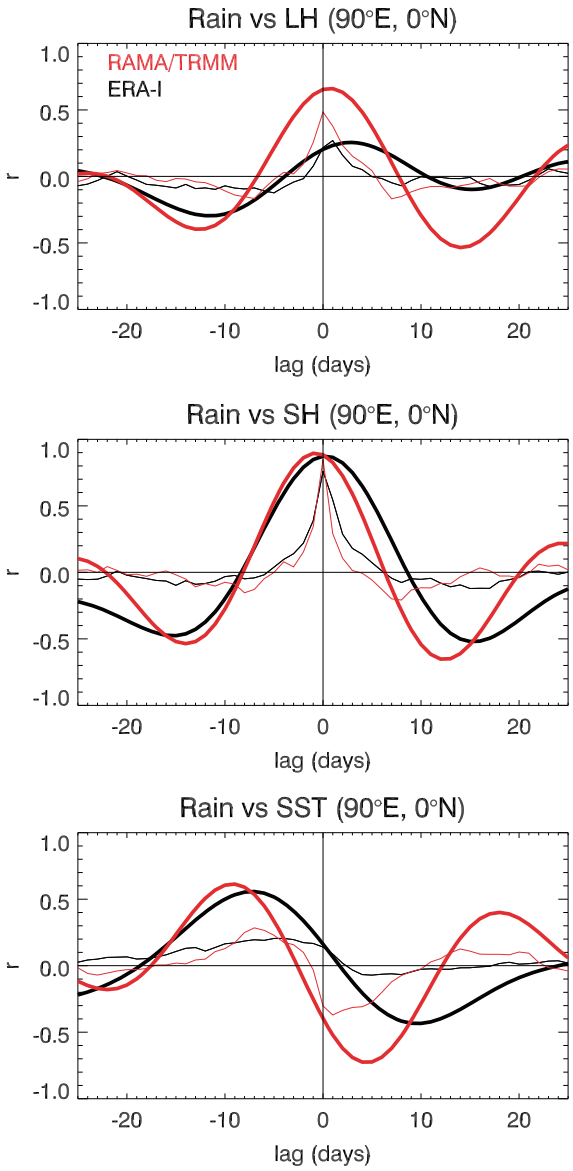


**Figure 5.** Lag correlation of latent heat flux (positive out of the ocean) and rainfall based on RAMA buoy data and TRMM 3B42 rainfall at 0°N, 90°E (red curves) and ERA-Interim reanalysis data (black curves) for unfiltered (thin) and filtered (thick) time series. Small asymmetries about lag = 0 in both time series are reflected as phase offsets for the filtered time series.

*Woolnough et al.*, 2000; *Inness and Slingo*, 2003; *Duvel and Vialard*, 2007]. This issue is demonstrated in Figure 5 using 2 years of RAMA buoy data at 0°N, 90.5°E and collocated European Centre for Medium-range Weather Forecasts (ECMWF) Interim reanalysis data (ERA-I) [*Dee et al.*, 2011]. Filtered and unfiltered RAMA (ERA-I) latent heat fluxes are lag correlated with filtered and unfiltered TRMM 3B42 (ERA-I) rainfall, respectively. For unfiltered data, maximum latent heat fluxes are either exactly (RAMA) or nearly (ERA-I) coincident with rainfall. Because the buildup and decay of the flux is not symmetric about maximum rainfall (i.e., elevated fluxes are observed only a few days prior to maximum rainfall but for many days following), filtered data maximum correlations are shifted to later lags. This misalignment of the flux and rainfall can lead to an underestimate of the ocean feedback contribution (via the flux) to MJO convection [e.g., *Zhang and Anderson*, 2003]. The use of time-filtered data is widespread in MJO studies because it simplifies analysis and emphasizes intraseasonal variations that are otherwise obscured without filtering. Its use, however, warrants care when considering the relative phasing of multiple variables.

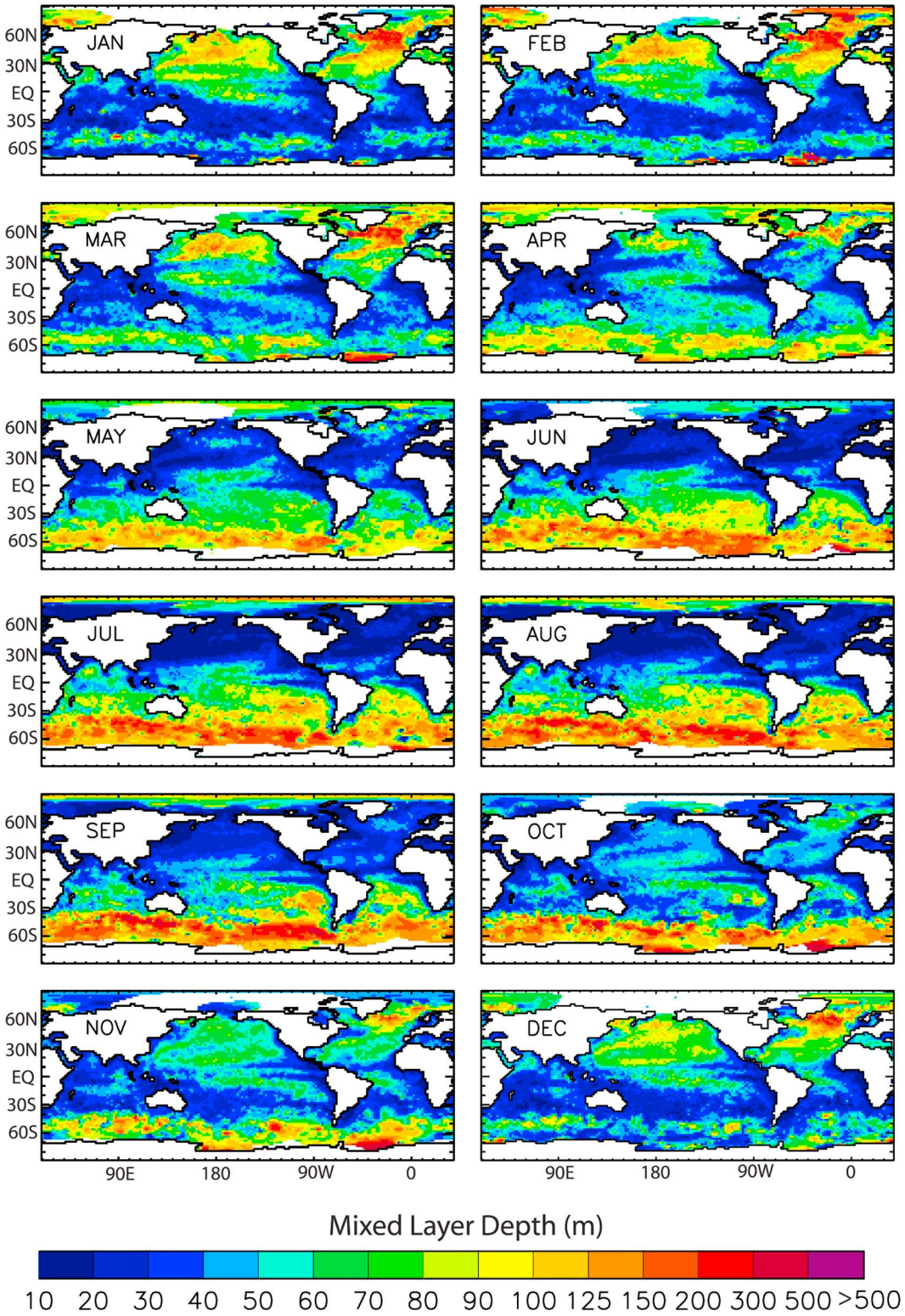


**Figure 6.** The monthly global climatology of ocean mixed layer depth based on ~4.5 million hydrographic profiles collected from 1941 to 2002 (reprinted from *de Boyer Montégut et al.* [2004], copyright 2004, with permission from American Geophysical Union).

The degree of surface flux asymmetry with respect to rainfall varies with location. For instance, when analyzing unfiltered data from a buoy at 0°N, 165°E near the eastern edge of the Warm Pool, *Zhang and McPhaden* [2000, Figure 6] demonstrate that the phasing of surface fluxes, precipitation, winds, and SST cooling support the "coincident" model. When the composite includes buoys between 143°E and 165°E (their Figure 8), surface variables still maximize with rainfall, but there is more asymmetry about the wind speed maximum than observed at 165°E alone, and precipitation maximizes 1 day earlier than wind speed. These differences are consistent with the decreasing phase offset between low-level winds and convection as the MJO propagates east [*Hendon and Salby*, 1994].

### 3.3. Ocean Response to MJO Forcing

#### 3.3.1. Processes Affecting the Upper Ocean

Turbulent mixing produces an ocean mixed layer of roughly uniform temperature and salinity in the upper 10∼100 m. The ocean mixed layer is functionally similar to the ∼1 km deep atmospheric boundary layer. Mixed layer stability is regulated by upper ocean density discontinuities, which are governed by processes that affect water buoyancy within this layer, known as buoyancy flux. *Anderson et al.* [1996] summarized the processes that regulate Warm Pool buoyancy flux and ocean stratification. Buoyancy fluctuations at the air-sea interface arise from the thermal response to radiative and surface heat fluxes and from the salinity response to water mass loss or gain through evaporation and precipitation. Buoyancy fluctuations also occur via mixing and diffusion at the mixed layer base [*Cronin and McPhaden*, 1997]. The mixed layer shoals (thins) in light-wind periods when the stabilizing effect of net positive buoyancy flux exceeds the buoyancy reduction by mechanical mixing (e.g., vertical advection and entrainment) and diffusion at the mixed layer base. As wind speed increases, shear-driven mixing at the mixed layer base reduces buoyancy and deepens the mixed layer until the surface buoyancy flux and mechanical mixing energy balance. Rainfall can offset some of the wind-driven buoyancy flux reductions [e.g., *Zhang and McPhaden*, 2000].

The mixed layer depth can be defined in terms of gradients or surface-to-depth differences of density, temperature, or salinity [e.g., *Anderson et al.*, 1996; *Sprintall and Tomczak*, 1992]. Gradient methods can more accurately identify discontinuities, but require finely resolved vertical profiles of temperature and salinity. The climatological distribution of mixed layer depth based on individual profiles is shown in Figure 6. From May to October, equatorial mixed layer depths in the tropical Indian Ocean and West Pacific are roughly similar (30∼80 m); during boreal winter (November–April), the tropical Indian Ocean mixed layer is shallower (10∼30 m) than in the West Pacific (20∼60 m).

The temperature and salinity gradients that define the mixed layer base are not always found at the same depth. When the upper ocean is more strongly stratified by salinity than by temperature, a barrier layer forms between the top of the thermocline—the transition layer between deep, cold water and the warmer upper ocean (analogous to the atmospheric tropopause)—and the base of the salinity gradient. This is illustrated schematically in Figure 7. In the Warm Pool, the deep thermocline ($O$(100 m)) and the salinity-stratified upper ocean leads to the frequent development of barrier layers [*Anderson et al.*, 1996; *Godfrey and Lindstrom*, 1989; *Lukas and Lindstrom*, 1991; *Sprintall and Tomczak*, 1992; *Mignot et al.*, 2007]. Local barrier layer formation or modification may also occur in the vicinity of existing salinity discontinuities, through processes such as oceanic advection and stretching and tilting of "salinity fronts" by strong surface winds [*Roemmich et al.*, 1994; *Cronin and McPhaden*, 2002]. Once formed, barrier layers resist mechanical mixing at the mixed layer base, confining surface heat and momentum fluxes to the shallow mixed layer, and effectively insulating mixed layer waters from the waters below the 20°C thermocline.

The oceanic response to intraseasonal fluxes of heat, precipitation, and momentum is observed as changes to upper ocean heat content, density stratification, and dynamics. In his review of the oceanic response to atmospheric intraseasonal forcing, *Kessler* [2005] noted that most of what was known at that time was specific to the better observed West Pacific Ocean. The Indian Ocean response to intraseasonal forcing was mostly understood via model diagnostics, as observing systems were just being deployed and modern regional campaigns were still being analyzed [e.g., JASMINE; *Webster et al.*, 2002] or planned. The physical processes governing the oceanic response to intraseasonal forcing are the same for the West Pacific and Indian Oceans, but differences in their mean states and seasonal cycles suggested different responses to intraseasonal forcing. The following subsections review the Indo-Pacific upper ocean response to intraseasonal MJO forcing. MJO-linked air-sea interactions in the East Pacific and Atlantic Oceans are summarized in section 3.5.

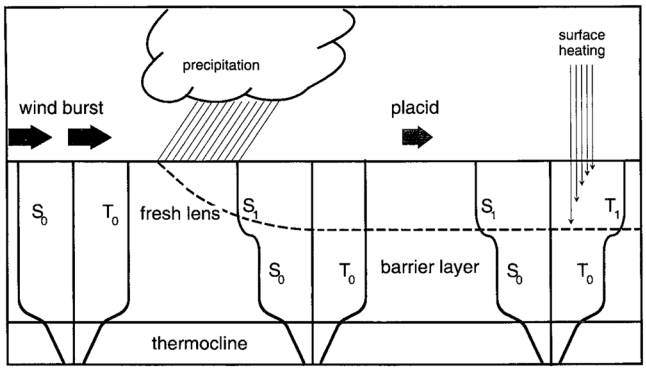


**Figure 7.** Schematic illustration of barrier and mixed layer development: wind mixing homogenizes temperature ($T_0$) and salinity ($S_0$) to the thermocline depth; subsequent rainfall generates a less saline fresh lens ($S_1$) and upper ocean stable layer (the mixed layer). Salinity stratification resists vertical mixing, and heating from solar radiation remains trapped in the upper ocean, leading to warming ($T_1$) (reprinted from *Anderson et al.* [1996], copyright 1996, with permission from American Meteorological Society).

### 3.3.2. Intraseasonal Mixed Layer Heat and Salinity Budgets

Variations in mixed layer depth can regulate the SST response to MJO forcing [e.g., *Duvel et al.*, 2004]. For a given surface heating, a shallower mixed layer has a smaller heat capacity and larger SST response, except for cases of very shallow mixed layers—where solar heating may penetrate below the mixed layer base—and very deep mixed layers—where surface heating is offset by entrainment of cold thermocline waters [*Anderson et al.*, 1996]. Regional and local variations in mixed layer depth have been observed on interannual [*Keerthi et al.*, 2013], seasonal [*de Boyer Montégut et al.*, 2004], and intraseasonal [*Drushka et al.*, 2012] time scales. *Duvel and Vialard* [2007] and *Vialard et al.* [2012] demonstrated that maximum intraseasonal SST variability is observed in regions with shallow mean mixed layer depth—the Seychelles thermocline ridge (5–15°S, 50–90°E) in the south equatorial Indian Ocean, the eastern Indian Ocean and Timor Sea, the South Pacific Convergence Zone near 20°S, and the shallow waters northwest of Australia.

Understanding what controls the mixed layer heat budget is important to understanding the local ocean feedback to the MJO. In the West Pacific, surface fluxes dominate mixed layer heating and cooling, with secondary contributions from ocean processes, consistent with the regionally deep (~180 m) thermocline [*Anderson et al.*, 1996; *McPhaden*, 2002; *Duvel and Vialard*, 2007]. Farther east, ocean processes, such as zonal advection in the Central Pacific, and vertical advection, entrainment, and meridional advection in the East Pacific dominate [*McPhaden*, 2002; *Lucas et al.*, 2010; *Halkides et al.*, 2011].

While the above studies identify surface heat fluxes as the primary regulators of the intraseasonal West Pacific mixed layer heat budget, horizontal and vertical advection and entrainment mixing at the mixed layer base may play a larger role in the Indian Ocean, where the thermocline is shallower (~100 m). This is especially true for the Seychelles thermocline ridge where Ekman pumping by the mean winds produces a shallow thermocline (~70 m) and a mixed layer that are predisposed to mixing by strong wind events.

The relative contributions of surface fluxes and ocean dynamics to the mixed layer heat budget of the thermocline ridge have been a subject of debate during the past decade. Some early studies of mixed layer intraseasonal heat budgets inferred the importance of ocean dynamics. For example, *Harrison and Vecchi* [2001] studied a single Indian Ocean cooling event and estimated that surface fluxes accounted for only ~20% of the observed cooling, implying a fundamental role for ocean dynamics. *Saji et al.* [2006] used 7 years of satellite observations to infer the need for ocean processes in mixed layer heat budgets based on pattern mismatches between maps of intraseasonal variance of SST, OLR (a proxy for solar flux), and QuikSCAT winds (a proxy for evaporation). On the other hand, *Duvel and Vialard* [2007] surmised that upper ocean heating processes dependent upon mixed layer depth—those involving surface fluxes and vertical processes (entrainment mixing and advection)—primarily controlled the mixed layer temperature. However, the high correlation of dSST/d$t$ to $Q_{net}$ ($r > 0.5$) suggested a dominant role for surface fluxes in setting mixed layer temperature, with secondary (but not negligible) contributions from vertical dynamic processes.

The above studies are limited in their inability to identify [*Harrison and Vecchi*, 2001; *Saji et al.*, 2006] or quantify [*Duvel and Vialard*, 2007] ocean processes important to the mixed layer temperature balance.

Vertical processes acting at the base of the mixed layer (entrainment, vertical advection, and diffusion) can be particularly difficult to measure. They are often grouped together as a single term and computed as a budget residual, either from in situ measurements of surface forcing and upper ocean temperature, salinity, and currents or with the aid of ocean GCMs (OGCMs). These residual estimates are subject to potentially large errors associated with forcing time series, resolution, and, in the case of model-derived quantities, parameterization assumptions [e.g., *Vialard et al.*, 2008; *Schott et al.*, 2009]. Nevertheless, efforts to analyze mixed layer heat budgets with observations or observationally constrained OGCMs have been fruitful.

*Duvel et al.* [2004] studied two thermocline ridge intraseasonal cooling events observed during the 1999 Indian Ocean Experiment field campaign [*Ramanathan et al.*, 2001]. An ocean model forced with reanalysis daily mean momentum and heat fluxes and relaxed to climatological temperature and salinity profiles produced good agreement with TMI SST observations. Their results over the Seychelles thermocline ridge pointed to the importance of surface fluxes in setting the mixed layer temperature, with very weak contributions from horizontal advection. Vertical advection and entrainment were quasi-constant cooling terms that varied little with the two MJO cooling events. *Vialard et al.* [2008] computed mixed layer budget terms for the two November 2007 to February 2008 MJO events using surface and ocean observations from the 8°S, 67°E mooring and TMI SST gradients. Estimates of vertical processes were subject to large errors resulting from sensor failures at 20 m. The authors concluded that atmospheric fluxes dominated the mixed layer heat balance for the two events, while vertical process contributions were unclear due to their large uncertainty. Lateral advection was generally small, but its episodic contributions were not phase locked with MJO cooling.

Other case studies provide stark contrasts to the "flux-dominated" cooling events. Using data from the 0°S, 80.5°E mooring, *McPhaden and Foltz* [2013] computed the heat budget for two cooling events from 23 October 2004 to 20 March 2005. For the first event, cooling was substantially aided by advection associated with an enhanced Wyrtki jet, while the second event was characterized by pronounced cooling by entrainment mixing. The different cooling mechanisms were attributed to the presence of a strong barrier layer during the first event, which trapped momentum inputs in the upper ocean, and its absence during the second event, which allowed vertical exchanges at the thermocline. The large impact of advection in the *McPhaden and Foltz* [2013] study may also be a consequence of its proximity to the equator, where surface currents are easily excited by wind forcing [e.g., *Horii et al.*, 2011; *Shinoda et al.*, 2013a; *Chi et al.*, 2014; *Halkides et al.*, 2015]. *Seiki et al.* [2013] describes off-equatorial advective cooling observed by the R/V *Mirai* (8°S, 80.5°E) during the November 2001 DYNAMO event. In this case, the advective cooling was linked to an oceanic Rossby wave.

The case studies summarized above present conflicting views on the leading processes governing intraseasonal mixed layer temperature perturbations. The differences may arise from event-to-event variability, interannual variability, or regional differences (equatorial versus off-equator cooling events). Several recent studies that combine long-term satellite observations or reanalysis fields with OGCMs help clarify some of these differences. *Vinayachandran and Saji* [2008] forced an OGCM with 9 years of observed daily winds, air temperature, specific humidity, surface radiation, rainfall, and weekly chlorophyll (to help parameterize penetrating radiation). For a region in the Seychelles thermocline ridge (4–12°S, 65–80°E), they found that the relative contributions of air-sea fluxes and vertical processes to intraseasonal cooling varied from event to event. Surface fluxes dominated events with deeper thermoclines and thicker mixed layers, while vertical processes played a larger role with shallow thermoclines and thin mixed layers.

*Lloyd and Vecchi* [2010] used a one-dimensional mixed layer model to study the mixed layer heat budget for 16 extreme (SST cooling more than 2.5 standard deviations) intraseasonal cooling events observed in the western Indian Ocean (5–15°S, 50–70°E) from 1998 to 2007. The model was forced with daily surface fluxes and winds and climatological temperature and salinity profiles. For most of the extreme cooling events, surface fluxes could only account for ~50% of the observed cooling, although some events—including those analyzed in *Duvel et al.* [2004] and *Vialard et al.* [2008]—were largely driven by surface fluxes. For more typical cooling events (those with maximum cooling between 1.5 and 2.5 standard deviations), surface fluxes accounted for ~75% of the mixed layer cooling. In agreement with *Vinayachandran and Saji* [2008], *Lloyd and Vecchi* [2010] found that ocean process contributions were more pronounced, and cooling events were larger when the thermocline was shallow, as is common with La Niña conditions.

*Jayakumar et al.* [2011] performed a study similar to that of *Vinayachandran and Saji* [2008]. As in the *Lloyd and Vecchi* [2010] study, they found that surface fluxes accounted for ~70% of cooling for the 1.5–2.5 standard

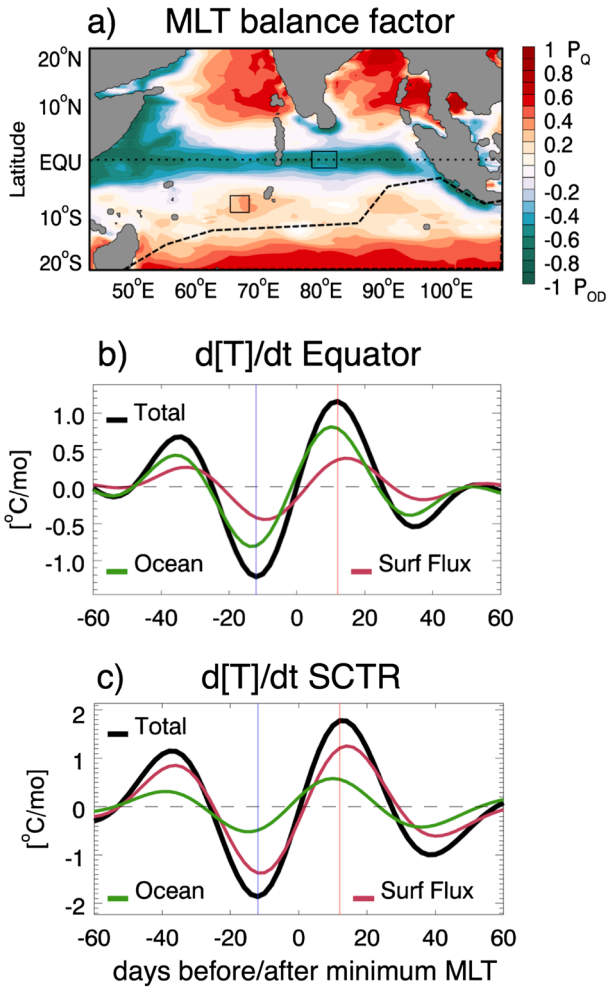


**Figure 8.** (a) All-season mixed layer temperature (MLT) "balance factor" as computed by *Halkides et al.* [2015] using ECCO ocean reanalyses: positive red (negative green) values indicate the relative contributions of surface fluxes (ocean dynamics) to the mixed layer temperature budget. Southern Hemisphere dashed line illustrates the approximate boundary between northern resolved and southern unresolved ocean processes. (b) Ocean dynamics (green) and surface flux (red) contributions to intraseasonal mean mixed layer temperature tendency, d[*T*]/d*t* averaged over the box centered on the equator. (c) as in Figure 8b but for the box near 10°E within the Seychelles-Chagos thermocline ridge (SCTR). In Figure 8b advection dominates the ocean processes. In Figure 8c vertical mixing dominates ocean processes. Adapted from *Halkides et al.* [2015].

deviation events. However, for the two events above the 2.5 standard deviation threshold, they again found that surface fluxes dominated. Reasons for the conflicting findings for the strongest cooling events are not clear. It may be a consequence of the different regions analyzed in the *Lloyd and Vecchi* [2010] (2.5–12.5°S, 50–70°E) and *Jayakumar et al.* [2011] studies (5–10°S, 60–90°E) or differences in models and forcing data.

Recently, *Halkides et al.* [2015] used 18 years of ocean reanalysis data from NASA's Jet Propulsion Laboratory (JPL) Estimating the Circulation and Climate of the Ocean (ECCO) project to study the Indian Ocean intraseasonal mixed layer heat budget. The JPL-ECCO 0.3° latitude spacing near the equator (telescoping to 1° at higher latitudes) sufficiently resolves surface forcing and ocean processes as far south as ~15°S (~5°S) in the western (eastern) part of the basin. The *Halkides et al.* [2015] analysis confirms that many of the ambiguities associated with studies of limited events or locations arise from either event-to-event differences or regional differences in the leading processes controlling the mixed layer heat budget. This is illustrated in Figure 8, which identifies ocean processes (primarily horizontal advection) as controlling the equatorial mixed layer budget, with off-equatorial events controlled primarily by surface fluxes, with secondary contributions from vertical entrainment. For each location, weaker cooling events were more sensitive to surface fluxes and

were sometimes attributable to the presence of a barrier layer. Cooling events at each location occasionally exhibited heat balance factors opposite of those shown in Figure 8.

*Drushka et al.* [2012] examined MJO modulation of the November–April mixed layer energy budget and depth using ~28,000 Argo temperature and salinity profiles from 2004 to 2010 [*Gould et al.*, 2004; *Alverson and Baker*, 2006]. The drifters reside at a nominal depth of 1000 m and profile the upper ocean (0–2000 m) with high accuracy (within 0.002°C) [*Abraham et al.*, 2013] every 10 days. In *Drushka et al.* [2012], the mixed layer heat budget was estimated using only observational data products (see their Table 1). Vertical velocities associated with Ekman pumping were calculated using gridded wind stress data. The Argo data composites revealed that MJO-modulated mixed layer depth variations in the Indian Ocean are widespread and large (>15 m), while those in the West Pacific are smaller and concentrated near the equator and ~150°–170°E. These estimates are likely subject to considerable uncertainties arising from the estimated Ekman pumping and the 10 day resolution of the Argo profilers. Mixed layer temperature variations were dominated by surface heat fluxes, but their importance varied with location and MJO phase, especially during MJO onset when vertical entrainment cooling at the mixed layer base was important. In the Indian Ocean, MJO-induced mixed layer depth perturbations modulated net surface heat flux and SST fluctuations by up to ~40%, a result that was later noted by *Halkides et al.* [2015].

Intraseasonal salinity fluctuations are driven by rainfall, evaporation, advection, and mixing. Availability of Argo and Aquarius satellite [*Lagerloef et al.*, 2010] sea surface salinity (SSS) measurements allow widespread assessment of the processes governing upper ocean salinity and fulfill a need highlighted in *Kessler* [2005]. *Matthews et al.* [2010] analyzed the upper ocean salinity budget of the MJO using Argo data, which revealed intraseasonal SSS ranges of ~0.2 psu (practical salinity units) that were consistent with precipitation minus evaporation ($P - E$) fluxes in the Indian Ocean and with $P - E$ and salinity advection in the West Pacific. *Grunseich et al.* [2013] analyzed 18 months of Aquarius SSS data and found a similar SSS amplitude but concluded that intraseasonal salinity fluctuations in both the Indian Ocean and West Pacific were governed by $P - E$. In a similar study of Aquarius SSS, *Guan et al.* [2014] pointed out that the time rate of change of SSS, rather than SSS itself (as in *Grunseich et al.* [2013]), should be evaluated against $P - E$. With this approach, the Aquarius data also suggest the need for advection in the West Pacific salinity budget, in agreement with *Matthews et al.* [2010]. However, *Guan et al.* [2014] found a more complex salinity budget in the Indian Ocean. There, intraseasonal $P - E$ explained SSS changes in the western Indian Ocean but not in the central and eastern Indian Ocean, implying the importance of ocean dynamics for surface SSS budgets. For both Indian and West Pacific Oceans, SSS variations driven by the MJO were shown to strongly regulate surface perturbation potential energy, the energy source for downward energy propagation. *Drushka et al.* [2014] used 13 years of Argo data to study MJO barrier layer feedbacks. Consistent with the *Matthews et al.* [2010] and *Guan et al.* [2014] studies, they found significant modulation of surface and upper ocean salinity by the MJO but little modulation of barrier layer thickness. Although not the focus of their study, their composite MJO ocean profiles (their Figure 5f) demonstrate the downward propagation of the temperature and salinity components of perturbation potential energy described in *Guan et al.* [2014], suggestive of $P - E$ forcing of SSS variations.

The Argo and Aquarius data provide large-scale estimates of upper ocean salinity controls, but freshening by rainfall is accomplished via a collection of smaller-scale events. Rain that falls over the tropical oceans is cooler and less saline than that of the upper ocean. The response of these competing effects depends upon the temperature and salinity stratification of the underlying ocean and the prevailing wind speed. When the density perturbation is dominated by temperature, the cold rain lens drives vertical mixing to depths of ~40 m over the course of several hours [e.g., *Wijesekera et al.*, 1999; *Anderson and Riser*, 2014], while the horizontal structure of the rain lens (diameters up to ~100 km) can be preserved for about a day via favorable interactions between the oceanic buoyancy discontinuity and overlying winds [*Soloviev and Lukas*, 1997]. In the absence of wind, large density differences between the mixed layer and fresh layer can resist mixing driven by temperature differences, and the lens spreads and thins [*Soloviev et al.*, 2015]. The presence of rain-induced cold lenses will reduce surface fluxes. Very thin lenses may be difficult for buoys to sample, potentially biasing surface flux estimates when influenced by their effect. The collective effect of cool fresh lenses on intraseasonal surface flux measurements is uncertain. On the one hand, their small spatial and short temporal scales suggest infrequent sampling by buoys. However, their frequent occurrence during calm conditions may have a nonnegligible impact on buoy flux estimates. More studies are needed to determine if cool lenses significantly bias buoy measurements or reduce surface turbulent fluxes during calm conditions.

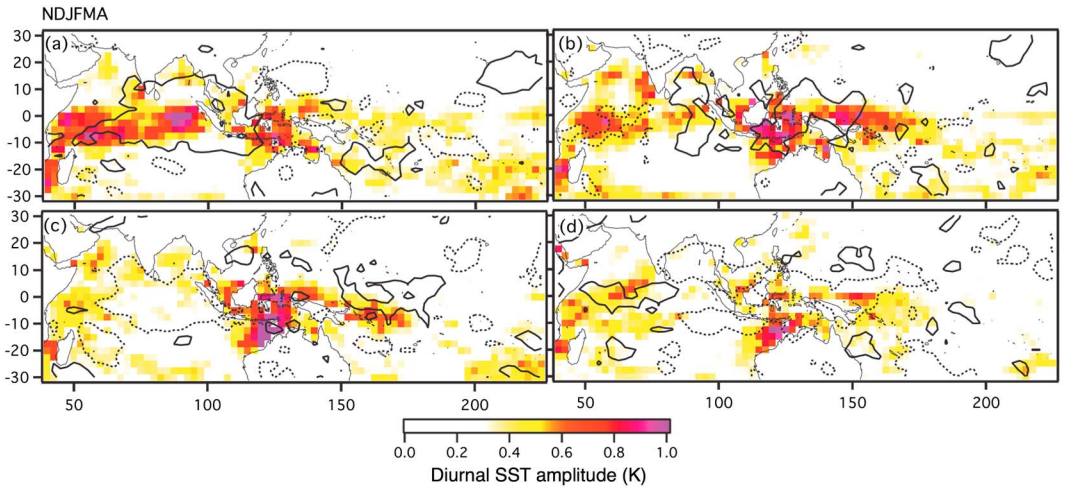


**Figure 9.** Modulation of the diurnal SST amplitude (colors) by the intraseasonal oscillation for November–April (18 ISO events) for the period 1979–2002. The four ISO phases are detected based on the filtered OLR signal around 0°N, 90°E: (a) maximum OLR; (c) minimum OLR; and (b, d) intermediate phases. The +10 W $m^{-2}$ (−10 W $m^{-2}$) OLR anomalies are overlaid with solid (dashed) contours (reprinted from *Bellenger and Duvel* [2009], copyright 2009, with permission from American Meteorological Society).

### 3.3.3. The Mixed Layer Diurnal Cycle

*Kawai and Wada* [2007] reviewed the diurnal variation of SST and its impact on the atmosphere and ocean. During convectively suppressed, low-wind conditions, surface heat flux into the ocean increases and mechanical mixing of the mixed layer decreases. In the absence of wind-driven mixing, heat from solar radiation remains in the upper ocean, producing a large SST response. Because the diurnal warming of SST is stronger and more rapid than cooling associated with nighttime ocean convection [*Lau and Sui*, 1997; *Soloviev and Lukas*, 2010; *Matthews et al.*, 2014], the mixed layer shoals [*Clayson and Weitlich*, 2005]. In the tropics, the SST diurnal cycle is typically 1–2 K but can be as high as 3K (Figures 2 and 3).

*Bellenger and Duvel* [2009] analyzed the climatology and intraseasonal variability of diurnal warm layers by forcing a simple mixed layer model with hourly interpolated ECMWF 40 year reanalysis (ERA-40) [*Uppala et al.*, 2005] surface radiative and turbulent fluxes. They found that diurnal warm layers are spatially broad ($O$(500 km)) and may persist for several days. The largest and most persistent diurnal warm layers occur in the Timor Sea in September–February and the western Indian Ocean and eastern equatorial Pacific in boreal spring. Diurnal warm layers are modulated by MJO phase (Figure 9) in a manner consistent with the mixed layer depth evolution over the MJO life cycle shown by *Drushka et al.* [2012]. The presence of diurnal warm layers and shallow mixed layers provides a near-surface "energy reservoir", in which heat inputs to the upper ocean during calm conditions are stored until they are "tapped" by the enhanced winds that accompany MJO convection.

### 3.3.4. Ocean Dynamic Response

As discussed in 3.3.2, the upper ocean responds dynamically to MJO wind forcing, as reflected in surface current accelerations and thermocline wave perturbations. Equatorial westerly wind bursts can force strong (~1 m $s^{-1}$) equatorial surface Yoshida jets [*Yoshida*, 1959], which can accelerate the seasonal wind-driven Wyrtki jet—the narrow, eastward flowing jet-like current on the equator of the Indian Ocean [*Wyrtki*, 1973]. The Yoshida jet is directly linked to MJO forcing [*Han et al.*, 2001; *Han*, 2005] and may reach as deep as 100 m but is usually distinct from the deeper Equatorial Countercurrent [*Sengupta et al.*, 2007]. Wyrtki and Yoshida jets impact the upper Indian Ocean heat balance by enhancing turbulent mixing at the mixed layer base and advecting surface waters. The enhanced Wyrtki jet associated with westerly wind events induces an anomalous wind stress curl on either side of the equator and excites upwelling equatorial Rossby waves characterized by a raised thermocline and cold SST anomaly [*Delcroix et al.*, 1991]. In DYNAMO, the November MJO westerlies >10 m $s^{-1}$ and the presence of a strong preexisting barrier layer (which reduced mixing) resulted in a 1.5 m $s^{-1}$ jet that persisted for several weeks beyond the wind forcing [*Shinoda et al.*, 2013b; *Moum et al.*, 2013]. Shear-driven turbulence cooling at the mixed layer base was comparable to warming by surface fluxes, which slowed SST recovery in the wake of MJO convection.

When westerly wind bursts are sufficiently strong, perturbations to the stably stratified thermocline can excite oceanic Kelvin waves, which can modulate upper ocean and deep-ocean temperature, salinity, and momentum budgets [*Zhang*, 1997]. In the West Pacific, intraseasonal Kelvin wave power is centered at 70–90 days with propagation speeds of about 2.1–2.8 m $s^{-1}$ [*Kessler et al.*, 1995; *Hendon et al.*, 1998]. Surface Ekman convergence and momentum transfer from atmosphere to ocean simultaneously deepen the thermocline and elevate the sea surface height (SSH), with typical displacements of 15–20 m and 15–20 cm, respectively [e.g., *Matthews et al.*, 2010]. The downwelling thermocline insulates the mixed layer from cold subsurface waters, leading to a warm SST anomaly signature as the wave propagates eastward [e.g., *Kessler and Kleeman*, 2000]. The SST anomaly may be as large 0.5 K in the eastern Pacific, where the mean thermocline depth is shallow, and less in the West Pacific [*Vecchi and Harrison*, 2000]. The Kelvin wave response is linked to intraseasonal eastward expansion of the Warm Pool [*Piquat et al.*, 1996] and East Pacific ENSO variability [*Lukas et al.*, 1984]. West Pacific MJO-driven wind bursts, especially successive bursts, have been linked to El Niño onset [*Zhang and Gottschalck*, 2002; *McPhaden*, 2004]. *Matthews et al.* [2010] analyzed equatorial salinity profiles using 4 years of Argo data and found that the MJO-forced oceanic Kelvin wave in the West Pacific drives salinity perturbations that extend into the deep ocean (at least 1400 m). Deep-ocean salinity perturbations in the Indian Ocean are also evident, but the shorter sampling period in that basin made their interpretation difficult.

In the Indian Ocean, the zonal and northern land barriers lead to a more complex ocean wave response to MJO westerly wind events [e.g., *Schott et al.*, 2009]. *Webber et al.* [2010] analyzed surface altimetry data from the TOPEX/POSEIDON-Earth Remote Sensing (T/P-ERS) satellite to study the ocean response to MJO wind forcing. As in the West Pacific, they found that Indian Ocean MJO wind events initiate a downwelling Kelvin wave, but upon encountering the west coast of Sumatra, the bulk of the wave energy is reflected into a *downwelling* equatorial Rossby wave, while the remainder is transformed into northward and southward propagating coastal Kelvin waves, the latter of which interacts with ocean mixing processes in the Indonesian Seas (section 3.5). The southward coastal Kelvin wave may "escape" the Indian Ocean via the Timor, Arafura, and Coral Seas, but the northward coastal Kelvin wave remains trapped. The reflected downwelling Rossby wave period depends on upper ocean stratification but typically crosses the Indian Ocean in 80–100 days. On average, the equatorial Rossby wave induces a 0.2–0.3 K warm SST anomaly (up to 1 K for individual events) when it reaches the western Indian Ocean, comparable to anomalies from intraseasonal surface heating; the SST anomaly may be linked to the initiation of primary MJO events [*Webber et al.*, 2012]. Modulation of the upper ocean was also observed during CINDY/DYNAMO [*Gottschalck et al.*, 2013; *Shinoda et al.*, 2013b]. In that case, the deepening of the Seychelles thermocline ridge in early 2012 is attributed to the arrival of an equatorial Rossby wave that was forced by the November 2011 MJO westerly wind event.

### 3.4. Ocean Feedbacks to the MJO

Ocean feedbacks are important to the MJO only if they impact the frequency, intensity, or duration of the disturbance. *Sobel et al.* [2010] cite the larger intraseasonal OLR variance over the tropical Indian and West Pacific Oceans compared to the Maritime Continent, the spatiotemporal correlation of precipitation and surface fluxes, and the improved simulation of the MJO in models with larger surface flux variability as evidence for the role of ocean turbulent fluxes in the MJO. The ocean feedback to the MJO involves two processes: the modulation of surface fluxes by variable SSTs and the response of the MJO to the SST-modulated fluxes. *Zhang* [2005] and *Hendon* [2005] note that the phasing of SST variations within the MJO cycle decreases latent and sensible surface flux amplitudes and shifts them slightly closer to the leading edge of MJO convection. Warm SSTs east of MJO convection were postulated to improve MJO propagation through either direct destabilization or by enhancing low-level moisture convergence. Assessments of the impact of ocean coupling on the MJO were hampered by the poor simulation of the MJO in most GCMs and a general lack of knowledge of processes important to MJO initiation, maintenance, and propagation [e.g., *Zhang et al.*, 2013]. While these challenges remain today, progress has been made on both fronts in the past decade. Surface fluxes associated with the MJO are sensitive to SST fluctuations on a variety of time scales via their influence on mean and anomalous $\Delta q$ and $\Delta T$ (e.g., equations (1) and (2)). Here we summarize ocean feedbacks forced by interannual, intraseasonal, and diurnal SST variability.

#### 3.4.1. Sensitivity to Interannual SST Variability

Major coupled modes of variability, such as ENSO and the Indian Ocean Dipole (IOD), drive interannual Warm Pool SST variations. These modes are each associated with large-scale wind, precipitation, and upper ocean anomalies [*Wyrtki*, 1975; *Ramage*, 1975; *Saji et al.*, 1999]. These changes in the basic state can potentially influence the initiation, maintenance, and propagation of the MJO, either independently of the air-sea interaction

processes or through altering air-sea interaction process within the MJO. Compared to La Niña conditions, MJO events during El Niño episodes are more frequent [*Jones et al.*, 2004b], have shorter durations [*Pohl and Matthews*, 2007], and propagate farther east into the Pacific Ocean [*Fink and Speth*, 1997; *Hendon et al.*, 1999; *Woolnough et al.*, 2000; *Bergman et al.*, 2001; *Kessler*, 2001; *Tam and Lau*, 2005]. The eastward expansion of the Warm Pool during El Niño events supports extended eastward propagation of the MJO [e.g., *Woolnough et al.*, 2000], enabling the westerly wind anomalies to further reinforce the El Niño state. This cooperative or multiplicative feedback of MJO winds and ENSO has been demonstrated with a variety of models [*Perez et al.*, 2005; *Gebbie et al.*, 2007; *Kapur and Zhang*, 2012; *Lopez et al.*, 2013]. *Gushchina and Dewitte* [2012] found that the modulation of MJO activity by ENSO depends upon whether the ENSO SST anomalies maximize in the eastern or central Pacific. During −IOD years, with cold (warm) SST anomalies in the western (eastern) Indian Ocean, MJO activity increases in the eastern Indian Ocean following an eastward shift of low-level moisture convergence [*Shinoda and Han*, 2005; *Wilson et al.*, 2013], while the opposite is true for +IOD events. As with ENSO, the IOD modulates the MJO period, with longer-period events during −IOD events [*Izumo et al.*, 2010].

These variations could potentially influence the air-sea interaction within the MJO through the following: changing the oceanic response to the MJO-associated surface fluxes as a result of the changing structure of the ocean mixed layer, changing the MJO-related surface fluxes (e.g., as a result of changing basic state low-level winds), or changing the atmospheric response to these intraseasonal SST variations. While some of the influences of basic state variations on air-sea interaction are discussed in the relevant sections, to the best of our knowledge there has been no systematic study of their influence on the basic state of air-sea interaction processes within the MJO.

#### 3.4.2. Sensitivity to Intraseasonal SST Variability

Intraseasonal SST maximum-to-minimum ranges routinely exceed 1°C (e.g., Figures 2 and 3). Using mean values observed during TOGA COARE, *Webster et al.* [1996] employed a bulk flux algorithm to estimate that a 1°C change in SST changes latent and sensible heat fluxes by 18.7 W $m^{-2}$ and 2.4 W $m^{-2}$, respectively. Because intraseasonal SST fluctuations are in quadrature with intraseasonal rainfall and winds (Figure 4), they can alter the phasing and magnitude of surface fluxes with respect to MJO convection. This effect was first demonstrated by *Shinoda et al.* [1998], who estimated the sensitivity of surface fluxes to SST variability by comparing fluxes calculated with the COARE bulk flux algorithm using observed weekly SSTs and 120 day low-pass filtered SSTs. Maximum surface fluxes using the full SST time series were about 10 W $m^{-2}$ (5–10%) lower than those with the filtered SSTs, because in the former calculation maximum winds acted on colder SST anomalies.

Intraseasonal SST variability also affects latent and sensible heat fluxes through its impact on $\Delta q$ and $\Delta T$ phase and amplitude (i.e., the first terms on the right-hand side of equations (1) and (2)), although this effect is secondary to the wind-SST interactions above. *Hendon and Glick* [1997] analyzed the phasing of SST, $q_{air}$, and $\Delta q$ in the Indian and West Pacific Oceans using 30–90 day filtered OLR and ECMWF operational analyses. In both basins, intraseasonal $\Delta q$ variations are largely driven by $q_{air}$ fluctuations. In the West Pacific, $q_{air}$ and $q^*_{SST}$ are in phase, yielding $\Delta q$ amplitudes (i.e., one half the intraseasonal range) of ~0.2 g $kg^{-1}$. However, in the Indian Ocean, $q_{air}$ and $q^*_{SST}$ are nearly in quadrature, so that $\Delta q$ amplitude is ~0.7 g $kg^{-1}$. It should be noted that these findings are based on filtered time series, which can exaggerate phase offsets (Figure 5). However, Figure 9 of *Benedict and Randall* [2007], which is based on unfiltered data, offers support for this argument and suggests that differences in $q_{air}$ and $q^*_{SST}$ phasing are a consequence of the more vertically "tilted" MJO convective structure in the West Pacific compared to the more "upright" convection of the Indian Ocean. This implies that Indian Ocean latent and sensible heat fluxes should be more sensitive to $\Delta q$ and $\Delta T$, respectively, than those in the West Pacific.

*Araligidad and Maloney* [2008] studied the sensitivity of MJO convection to latent heat flux using data from two West Pacific buoys, finding that intraseasonal latent heat flux predicted about 20% of contemporaneous precipitation. (These values are based on regressing rainfall onto LH. However, regressing LH onto rainfall is perhaps a calculation more directly relevant to moisture mode theory and yields a 5~10% contribution of LH to rainfall [e.g., *Riley Dellaripa and Maloney*, 2015].) Fluxes computed using long-term means of SST and near-surface humidity were about 20% greater than those using observed SST and humidity variations, generally consistent with *Shinoda et al.* [1998]. This reduction in surface fluxes by intraseasonal SST variations presents an apparent conflict with the enhanced MJO activity that often results from air-sea interactions in coupled models (section 5); the conflict is resolved when the relative phasing of the reductions are considered. Latent heat flux reductions by intraseasonal SST variations are not uniformly distributed

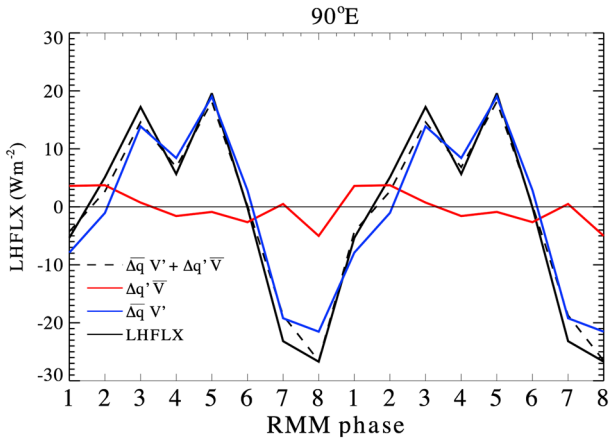


**Figure 10.** Composited all-season latent heat flux anomalies and linearized latent heat flux terms shown in equation (1) for MJO phases at the 0°N 90°E RAMA buoy. Latent heat flux was calculated using 10min average wind speed, SST, air temperature, and relative humidity buoy data and COARE v3.0 bulk flux algorithm [*Fairall et al.*, 2003] and averaged by MJO phase using the Real-time Multivariate MJO (RMM) index [*Wheeler and Hendon*, 2004]. For the linearized component terms, overbars are average quantities over the entire MJO cycle, while primes represent intraseasonal deviations. MJO convection maximizes during phases 3 and 4. Figure courtesy of Emily Riley-Dellaripa.

across the MJO life cycle. Rather, they occur during the westerly wind (active and transition to suppressed conditions) phase and are partially offset by surface flux enhancements during the suppressed and developing stages [*Shinoda et al.*, 1998]. *Riley Dellaripa and Maloney* [2015] demonstrate this result using data from an Indian Ocean RAMA buoy (Figure 10). This finding suggests two possible feedbacks to the MJO by SST-modulated latent heat fluxes: first, the SST-enhanced flux during MJO developing and active phases increases available boundary layer moisture and amplifies and maintains the developing convective anomalies, respectively, via a so-called "modified WISHE" effect [*Maloney and Sobel*, 2004]; second, the westerly wind during the transition-to-suppressed phase impacts the ocean mixed layer energy budget and influences the SST recovery time.

SST-enhanced surface fluxes may also augment frictional wave-CISK moisture convergence (section 2.2), which is associated with MJO propagation [e.g., *Hendon and Salby*, 1994; *Sperber*, 2003; *Weare*, 2006]. Sensible heat fluxes driven by the warm SST anomaly induce surface low-pressure anomalies and convergence [e.g., *Lindzen and Nigam*, 1987; *Back and Bretherton*, 2009] approximately collocated with the dynamically driven low-pressure response to deep convective heating. This SST-driven convergence is proportional to the SST Laplacian ($-\nabla^2$SST), which maximizes on the warm side of SST gradients. Consequently, the SST-driven sensible heat fluxes and convergence might be effectively hidden, since they occur in a location where fluxes are suppressed due to lower wind speeds. Simple scaling arguments suggest that boundary layer winds adjust to SST gradients in 1∼3 days for 2∼5 m s$^{-1}$ wind speeds typical of the MJO suppressed phase. (The adjustment time scale for winds to respond to the SST gradient can be estimated as the inverse of the frictional drag, $\frac{h}{w_d}\mathbf{U}$, where $\mathbf{U}$ and $h$ are the boundary layer wind and height, respectively, and $w_d$ is a linearized friction coefficient [e.g., *Back and Bretherton*, 2009, Eq. 1]. Here we assume $w_d = 10^{-3}$ and $h$ = 500m.) This adjustment time scale is much shorter than the ∼10–20 day suppressed phase, so SST-driven boundary layer convergence is active during most of this time. Estimating the SST-driven component of boundary layer convergence and its contribution to the dynamically forced convergence is difficult, in part because it requires knowledge of the boundary layer height. *Hsu and Li* [2012] estimate $\sim 10^{-7}$ s$^{-1}$ SST-boundary layer convergence over the Maritime Continent when MJO convection is in the eastern Indian Ocean. This represents a 10–25% contribution to total boundary layer convergence for boundary layer depths corresponding to 850 and 700 hPa, respectively. *Hsu and Li* [2012] calculated this quantity using coarse (2.5°) resolution SST data over the Maritime Continent, where islands reduce the number of grid points available for the $-\nabla^2$SST calculation and may disrupt dynamically driven moisture convergence, both of which may impact the estimated contribution of SST-driven moistening. Nevertheless, their study represents the first attempt to quantify the role of ocean feedbacks via this potentially important mechanism.

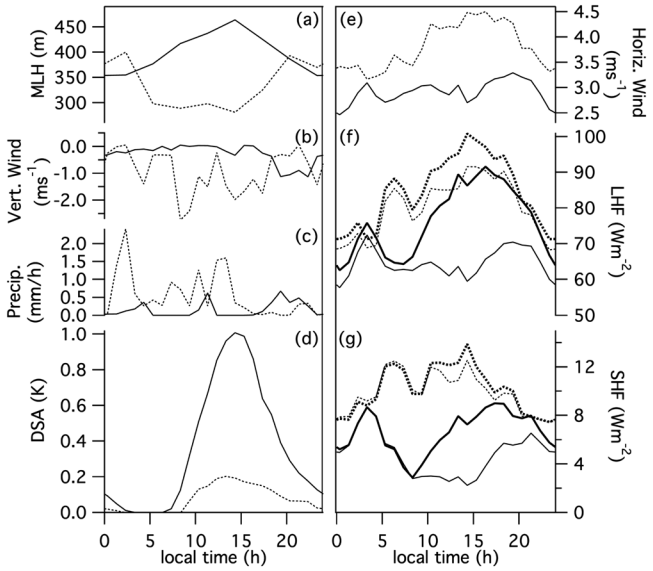


**Figure 11.** Average diurnal evolution observed by the R/V *Mirai* during the Indian Ocean MISMO field experiment for days with (solid) and without (dashed) strong diurnal warm layers (DWLs) of (a) mixed layer height (or depth; m), (b) the 300–800 m height average vertical wind (m s$^{-1}$), (c) precipitation rate (mm h$^{-1}$), (d) diurnal SST amplitude (DSA; K), (e) horizontal wind speed (m s$^{-1}$), (f) surface latent heat flux (W m$^{-2}$), and (g) sensible heat flux (W m$^{-2}$). For surface fluxes, thick lines represent heat fluxes computed with DWL-induced SST variations and thin lines represent heat fluxes computed with bulk SST from which the DWL effect has been removed (reprinted from *Bellenger et al.* [2010], copyright 2010, with permission from American Meteorological Society).

There is some evidence to suggest that boundary layer convergence driven by small-scale SST gradients can generate precipitating clouds. *Li and Carbone* [2012] measured West Pacific rain onset events as a function of $\nabla^2$SST using 25 km resolution satellite rainfall and SST measurements. They found that onset events were more than twice as likely the day after a negative $\nabla^2$SST was observed (boundary layer convergence) than when positive $\nabla^2$SST (boundary layer divergence) was observed. Because large local SST variations of >2°C were observed over relatively small scales (~100 km), $-\nabla^2$SST was large, inducing convergence of $\sim 10^{-5}$ s$^{-1}$, an order of magnitude larger than the background convergence. The small-scale rain onset events were most frequent for SSTs warmer than 29°C, suggesting a preference for MJO suppressed and developing phases, later confirmed by *Carbone and Li* [2015]. These phases are also characterized by large diurnal SST variations which are also linked to convective onset events, as discussed in the following section. It is presently not clear if SST gradients or SST diurnal variability (or other processes) are more important for initiating suppressed phase rain events.

### 3.4.3. Sensitivity to Diurnal SST Variability

Mixed layer shoaling during suppressed conditions is frequently associated with diurnal warm layers with 1–3 K diurnal SST variations (e.g., Figures 2 and 3) [*Anderson et al.*, 1996; *Shinoda and Hendon*, 1998; *Shinoda*, 2005; *Bernie et al.*, 2005; *Moum et al.*, 2013]. These variations can increase surface heat fluxes (latent + sensible) by 50–70 W m$^{-2}$ during the day and by 10 W m$^{-2}$ for the 24h mean [*Fairall et al.*, 1996b; *Schiller and Godfrey*, 2005; *Bellenger and Duvel*, 2009]. *Zeng and Dickinson* [1998] used hourly SSTs from West Pacific buoys to diagnose a 19.7 W m$^{-2}$ (5.6 W m$^{-2}$) mean diurnal range for the latent (sensible) heat flux. If daily or monthly SSTs were used to compute the fluxes, the diurnal flux variations essentially disappeared. *Parsons et al.* [2000] reported mean diurnal ranges of latent (45 W m$^{-2}$) and sensible (4 W m$^{-2}$) fluxes from the TOGA COARE Intensive Flux Array buoy during one MJO suppressed phase (11–22 November 1992).

More recently, *Bellenger et al.* [2010] calculated diurnal surface fluxes using data collected in the Indian Ocean (near 0°N, 80°E) during MISMO. The 30 day observation period was partitioned into days with and without diurnal warm layers (DWLs) >0.5 K (Figure 11), which effectively selected suppressed and weakly disturbed conditions, respectively. The latent (sensible) heat flux diurnal range is ~30 W m$^{-2}$ (~5 W m$^{-2}$) for both DWL and non-DWL days (heavy lines in Figures 11f and 11g). DWL fluxes are weaker than non-DWL fluxes and are primarily driven by SST (Figure 11d), while non-DWL fluxes are mostly sensitive to wind speed (Figure 11e). This difference is reflected in the diurnal composites using daily mean SSTs (thin lines in Figures 11f and 11g).

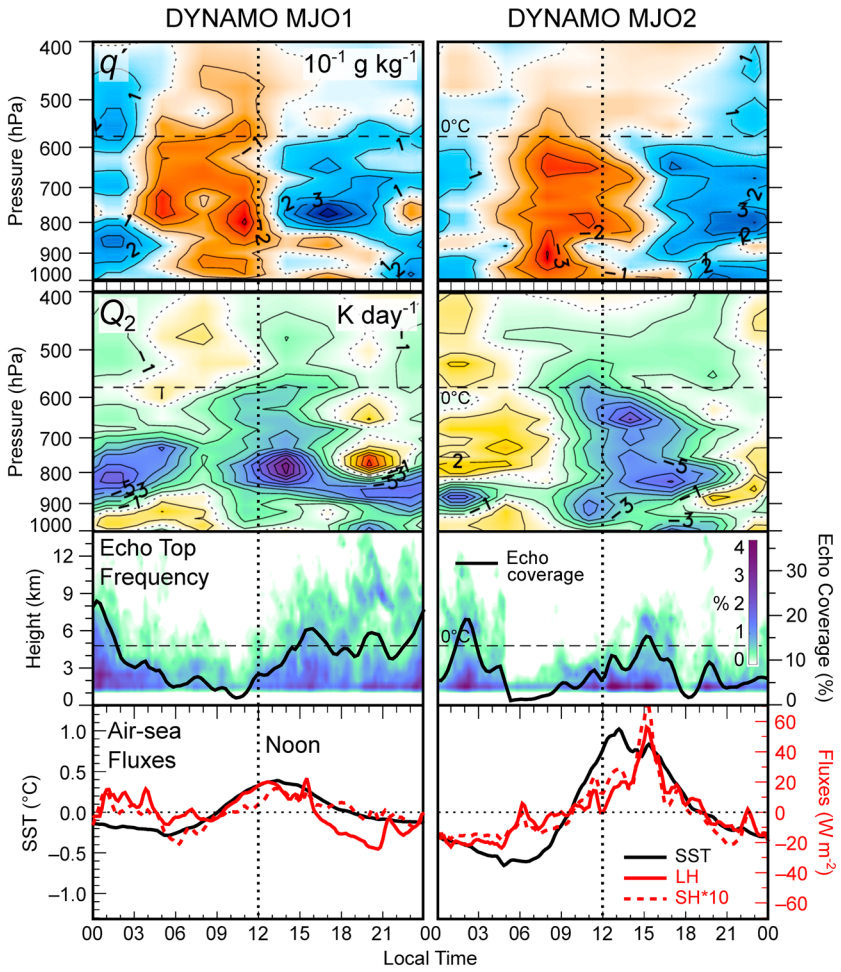


**Figure 12.** Composite diurnal cycle during the MJO suppressed phase for the DYNAMO (left column) October (right column) and November (MJO2) MJO events: (first row) anomaly specific humidity ($q'$; $10^{-1}$ g kg$^{-1}$); (second row) DYNAMO northern sounding array apparent moisture sink ($Q_2$; K day$^{-1}$) [*Yanai et al.*, 1973]; (third row) radar echo top frequency (%; shaded) and echo coverage (%; black line); and (fourth row) anomaly SST (SST; °C; black; left ordinate), anomaly latent heat flux (LH; W m$^{-2}$; solid red), and anomaly sensible heat flux (SH; W m$^{-2}$; dashed red) multiplied by 10 (reprinted from *Ruppert and Johnson* [2015], supplemental figure, copyright 2015, with permission from American Meteorological Society).

*Sui et al.* [1997] demonstrated the link between convection and diurnal SST and surface flux variations during TOGA COARE, noting distinct differences in the diurnal cycle of rainfall during disturbed and suppressed MJO phases. As is typical for oceanic rainfall in cloudy conditions, radiative-dynamic interactions associated with nighttime cloud top cooling [*Gray and Jacobson*, 1977; *Randall et al.*, 1991] or surface-cloud-radiation interactions [*Chen and Houze*, 1997] result in a diurnal rainfall maximum a few hours after local midnight [e.g., *Janowiak et al.*, 1994; *Yang and Slingo*, 2001]. However, during suppressed conditions, diurnal rainfall exhibited a more land-like character, maximizing a few hours after local noon, suggesting that diurnal SST variations are large enough to destabilize the lower atmosphere and initiate convection.

*Ruppert and Johnson* [2015] analyzed the impact of diurnally forced suppressed phase convection by compositing a variety of in situ DYNAMO measurements, including apparent moisture sink ($Q_2$) [*Yanai et al.*, 1973] diagnosed from the Northern Sounding Array, for each of two suppressed periods during DYNAMO (6–11 October and 13–16 November 2012; Figure 12). During the October case, mean surface wind speeds were about 5m s$^{-1}$, and the mean diurnal ranges of SST, latent heat, and sensible heat fluxes were 0.65 K, 36 W m$^{-2}$, and 5 W m$^{-2}$, respectively. For the November case, mean wind speeds were only 2 m s$^{-1}$, and the diurnal ranges increased to 1.6 K, 81 W m$^{-2}$, and 9.9 W m$^{-2}$. During both periods, rapid SST warming began about 0900 LT, a few hours after sunrise, and caused most of the $\Delta T$, as seen by comparing the SST and air

temperature traces in the lower panels of Figure 12. Convection and $-Q_2$ increased sharply around local noon, followed by increased midlevel moisture anomalies. This sequence was repeated daily over both periods, which were characterized by progressively deeper diurnal moistening and greater organization of the cloud field (not shown). It is difficult to assess if the enhancement of diurnal moistening contributed directly to local moistening and cloud organization or whether such moistening was accomplished by larger-scale circulations [*Chen et al.*, 2015], which integrate moistening from a variety of time scales and space scales, including the diurnal. In other words, the suppressed phase ocean feedback to the atmosphere on diurnal time scales seems clear, but the mechanisms that rectify the diurnal moistening onto MJO time scales are not.

### 3.5. Air-Sea Interactions in Other Tropical Regions and Seasons

The MJO also modulates the upper ocean in other basins and seasons, either remotely via oceanic Kelvin waves or via propagating large-scale atmospheric circulation anomalies. During boreal winter, circulation anomalies associated with the MJO impose 40∼60 day wind variations in the tropical Atlantic that modulate surface fluxes, sea level, and thermocline depth [e.g., *Foltz and McPhaden*, 2004; *Yu et al.*, 2011]. Some of the Atlantic intraseasonal wind variations may also be driven by the MJO-regulated Northern Annular Mode [*Lin et al.*, 2009]. The boreal winter Indian and Pacific Ocean responses to MJO forcing are discussed in section 3.3.4. During boreal summer, the MJO drives tropical East Pacific SST variations of 0.4-0.5°C [*Maloney and Kiehl*, 2002]. The JPL-ECCO reanalysis indicates that, on the equator, these variations are primarily driven by vertical advection processes associated with oceanic Kelvin waves, while wind-driven mixing and horizontal advection control the mixed layer temperature budget within as little as 3° latitude away from the equator [*Halkides et al.*, 2011].

The MJO may drive and respond to air-sea interactions over the Maritime Continent, which is home to a variety of oceanic and atmospheric processes that may impact the ocean feedbacks to the atmosphere [*Zhang et al.*, 2013]. In contrast to the deep, open Indian and Pacific Oceans, the Maritime Continent features complex bathymetry, deep seas, shallow continental shelves, enclosed and semienclosed seas, and deep, narrow channels that serve as conduits and mixing chambers for the Pacific-to-Indian Ocean Indonesian Throughflow [e.g., *Gordon*, 2005]. The Indonesian Seas experience intense tidal mixing which is thought to reduce SST and limit the occurrence of deep atmospheric convection [*Koch-Larrouy et al.*, 2011; *Sprintall et al.*, 2014]. The Indonesian Throughflow cools and freshens the eastern Indian Ocean [*Gordon*, 2005]. Indian Ocean Kelvin waves forced by westerly wind bursts (section 3.3.4) are partially transformed to coastal Kelvin waves, where they can modulate the Throughflow [*Gordon*, 2005; *Sprintall et al.*, 2009; *Gordon et al.*, 2010; *Drushka et al.*, 2010; *Sprintall et al.*, 2010; *Iskandar et al.*, 2014] and tidal mixing [e.g., *Schiller et al.*, 2010]. From the perspective of MJO convection, the Maritime Continent presents reduced ocean area, steep island terrain, and strongly forced diurnal convection, all of which may interfere with the intraseasonal convection and associated air-sea interactions. How these features influence air-sea interactions within the MJO is not well understood. *Peatman et al.* [2014] observed an amplified diurnal cycle of land-based convection about 10 days before the arrival of MJO convection. The increased convection may indirectly influence air-sea feedback mechanisms. For example, increased river discharge freshens and stabilizes the nearby upper ocean, modifying the response of the ocean to air-sea fluxes. Whether the diurnal cycle of convection is significantly modulated by ocean feedbacks and how it may be rectified onto the MJO are central questions to understanding the Maritime Continent's influence on the MJO.

### 3.6. Other Air-Sea Interactions

Intraseasonal air-sea interactions involving surface waves, turbulence, sea spray, bubbles, surface foam layers, gas exchange, biological processes, and aerosol formation have attracted less attention than the processes described elsewhere in this review. Two recent studies examined MJO influences on global ocean surface waves. *Stopa et al.* [2013] analyzed surface wave reanalysis data and noted global scale correlations of significant wave height with MJO amplitude, although the impacts were not examined as a function of MJO phase. *Marshall et al.* [2015] used output from an ocean wave model forced with global atmospheric reanalysis data to study significant wave height, energy flux, and period as a function of MJO phase. Wave height and energy flux were significantly modulated by MJO zonal wind anomalies in all ocean basins, including high-latitude waves forced by winds associated with MJO teleconnections. In the North Atlantic, MJO forcing was indirectly communicated to the ocean waves via its impact on the North Atlantic Oscillation. Perturbations to the ocean wave state associated with MJO onset were directly observed during the DYNAMO field campaign [*Moum et al.*, 2013]. *DeWitt et al.* [2013] analyzed aerosol concentrations during DYNAMO and noted the enhancement of sea salt aerosol particles, which are associated with sea spray, during MJO westerly wind events. Sea spray

can impact momentum and surface turbulent fluxes [*Veron et al.*, 2008] and represents an ocean feedback to the atmosphere independent of SST, although its variability within the MJO has received scant attention thus far. We found no publications assessing how the MJO affects air-sea gas exchanges, although *Li et al.* [2010] have noted MJO-driven modulations of atmospheric $CO_2$.

On the other hand, regulation of phytoplankton and chlorophyll by the MJO has emerged as an area of air-sea interaction research, both from the perspective of the fishing industry and because of the potential biological feedbacks on mixed layer salinity and temperature [*Siegel et al.*, 1995; *Murtugudde et al.*, 1999; *Strutton et al.*, 2000]. These studies use data from the Sea-Viewing Wide Field-of-View Sensor [*McClain et al.*, 2004], which provides daily near-global measurements of surface chlorophyll (a proxy for phytoplankton) or similar measurements from the Moderate Resolution Imaging Spectroradiometer [*Franz et al.*, 2005; *Bailey and Werdell*, 2006]. Significant MJO modulation of ocean surface chlorophyll has been observed over the northern Indian and northwestern tropical Pacific Oceans [*Waliser et al.*, 2005; *Jin et al.*, 2012, 2013], coastal areas in the far eastern Pacific [*Waliser et al.*, 2005; *Xie et al.*, 2005], the Seychelles thermocline ridge [*Resplandy et al.*, 2009], and the South China Sea and surrounding areas during boreal summer [*Isoguchi and Kawamura*, 2006; *Liu and Wang*, 2012]. In most regions, the phytoplankton blooms follow strong wind events by about 6 days [*Waliser et al.*, 2005; *Jin et al.*, 2013], as the upper ocean is fertilized with cold-water nutrients either by turbulent mixing or Ekman pumping [*Jin et al.*, 2013]. Nutrient availability for such blooms may depend on the erosion of preexisting barrier layers [*Murtugudde et al.*, 1999; *Madhu et al.*, 2006; *Cabrera et al.*, 2011; *Girishkumar et al.*, 2012]. Some blooms, such as those in the northern Arabian Sea, appear to be light driven [*Waliser et al.*, 2005]. Dense phytoplankton communities increase upper ocean absorption of solar radiation [*Jerlov*, 1968; *Paulson and Simpson*, 1977] and so may influence upper ocean salinity and SST, and hence possibly also atmospheric circulations [e.g., *Isobe et al.*, 2014]. *Robertson* [2012] used a 1-D ocean mixed layer model coupled to a four-compartment (Nutrient-Phytoplankton-Zooplankton-Detritus) model, forced with observed fluxes from TOGA COARE, to conclude that the MJO-modulated chlorophyll concentrations can enhance SST warming during the MJO suppressed phase by approximately 0.05°C.

### 3.7. Summary

Tropical atmosphere-ocean interactions on intraseasonal time scales can be interpreted as a three-step feedback loop: (1) ocean forcing by the atmosphere, (2) the ocean mixed layer response to rainfall, surface turbulent fluxes, and momentum fluxes, and (3) the response of the atmosphere to SST perturbations that arise from (2). Over the Warm Pool, the intraseasonal surface energy budget is dominated by variations in net surface shortwave radiation and latent heat fluxes. Cloudiness controls the surface shortwave variations. Latent heat flux variability is primarily driven by wind speed variations but is modulated by the underlying SST at a rate of 5–10% (9∼18 W $m^{-2}$) per 1°C (depending on low-level atmospheric humidity and wind). The ocean mixed layer responds to MJO forcing by warming and shoaling during the suppressed (calm) phase and cooling and deepening during the active (convective) phase so that maximum SSTs lead convection by about one quarter cycle. Typical SST maximum-to-minimum ranges associated with the MJO are 0.2∼0.5°C, although single-event variations can be larger than 1°C. The mixed layer response is modulated by the climatological mixed layer depth, with deeper (shallower) mean mixed layers having a larger (smaller) heat capacity and smaller (larger) SST response. The mixed layer response to MJO forcing can be modulated from one event to the next by factors such as salinity stratification (i.e., barrier layers), heat and salt advection by surface currents, vertical advection by wind-driven Ekman pumping and current shear, and turbulent mixing with subsurface waters. These processes have a potentially larger impact with shallower mixed layers and stronger MJO forcing. The atmospheric response to intraseasonal SST variations is driven by the amplitude and phase of the thermodynamic parts of latent and sensible heat fluxes ($\Delta q$ and $\Delta T$; equations (1) and (2)) relative to MJO convection. The atmospheric response to the SST-modulated fluxes may be reflected in changes to the cloud field.

During suppressed (calm) conditions, the thin mixed layer, light winds, and large net solar radiation into the ocean surface results in a large SST diurnal cycle (Figures 2 and 3) with a range of 1–3°C. These diurnal warm layers have diameters *O*(1000 km) and can persist for several days. The land-like diurnal surface temperature cycle can enhance shallow convection and its moisture detrainment into the lower troposphere. How this diurnally enhanced shallow convection impacts the MJO is unclear, but it may contribute directly to low-level tropospheric moistening, promote the upscale organization of convection, or amplify the aggregation of moisture by large-scale convergence. Continued progress on this front will likely require modeling studies that resolve cumulus scale motions over mesoscale domains.

Progress during the past decade has addressed, or even answered, several of the outstanding questions identified by *Zhang* [2005], *Hendon* [2005], and *Kessler* [2005]. Improved understanding of MJO air-sea interactions is the result of enhanced observing systems, intensive field campaigns, new paradigms for the MJO, and advances in modeling. From an observational standpoint, a rich array of new satellite sensors focused on ocean measurements have filled critical gaps in our ability to observe atmosphere-ocean coupled processes in data-sparse regions. QuickSCAT and its successors provide low-level wind estimates over the oceans. Ocean Surface Current Analyses-Real time [*Lagerloef et al.*, 1999] surface currents provide information on the upper ocean response to intraseasonal momentum forcing, while SSH data from TOPEX/POSEIDON reveal the deeper ocean inertial response. TRMM TMI and AMSR-E microwave radiometers provide estimates of both rainfall and SST variations, the Aquarius satellite measures ocean salinity changes, and the CloudSat project provides detailed information on the cloud field [*Riley et al.*, 2011]. The expansion of these remote sensing systems occurred in conjunction with new in situ observing systems, such as the RAMA buoy array in the Indian Ocean and the deployment of the global Argo drifter network. Field programs, such as MISMO and CINDY/DYNAMO, provided opportunities to deploy modern observing instruments in the Indian Ocean, where they together sampled the moistening and initiating phases of the MJO in the Indian Ocean and the associated air-sea interactions. These field campaigns also provided valuable "ground truth" measurements for satellite-based sensors [e.g., *Shinoda et al.*, 2013b]. Improved understanding of the close relationship of MJO convection to tropospheric moisture has reshaped MJO thinking and spearheaded efforts to improve its simulation.

Assessment of ocean feedbacks to the MJO remains challenging, especially in light of the growing recognition of the importance of free tropospheric moisture to the MJO and the multitude of physical processes present within the MJO life cycle. The challenges of understanding air-sea interactions as either contributors to or simply consequences of the MJO are pervasive in both observational and modeling studies. For example, *Hirata et al.* [2013] studied composites of observed intraseasonal convective events that did and did not propagate from the Indian Ocean to the West Pacific. Propagating events were associated with larger SST anomalies than nonpropagating events but also exhibited larger radiative, wind, and surface pressure anomalies which may have contributed to the larger SST anomalies. Assessment of ocean feedbacks to the MJO should be made within the context of existing MJO knowledge and theories but may require new theories that explicitly include the role of SST-modulated fluxes.

## 4. Theory and Idealized Modeling

Relatively few theoretical models have been developed for the role of air-sea interaction in the MJO. Section 4.1 discusses these models and a statistical modeling approach to the role of air-sea coupling; section 4.2 discusses idealized modeling studies that aim to understand the sensitivity of the atmosphere to intraseasonal SST anomalies in the context of the MJO.

### 4.1. Theoretical and Statistical Models of Air-Sea Interaction

*Wang and Xie* [1998] examine the role of air-sea coupling in the equatorial-wave modes of *Matsuno* [1966] in the Warm Pool region by considering a system of coupled atmosphere-ocean equations, comprising a set of linearized shallow-water equations for the first baroclinic mode of the tropical atmosphere coupled to a linearized model of the upper ocean dynamics and thermodynamics.

The atmospheric model describes the linear motion of the lowest internal baroclinic mode of the atmosphere following, e.g., *Gill* [1980], modified through latent heat release due to wave-induced moisture convergence following, e.g., *Wang* [1988b] and an additional atmospheric heating that depends linearly on SST perturbations. The source of this relationship is not clearly defined, but the authors noted a number of alternative justifications for this response, including enhanced evaporative fluxes [e.g., *Zebiak*, 1986] and convergence induced by surface temperature gradients [e.g., *Lindzen and Nigam*, 1987; *Neelin*, 1989], although their parameter choices are based on an SST enhancement of the moisture fluxes. The uncertainty about the nature of this relationship between SST and heating characterizes our lack of understanding of the role of air-sea interaction in the MJO, and we will return to it later.

The ocean model of consists of a linearized $2\frac{1}{2}$ layer ocean in which a mixed layer of variable depth is embedded within an active upper ocean bounded by a time-varying thermocline. Mixed layer temperature (SST) is determined prognostically and can respond to surface flux forcing, wind mixing entrainment, and variations in the mixed layer depth and thermocline depth driven by Ekman transport and wind-driven oceanic waves and

currents. The surface flux forcing includes evaporative fluxes and longwave and shortwave radiative fluxes. The latent heat flux perturbations depend linearly on surface wind perturbations from a mean westerly wind and mixed layer temperature perturbations. The shortwave flux perturbations depend on an assumed linear relationship between surface convergence and cloudiness; the longwave perturbations respond linearly to mixed layer temperature perturbations. By further simplifying the forcing of the ocean by removing separately (a) the coupling between the winds and the thermocline depth and (b) the shortwave feedback (Cloud Radiative Feedback, CRF), *Wang and Xie* [1998] show that the wind entrainment mixing and evaporation feedback (WEEF) is sufficient to generate unstable modes with horizontal structures that are broadly consistent with the observed structure of the MJO, with largest growth rates for the longest waves. They further show that the CRF has only moderate effects on the unstable modes for WEEF and CRF strengths appropriate to the Warm Pool, although for weaker WEEF the CRF tends to favor the shortest wavelengths. Including ocean wave dynamics has little impact. The available potential energy for wave growth comes from the correlation between negative low-level geopotential and the heating associated with the SST perturbations; the selection of longer waves is controlled by the small amplitude of SST anomalies associated with the shorter waves. Subsequently, *Liu and Wang* [2013] coupled the frictional skeleton model of *Liu and Wang* [2012] to the same ocean model through a similar SST-dependent heating. They find again that westerly mean winds are critical for eastward moving unstable modes.

While *Wang and Xie* [1998] and *Liu and Wang* [2013] demonstrated the possibility of destabilizing neutral or decaying modes of an idealized atmospheric model by the introduction of air-sea coupling appropriate for the Warm Pool region, *Newman et al.* [2009] adopt a statistical approach to considering the role of air-sea coupling by constructing a linear inverse model of the tropical atmosphere-ocean system. The state vector consists of the leading empirical orthogonal functions (EOFs) of the 7 day running mean anomalies from the annual cycle of stream function, at 250, 550, and 850 hPa; velocity potential at the same levels; diabatic heating at 400, 700, and 1000 hPa; and SST. The dynamical evolution operator is constructed from 6 day lagged covariances. They examine the impact of air-sea coupling on the behavior of their linearized system by zeroing the coefficients in the dynamical evolution operator that represent atmosphere-ocean interactions. They find that evolution of the atmospheric component of the eigenmodes which capture the MJO is largely unchanged between the coupled and uncoupled evolution operators. It is worth noting that the dynamical evolution operator is constrained to be dissipative (i.e., decaying eigenmodes) and hence must represent a fundamentally different system to that in *Wang and Xie* [1998] and *Liu and Wang* [2013] in which growing modes are permitted and indeed actively sought.

The linearized models of *Wang and Xie* [1998] and *Liu and Wang* [2013] express the atmospheric response to SST anomalies through a heating which is proportional to and in phase with those anomalies. However, the nature of this heating is not clearly defined and its relationship and the justification for its form is unclear; the authors cite several possible justifications for this form, but all essentially rely on increased surface turbulent fluxes associated with increasing SST. As discussed in section 3.4.2 the intraseasonal modulation of SST may offset around 10% of the wind-driven modulation of the surface fluxes. These surface fluxes may warm the boundary layer—relative to a boundary layer without the SST anomaly—and moisten the boundary layer by SST-induced boundary layer convergence [e.g., *Hsu and Li*, 2012], but it is difficult to detect these effects in observational and modeling studies. The choice of parameters for the SST-induced heating in *Wang and Xie* [1998] and *Liu and Wang* [2013] is justified essentially by a linearization of the evaporation response to SST, neglecting the wind speed variations, which are observed to be larger and drive the SST variations in their model. Furthermore, the non-SST related part of the heating in both these models relies on an implied precipitation-moisture convergence relationship but takes no account of the wind-induced evaporation changes as a source of atmospheric water vapor.

### 4.2. Idealized Modeling of the Atmospheric Response to Intraseasonal SST Anomalies

A number of modeling studies have attempted to examine the impact of intraseasonal SST anomalies on the MJO either through imposing intraseasonal SST anomalies as a forcing or through simplified representations of air-sea coupling in aquaplanet configurations.

*Sobel and Gildor* [2003] and *Maloney and Sobel* [2007] examine the response to an idealized SST "hot spot" in both a simple zero-dimensional model (i.e., a single column with fixed vertical structure) coupled to a slab ocean and an aquaplanet GCM coupled to a slab ocean. In both experiments they find that the atmospheric response to the hot spot is to increase precipitation, with a consequent SST cooling. For some parameters in

the simple zero-dimensional atmosphere they find oscillatory responses, although not for the more complex aquaplanet configuration.

*Woolnough et al.* [2001] impose an eastward propagating SST dipole with a structure similar to observed MJO SST anomalies in an aquaplanet configuration of a then state-of-the-art GCM. The precipitation response to this forcing consists of a maximum precipitation in quadrature with the SST anomaly, consistent with the observed structure of the MJO. By varying the propagation speed of the SST anomaly, they show that for slowly propagating anomalies the precipitation response is larger than for fast-moving anomalies, but the phase remains largely unchanged until the dipole becomes stationary. They attribute the phase lag between the SST maximum and precipitation maximum to a lag associated with the moistening of the free troposphere in response to the SST anomalies and the sensitivity of the precipitation to this free tropospheric humidity. The phase speed dependence of the precipitation response would be consistent with a preferred temporal scale for propagation in a coupled system.

*Flatau et al.* [1997] and *Grabowski* [2006] examine the response to coupling in aquaplanet configurations of a GCM. *Flatau et al.* [1997] couple a relatively coarse resolution AGCM to a slab ocean, with SST tendencies given by an idealized dependence on surface winds. They find that coupling slows the preexisting eastward moving modes of the uncoupled model, which depend on the WISHE mechanism [*Emanuel*, 1987; *Neelin et al.*, 1987]. *Grabowski* [2006] performed a set of experiments in an aquaplanet configuration of a GCM using the super-parameterization framework, with a 2-D cloud-resolving model embedded in each grid box of the large-scale model. This cloud-resolving model is used to produce the tendencies of heat and moisture which would normally be provided by the GCM subgrid parameterizations (including the radiative tendencies in this example). In an uncoupled configuration, the model spontaneously produces large-scale (slowly) eastward moving convective disturbances through a moisture-convection feedback. The presence of an interactive upper ocean of reducing thermal capacity (i.e., smaller mixed layer depth) slows down this aggregation, due to a competition between the moisture feedback which tends to favor convection in already convecting areas and an SST feedback which tends to favor convection in clear (increased shortwave warming) areas. However, propagation speed is increased as mixed layer depth is reduced. In experiments with mature eastward propagating disturbances, they argue that the presence of coupling has only a small impact on their propagation, although inspection of the precipitation Hovmöller [*Grabowski*, 2006, Figure 10] and system-relative composites [*Grabowski*, 2006, Figure 14] suggests more coherent disturbances for the coupled simulations. *Grabowski* [2006] argues that sensitivity of GCM simulations of the MJO to air-sea coupling is an artifact of too-weak representation of the moisture-convection feedback in traditional parameterization approaches, although this is perhaps contradicted by *Klingaman and Woolnough* [2014b], who show larger positive impact of air-sea coupling on MJO simulation in a GCM in which this feedback has been increased through enhanced entrainment mixing in the convection scheme, compared to the impact of coupling in the standard model configuration.

These aquaplanet configurations suggest a role for the intraseasonal SST anomalies in the maintenance and propagation of the MJO; however, in many respects they suffer from the same weakness as the theoretical models of, e.g., *Wang and Xie* [1998] and *Liu and Wang* [2013] with respect to the evaporative (and sensible) fluxes. Because of the presence of mean state easterlies, the latent heat fluxes ahead of the convection are increased by both the wind anomalies and the SST anomalies; however, these wind-induced latent heat flux anomalies are inconsistent with the observed mechanism for producing the intraseasonal SST anomalies associated with the MJO. This discrepancy, and our wider lack of understanding of how atmospheric convection responds to SST perturbations, limits our understanding of the role of air-sea interaction in the MJO.

## 5. Modeling

The decade since the reviews of *Zhang* [2005], *Hendon* [2005], and *Slingo et al.* [2005] has witnessed a substantial expansion in the number and variety of GCM sensitivity experiments aiming to improve the representation of the MJO. Many of these experiments target atmospheric resolution or subgrid-scale parameterizations (section 2.3); in this section, we discuss those that focus on the role of atmosphere-ocean interactions. While coupling often has been found to improve the simulated MJO, these experiments have identified two key barriers to MJO simulation in coupled GCMs: a poor simulation of the response of the upper ocean to atmospheric forcing (section 5.1) and large systematic errors in tropical SSTs and circulation in coupled models (section 5.3). The importance of the former argues strongly against using ocean models with coarse vertical

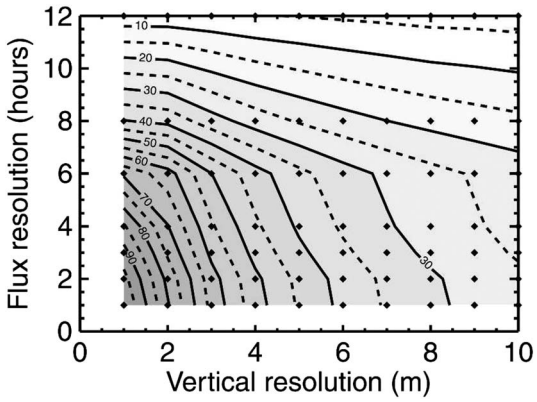


**Figure 13.** Phase diagram showing the diurnal SST variability, simulated by the one-dimensional KPP ocean model, as a function of the temporal resolution of the driving surface fluxes and the depth of the uppermost model level. Contours show the percentage of the magnitude of the diurnal variability in the control integration, which used 1 m depth and 1 h flux resolution. The contour interval is 5%, with alternating solid and dashed lines (reprinted from *Bernie et al.* [2005], copyright 2005, American Meteorological Society).

resolution for MJO studies, particularly zero-dimensional slab oceans (section 5.2). We also caution against prescribing high-frequency SST variability in atmosphere-only models, based on recent evidence of erroneous surface flux feedbacks (section 5.4). We review the impacts of air-sea coupling and SST variability on MJO prediction, a field of study that has grown considerably in the last decade as forecasting centers have explored the use of coupled GCMs for subseasonal prediction (section 5.5). Finally, we summarize this section and discuss outstanding issues for understanding and improving air-sea interactions in GCMs (section 5.6).

### 5.1. Upper Ocean Response to Atmospheric Forcing

In the past decade, one of the greatest advances in simulating the MJO in coupled GCMs (CGCMs) is the recognition of the importance of the upper ocean response to diurnal and subseasonal atmospheric forcing. This response includes variations in upper ocean stratification over the MJO cycle (section 3.3.2), as well as the diurnal variability that can rectify onto intraseasonal temporal scales (sections 3.3.3 and 3.4.3). To capture this response, CGCMs must include the diurnal cycle at the air-sea interface and have sufficient vertical resolution to represent the observed diurnal and subseasonal variations in mixed layer depth and stratification.

*Bernie et al.* [2005] and *Shinoda* [2005] demonstrated the rectification of diurnal atmosphere-ocean interactions on subseasonal temporal scales using one-dimensional (1-D) thermodynamic ocean models forced by TOGA COARE fluxes. In both studies, the authors varied the temporal resolution of the surface forcing and the vertical resolution of the ocean columns. They demonstrated that the diurnal maximum SST during the MJO suppressed phase warmed the daily mean SST and increased subseasonal variability. *Bernie et al.* [2005] concluded that a 1 m oceanic vertical resolution and 3h sampling of the surface fluxes were necessary to capture 95% of the TOGA COARE diurnal SST variability in the *K* Profile Parameterisation model (KPP; Figure 13), which translated to 90% of the subseasonal SST variability associated with the MJO cycle. Using forced simulations of a 300-level configuration of the 3-D Océan Parallélisé (OPA) OGCM with 1 m spacing in the top 100 m, *Bernie et al.* [2007] found that including the diurnal cycle of surface fluxes increased the SST response to the MJO by 20%, due to enhanced warming in the MJO suppressed phase. *Li et al.* [2013] reached similar conclusions with forced simulations of the Hybrid Coordinate Ocean Model.

CGCM experiments confirmed that the MJO could be improved by accurately representing the upper ocean response to diurnal and subseasonal atmospheric forcing. *Bernie et al.* [2008] performed the first CGCM simulations with very fine OGCM vertical resolution, conducting two experiments with HadAM3 (3.8° × 2.5°, L30) coupled to the 300-level OPA OGCM: the AGCM and OGCM were coupled by 3h means in one simulation and daily means in the other. Diurnal coupling warmed the mean tropical SST by 0.2–0.3°C, reducing the typical equatorial cold bias and weakening the Pacific double ITCZ. The MJO was stronger and more coherent with diurnal coupling, particularly near the Maritime Continent and particularly in precipitation, leading the authors to conclude that Maritime Continent biases could be reduced by strengthening thermodynamic air-sea coupling on diurnal and intraseasonal scales. Using HadAM3 coupled to many columns of the KPP 1-D ocean, *Klingaman et al.* [2011] found that MJO amplitude and propagation were improved with 1 m upper

ocean vertical resolution and 3h coupling, compared to 10 m resolution and 24h coupling. Since CGCM mean state errors can degrade the simulation of the MJO (section 5.3), we note that several other studies have also found that including the diurnal cycle of air-sea coupling reduced tropical SST and rainfall biases [e.g., *Danbasoglu et al.*, 2006; *Ham et al.*, 2010].

Most recently, *Ham et al.* [2014] examined the role of the diurnal cycle of coupling with the Global/Regional Integrated Model System (1.9° × 1.9°, L28). Although the OGCM used a 10 m near-surface vertical resolution and the AGCM and OGCM were coupled by daily means, *Ham et al.* [2014] implemented a separate mixed layer parameterization to represent wind-driven mixed layer cooling and diurnal variations in the surface energy budget, feeding the diurnal cycle of SST back to the AGCM. Comparing the diurnally resolved CGCM to the AGCM with AMIP SSTs showed that coupling reduced the AGCM overestimation of 20–100 day precipitation variability and concentrated power near the observed 50 day MJO peak. Resolving the diurnal cycle at the air-sea interface also improved the precipitation spectra, as the CGCM with daily mean coupling produced a too-strong peak around 50 days, suggesting that in this model diurnal SST variability reduces the (too-strong) magnitude of intraseasonal precipitation variability. *Seo et al.* [2014] found that subdaily coupling improved MJO prediction skill during the DYNAMO period in a tropical-channel configuration of the National Center for Atmospheric Research (NCAR) Weather Research and Forecast model (40 km) coupled to the Regional Ocean Modeling System. The authors concluded that subdaily coupling increased tropospheric moistening during the MJO suppressed phase, because the peak diurnal SST warming induced a similarly timed peak in the surface latent heat flux, which increased column moist static energy.

The evidence from observations and models for the role of diurnal forcing and ocean stratification in subseasonal SST variability, and in the atmospheric response to that variability, argues strongly for simulations of the MJO to use CGCMs capable of capturing this response. These effects may be strongest in the Maritime Continent region, where the MJO interacts strongly with the diurnal cycle of atmospheric convection [e.g., *Peatman et al.*, 2014] and where shallow seas can lead to intense diurnal SST variability. There are recent indications that some high-resolution models can capture these effects to a limited extent [e.g., *Peatman et al.*, 2015]. However, most contemporary CGCMs used to study the MJO—including many of those discussed in the following sections—still employ a ~10 m upper ocean vertical resolution and couple via daily means of SSTs and surface fluxes. Subseasonal SST variability should be strongly damped in these CGCMs relative to observations, which suggests that they underestimate the effects of air-sea interactions on the MJO. If subseasonal SST variability is not damped, but instead is similar to or greater than observations, it is likely that these models suffer from either excessive subseasonal surface flux variability or a too-strong sensitivity of SST to surface forcing, producing subseasonal SST variability by the wrong physical mechanisms.

### 5.2. Slab Ocean Models

Similar arguments can be made against the use of CGCMs with a one-layer, thermodynamic "slab" ocean. These models usually have a constant ocean mixing depth in space and time—some experiments use spatially varying but temporally fixed mixing depths [e.g., *Benedict and Randall*, 2011]—that is several tens of meters thick. They also neglect the diurnal cycle of air-sea interactions. CGCMs with slab oceans were common research tools until approximately 10 years ago, when increased computational resources and more mature 3-D OGCMs enabled a gradual transition to CGCMs with 3-D oceans, but slab ocean CGCMs are still occasionally used for MJO studies. Since previous reviews of the MJO [e.g., *Zhang*, 2005] have not discussed in detail the effects of air-sea interactions on the representation of the MJO in CGCMs, including CGCMs with slab oceans, we describe briefly the results of these historical experiments for completeness and to argue against the further use of slab ocean CGCMs to study the MJO.

*Waliser et al.* [1999] compared the Goddard Laboratory (4°× 5°, L17) in slab-coupled and AGCM configurations. *Waliser et al.* [1999] applied an SST restoring term—relaxing to zero anomaly with a 50 day time scale—to account for the lack of oceanic heat transport. Such relaxations artificially damp variability on temporal scales longer than the relaxation scale, which is often close to the MJO period in slab ocean experiments. The Goddard AGCM demonstrated poor intraseasonal variability and little propagation; coupling to the slab ocean improved eastward propagation while also concentrating the spectral power at frequencies near the observed 55 day and 25 day peaks.

Using the Commonwealth Scientific and Industrial Research Organisation (CSIRO) Mk2 GCM (5.6° × 3.2°, L9), *Watterson* [2002] varied the slab ocean depth between 10 m and 50 m. All coupled simulations displayed improved MJO amplitudes and propagation compared to the AGCM. Shallower slab depths produced

stronger SST anomalies due to reduced thermal inertia, which enhanced the low-level MJO circulation anomalies. As the author noted, the slab depth can be used to tune MJO amplitude and propagation, by varying the SST sensitivity to surface fluxes to artificially compensate for biases in the subseasonal variability of those fluxes. The results of slab ocean experiments often depend strongly, and unphysically, on the subjective choice of the slab depth.

This effect was confirmed by *Maloney and Sobel* [2004], which varied slab depths in the National Center for Atmospheric Research (NCAR) Community Atmospheric Model 2.0.1 (CAM2) (2.8° × 2.8°, L26) between 2 m and 50 m. While the 2 m experiment generated the strongest SST variability, the very fast SST response resulted in SST anomalies that opposed the wind-driven evaporative anomalies and hence reduced latent heat flux anomalies. This strongly degraded MJO amplitudes and intraseasonal precipitation variability in general, demonstrating the importance of WISHE for CAM2, in line with results from the *Sobel and Gildor* [2003] idealized model.

*Marshall et al.* [2008] coupled the Bureau of Meteorology AGCM (2.5° × 2.5°, L17) to a 30 m slab with a 60 day SST restoring time scale. Coupling quickened the too-slow MJO propagation in the AGCM and produced warm SSTs east of the active phase that increased local evaporation relative to the AGCM, leading the authors to suggest that coupling promoted propagation by reducing atmospheric stability. However, the larger thermal inertia of the 30 m slab relative to the much shallower mixed layers observed during the MJO suppressed phase (section 3.3.2) may have led the authors to underestimate the magnitude of the warm SST anomalies and associated increased evaporation.

*Benedict and Randall* [2011] found that air-sea feedbacks improved the SST-rainfall phase relationship and MJO propagation in the Super-Parameterized CAM3 (SPCAM3; 2.8° × 2.8°, L26) coupled to a slab ocean. East of the active phase, the CGCM produced stronger moisture convergence and enhanced moist static energy, highlighting the roles of frictional convergence [e.g., *Wang*, 1988b] and shallow and congestus heating during the MJO transition phase. Regressions of net surface fluxes on SSTs showed excessive sensitivity of the slab ocean SSTs relative to observations, however, which may have led *Benedict and Randall* [2011] to overestimate the effects of coupling feedbacks, particularly in regions with shallow mixed layers.

The deficiencies inherent in the design of slab ocean CGCM experiments, along with the observational (section 3.3.2) and modeling (section 5.1) evidence for the role of variability in upper ocean stratification on SSTs throughout the MJO cycle, cautions strongly against using slab ocean CGCMs for MJO experiments. We return to this point in section 6.

### 5.3. The Coupled Model Mean State

To capture the MJO, CGCMs must represent accurately not only the diurnal and subseasonal variability in atmosphere-ocean coupled system but also the mean climate about which those variations occur. *Zhang* [2005] briefly reviewed several studies that suggested that the CGCM mean state was crucial for MJO fidelity, but the author concluded that "the exact role of the mean background state has yet to be quantified." Here we consider studies performed since *Zhang* [2005] that have demonstrated that CGCM mean state errors degrade the simulation of the MJO; motivated by those findings, we also examine in greater detail the studies included in *Zhang* [2005] to support our recommendation that future MJO studies be performed in CGCMs with realistic mean climates (section 6.2).

*Kemball-Cook et al.* [2002] compared the Hamburg AGCM (ECHAM4; 3.8° × 3.8°, L19), forced by monthly mean SSTs, to a simulation in which ECHAM4 was coupled to a $2\frac{1}{2}$ layer ocean model. While the AGCM displayed a "seesaw"-like intraseasonal oscillation between the Indian Ocean and the West Pacific (i.e., opposite-signed anomalies in the two basins that occasionally reversed polarity with no evidence of eastward propagation), the CGCM produced smooth eastward propagation through the Maritime Continent that the authors attributed to enhanced low-level moisture convergence. Imposing the climatological CGCM SSTs in the AGCM produced the same disconnected seesaw oscillation, suggesting that the CGCM propagation arose from air-sea feedbacks, not the CGCM mean climate. However, *Liess et al.* [2004] found that coupling degraded the MJO in ECHAM4 (2.8° × 2.8°, L19) coupled to the Ocean model in isopycnic coordinates 3 (OPYC3) OGCM. The CGCM produced faster propagation than the AGCM with observed SSTs, worsening the AGCM bias. Prescribing climatological CGCM SSTs to the AGCM improved MJO amplitude and propagation relative to the CGCM. The authors attributed the discrepancy with *Kemball-Cook et al.* [2002] to differences in the CGCM mean state

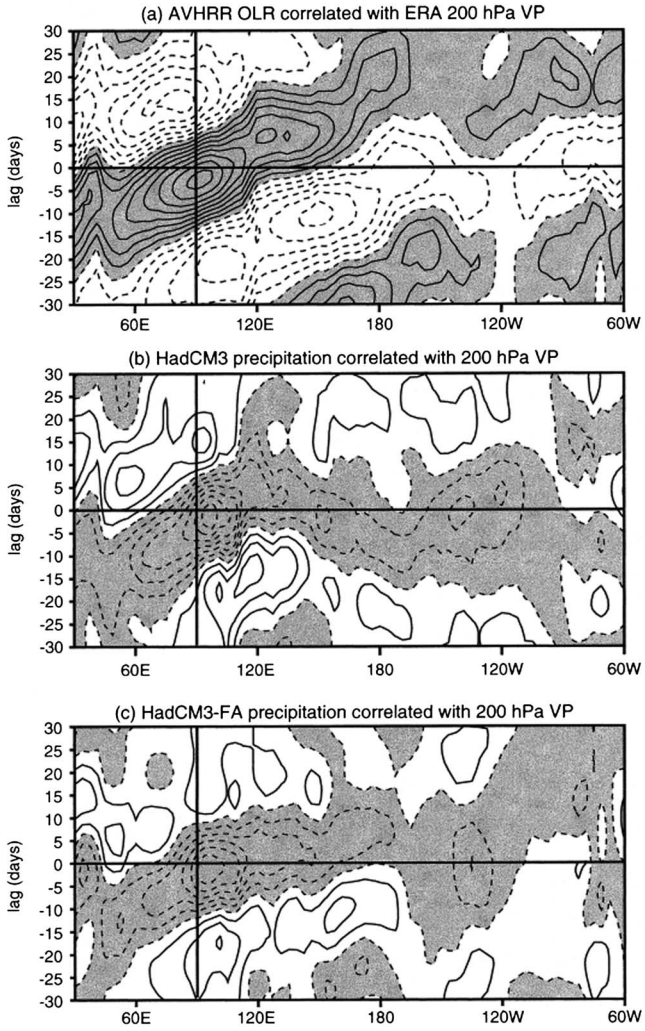


**Figure 14.** Lag correlation plots of OLR or convective precipitation averaged between 10°N and 10°S with 200hPa velocity potential (VP) at 90°E, also averaged between 10°N and 10°S: (a) NOAA advanced very high resolution radiometer (AVHRR) OLR correlated with ECMWF reanalysis VP, (b) HadCM3 control simulation precipitation and VP, and (c) HadCM3 flux-adjusted simulation precipitation and VP. Shading indicates negative correlations between precipitation and VP. Contour interval is 0.1. All data are 20–100day bandpass filtered (reprinted from *Inness et al.* [2003, Figure 7], copyright 2003, American Meteorological Society).

caused by the different ocean model: *Kemball-Cook et al.* [2002] found strong cold SST biases near the Maritime Continent, but in *Liess et al.* [2004] the cold SST error reached a maximum in the central Pacific. *Liess and Bengtsson* [2004] showed that MJO propagation through the Maritime Continent in ECHAM4 was highly sensitive to the local SST specification, with much stronger propagation when the AGCM was forced by the *Reynolds and Smith* [1994] SST analysis instead of the standard AMIP data set. Propagation also improved when weekly mean observed SSTs were used instead of monthly means; we return to this topic in section 5.4.

Similarly, *Inness and Slingo* [2003] and *Inness et al.* [2003] demonstrated that CGCM mean state biases could influence the effect of coupling on the MJO in the Hadley Centre model (HadCM3; 3.8° × 2.5°, L30). *Inness and Slingo* [2003] showed that air-sea feedbacks modestly improved the MJO: HadCM3 produced propagation from the Indian Ocean to the Maritime Continent (Figure 14b), whereas the AGCM (HadAM3) displayed a seesaw oscillation similar to ECHAM4 in *Kemball-Cook et al.* [2002]. In *Inness et al.* [2003], a flux-corrected HadCM3 simulation removed the 1–4°C Warm Pool cold SST errors and changed the mean near-equatorial zonal winds from easterly to westerly, in agreement with observations. This simulation showed strong MJO propagation through the Maritime Continent (Figure 14c), demonstrating that mean state biases in the standard HadCM3 caused the lack of propagation and consequent low MJO variability in the Pacific. A third

CGCM simulation, involving HadAM3 coupled to the Océan Parallélisé (OPA) OGCM without flux corrections, produced warmer tropical mean SSTs than the standard HadCM3 but still showed weak MJO propagation through the Maritime Continent. *Inness et al.* [2003] hypothesized that the poor propagation was due to the presence of equatorial mean easterlies, despite the warmer SSTs, and conjectured that the improved MJO in the flux-corrected HadCM3 was due to the improved equatorial zonal winds correcting the surface flux-convection phasing. *Seo et al.* [2007] also found that a flux-corrected CGCM, the National Centers for Environmental Prediction Coupled Forecasting System (CFS; 1.9° × 1.9°, L64), produced improved propagation due to warmer mean SSTs, low-level equatorial westerlies rather than easterlies, and stronger vertical wind shear, relative to the uncorrected CGCM and the AGCM with AMIP SSTs.

*Sperber* [2004] concluded that several mean state errors in the NCAR Community Climate System Model (CCSM2; 2.8° × 2.8°, L26) severely limited MJO propagation: a substantial equatorial Pacific cold SST bias, a preference for off-equatorial convection that produced a double Intertropical Convergence Zone (ITCZ), and erroneous mean easterlies in the eastern Indian Ocean and West Pacific. CCSM2 generated some eastward propagation in the Indian Ocean, an improvement over the westward propagation in the AGCM, and similar to HadCM3 in *Inness and Slingo* [2003]. Experiments with CSIRO Mk3 (1.9° × 1.9°, L18) also showed that MJO propagation in the CGCM was limited by the spatial extent of mean equatorial westerlies [*Watterson and Syktus*, 2007]; propagation was stronger in El Niño years when the westerlies extended further into the Pacific. The Mk3 AGCM produced only a standing intraseasonal oscillation, while the MJO was considerably improved in a slab ocean configuration with flux corrections that maintained the observed mean SST. *Wang and Seo* [2009] found that air-sea feedbacks improved the coupling between anomalous convection and circulation in the CFS (1.9° × 1.9°, L64), relative to the AGCM, which produced strong MJO events but which too quickly moved convection from the Indian Ocean to the Pacific. However, the CFS showed poor eastward propagation in the Pacific, which the authors concluded was due to very weak mean westerlies there that produced an incorrect SST-surface flux phasing and increased easterly vertical shear.

The model comparisons of *Sperber et al.* [2005] and *Zhang et al.* [2006] confirmed that mean state fidelity in CGCMs strongly influenced both the overall representation of the MJO and the impact of air-sea feedbacks. *Sperber et al.* [2005] analyzed the boreal winter MJO in long simulations of ECHAM4 coupled to three OGCMs: OPYC (2.8° × 2.8°, L19), as in *Liess et al.* [2004]; the Hamburg Ocean Primitive Equation model (3.8° × 3.8°, L19); and OPA (3.8° × 3.8°, L19). The former two employed flux corrections and produced much more realistic eastward propagation than either the OPA-coupled CGCM or the ECHAM4 AGCM, which the authors attributed to the more realistic basic state, particularly the mean SST, low-level winds, and moisture convergence, and the phasing between subseasonal anomalies of those variables and MJO convection. The OPA-coupled CGCM produced strong cold tropical SST biases that reduced convective organization and inhibited moisture convergence east of the MJO active phase. Only in the OPYC-coupled simulation did the enhanced latent heat flux anomalies, located west of the MJO active phase, travel east with the propagating convection, as in observations. *Sperber et al.* [2005] argued that this was due to the higher atmospheric horizontal resolution rather than air-sea coupling or the OGCM employed. The OPYC-coupled results conflicted with *Liess et al.* [2004], which found little effect of coupling in the same model; *Sperber et al.* [2005] suggested that this was due to applying different MJO indices or a focus on boreal winter (*Liess et al.* [2004] analyzed all seasons).

*Zhang et al.* [2006] compared four CGCMs—the Bureau of Meteorology CGCM (2.5° × 2.5°, L17), the CFS (1.9° × 1.9°, L64), the CCSM2 (2.8° × 2.8°, L26), and the ECHAM4-OPYC model from *Sperber et al.* [2005]—to their AGCM counterparts. While all AGCMs and CGCMs produced a spectral peak in the 30–90 day MJO band in 850 hPa zonal wind, air-sea feedbacks improved subseasonal, eastward propagating power in rainfall in all models. *Zhang et al.* [2006] found a lack of convection-circulation coupling in all models, particularly the AGCMs, which the authors attributed to mean state errors associated with a double Pacific ITCZ. There were substantial inter-GCM inconsistencies in the effects of coupling on other aspects of the MJO, including horizontal and vertical structure, the seasonal cycle of MJO activity, and the spatial distribution of intraseasonal variability, which *Zhang et al.* [2006] hypothesized were due to inter-GCM variability in the magnitudes and spatial patterns of mean state biases.

Recently, *Klingaman and Woolnough* [2014b] showed that CGCM mean state errors could substantially impact the "perceived effects" of subseasonal air-sea interactions. In that study, the Met Office Unified Model (MetUM; 1.9° × 1.3°, L85) was coupled to many columns of the KPP 1-D ocean within the Indo-Pacific Warm Pool.

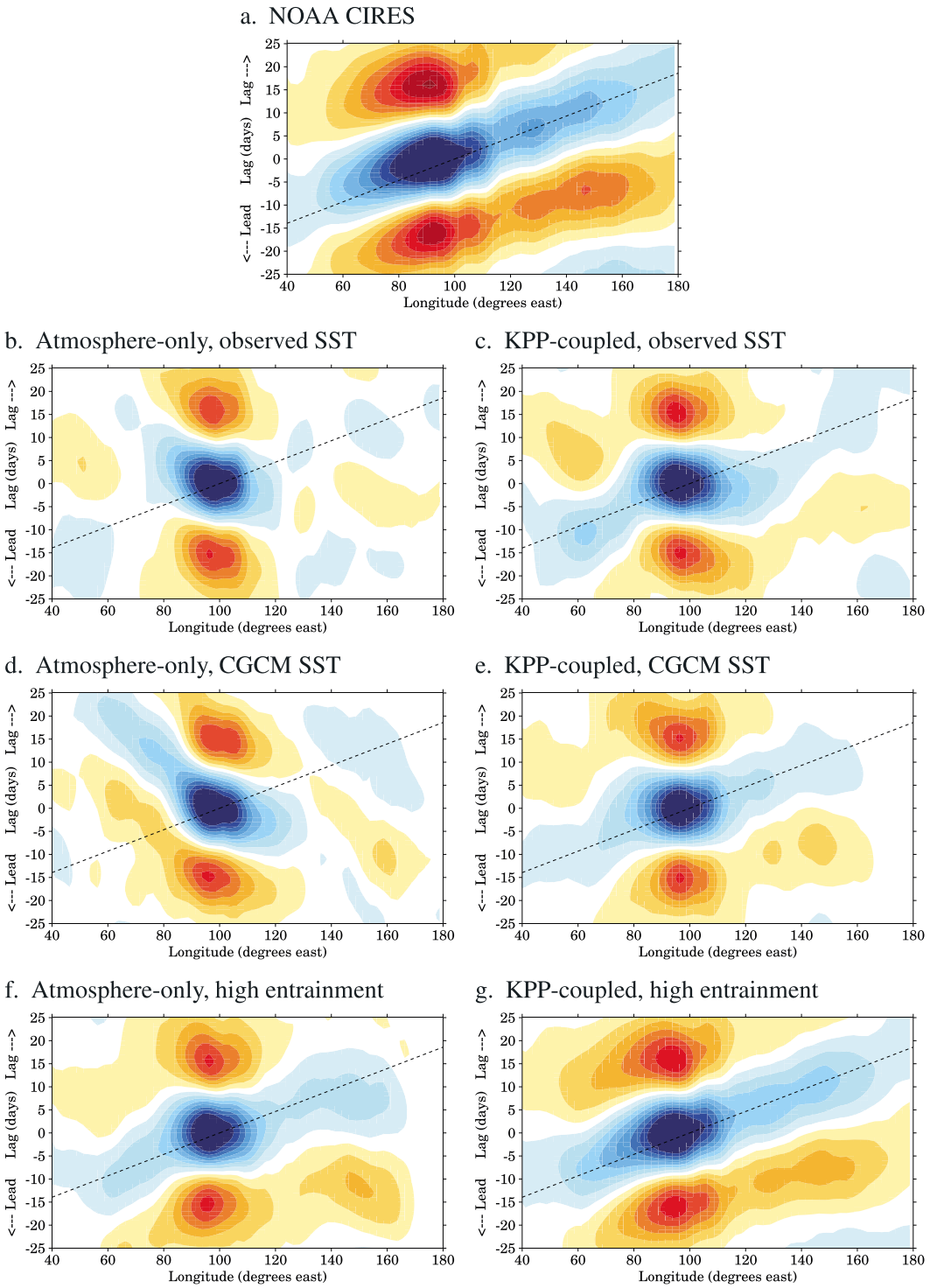


**Figure 15.** Lag regressions of 10°S–10°N averaged, 20–100 day bandpass-filtered OLR against the same at 100°E for (a) NOAA OLR (1989–2008) and (in Figures 15b–15g) 20 year simulations of MetUM GA3.0 (b) AGCM with climatological observed SSTs, (c) coupled to the KPP 1-D ocean model and constrained to observed climatological SSTs, (d) AGCM with climatological SSTs from the MetUM CGCM with the NEMO dynamical OGCM, (e) coupled to KPP and constrained to the MetUM CGCM SST, and (f, g) as in Figures 15b and 15c but with a 50% increase to the convective entrainment and detrainment rates. Adapted from *Klingaman and Woolnough* [2014b, Figures 4 and 9].

In one simulation, flux corrections were employed to maintain the observed mean ocean state; in another, they were used to maintain the mean ocean state from the MetUM CGCM (i.e., coupled to a 3-D OGCM). Outside the KPP-coupled region, the climatological annual cycle of SSTs from either observations or the MetUM CGCM were prescribed. Corresponding AGCM simulations were conducted using the same prescribed SSTs. The MetUM AGCM with observed SSTs (Figure 15a) and the MetUM CGCM (not shown) had similarly poor MJO activity. By comparing the AGCM and KPP-coupled experiments, *Klingaman and Woolnough* [2014b] showed that air-sea coupling under both the observed (Figures 15b and 15c) and CGCM mean states (Figures 15d and 15e) produced modest improvements in MJO amplitude and propagation. Comparing the two KPP-coupled experiments demonstrated that in the CGCM, the improvements from coupling were offset by degradations from mean state biases.

CGCM mean state errors—particularly tropical cold SST and easterly low-level wind biases—have been consistently shown to diminish simulated MJO amplitude and propagation. Yet often, studies have quantified the impact of air-sea coupling by driving the AGCM with CGCM SSTs [e.g., *Liess et al.*, 2004; *Rajendran and Kitoh*, 2006; *DeMott et al.*, 2014], using either temporally smoothed daily SSTs (e.g., 5 day means, monthly means) or a repeating climatological annual cycle. The former likely provides a cleaner comparison than the latter, because it ensures that the AGCM and CGCM have the same interannual SST variability. While these experiment designs impose a similar mean state in the AGCM as in the CGCM, that mean state is biased by the same CGCM systematic errors that often degrade the representation of the MJO. Therefore, this type of experiment design is a poor approximation of the impact of air-sea interactions in the real-world MJO, especially given that many CGCMs fail to capture the upper ocean response to diurnal and subseasonal atmospheric forcing (section 5.1). We recommend performing future investigations of air-sea interactions in the MJO in a CGCM in which the ocean mean state can be held close to observations (section 6.2).

### 5.4. High-Frequency SST Forcing

Separate from the issues surrounding prescribing CGCM SSTs with mean state biases in an AGCM, recent studies have provided evidence against forcing an atmosphere-only model, whether a global or regional model, with "high-frequency" (i.e., submonthly, usually pentad or daily means) SSTs, either from a CGCM or observations. At first glance, prescribing high-frequency CGCM SSTs may appear more desirable than prescribing monthly means or prescribing observed high-frequency SSTs, because it minimizes differences in subseasonal SST variability between the CGCM and the atmosphere-only model. However, using high-frequency SSTs may degrade atmospheric model SST-precipitation and SST-surface flux relationships and spuriously increase subseasonal convective variability, as we discuss below. These drawbacks make this approach unsuitable for studying the MJO, in which the phasing between convection, surface fluxes, and SSTs is critically important. For clarity, we first discuss experiments that have examined the effects of prescribing high-frequency observed SSTs before discussing studies using high-frequency CGCM SSTs.

In experiments to identify controls on MJO propagation through the Maritime Continent in ECHAM4 ($2.8° \times 2.8°$, L19), *Liess et al.* [2004] compared AGCM simulations with weekly and monthly SST forcing from the ECMWF 15 year reanalysis (ERA-15), derived from *Reynolds and Smith* [1994]. Using weekly mean SSTs lengthened the MJO period from ~40 to ~50 days, in closer agreement with observations. Using large ensembles of HadAM3 simulations ($1.3° \times 0.8°$, L30) driven by daily, pentad, or monthly mean satellite-derived SSTs, *Klingaman et al.* [2008] concluded that high-frequency SST forcing greatly improved the magnitude of tropical intraseasonal variability, as well as its northward propagation in boreal summer; eastward propagation was only modestly affected. *DeMott et al.* [2014] found that specifying pentad mean instead of monthly mean CGCM SSTs slightly enhanced eastward propagation in SPCAM3, CAM3, and CAM4. Several prediction studies also have shown that prescribing high-frequency SSTs improved MJO forecast skill, relative to weekly, monthly, or persisted SSTs; we discuss these in section 5.5.

However, all of the studies above noted that the AGCMs produced incorrect, coincident SST-rainfall phase relationships, regardless of SST forcing frequency. In observations and CGCMs, SSTs and rainfall have a near-quadrature phase relationship with a 6–10 day lag (Figure 5). This suggests that the improved MJO in AGCMs with high-frequency SST forcing arises from incorrect temporal relationships between the prescribed SSTs, surface flux anomalies, and convection.

*Zheng et al.* [2004] was among the first to analyze the MJO in an AGCM with daily CGCM SSTs, employing a version of the Geophysical Fluid Dynamics Laboratory AGCM ($2.8° \times 2.8°$, L18) that had been shown to produce substantial intraseasonal variability [*Waliser et al.*, 2003]. The CGCM was coupled every 2h. Both the CGCM

and AGCM produced stronger intraseasonal precipitation variability than observed, by ~30%, with propagation similar to observations. The AGCM also exhibited the typical coincident SST-rainfall phase relationship; the CGCM reproduced the observed near-quadrature relationship. In terms of the MJO, however, the two simulations were highly similar, suggesting that coupling had little impact.

On the other hand, *Pegion and Kirtman* [2008b] concluded that coupling enhanced the organization and eastward propagation of convection in the CFS CGCM (1.9° × 1.9°, L64), relative to the AGCM with daily CGCM SSTs. Although the AGCM and CGCM both overestimated Warm Pool intraseasonal precipitation variability, the CGCM reduced this overestimation considerably. Indeed, *Pegion and Kirtman* [2008b] emphasized that the AGCM, when provided with "realistic" daily SST variability, produced excessive SST-forced precipitation variability across the tropics, with a coincident SST-rainfall relationship and weak SST-surface flux correlations. The CGCM reproduced the observed SST/rainfall/surface flux phasings, which the authors hypothesized were responsible for the improved MJO propagation. However, the observed MJO amplitude and propagation were best represented by the AGCM with a prescribed repeating climatological annual cycle of CGCM SSTs, which was attributed to reduced mean tropical circulation biases. While internal atmospheric dynamics clearly drove the MJO in the CFS, air-sea coupling reduced erroneously strong SST-forced precipitation and maintained observed phase relationships between SSTs, rainfall, and surface fluxes. Similar results have been found for extratropical variability [e.g., *Barsugli and Battisti*, 1998].

The degraded SST/surface flux/precipitation phase relationships and the artificially strong SST-forced precipitation variability make global or regional atmosphere-only models with prescribed high-frequency SST variability poor tools for studying the MJO. Additionally, as in all atmosphere-only model experiments, the ocean is assumed to have an effectively infinite heat capacity, such that the negative feedback between turbulent fluxes and SSTs is missing. Atmosphere-only models with observed high-frequency SSTs should not be used as a substitute for CGCMs that are able to capture the observed level of subseasonal upper ocean variability in response to atmospheric forcing.

### 5.5. Air-Sea Interaction and MJO Prediction

A number of studies have examined the role of air-sea interaction in the context of MJO prediction. These studies serve two purposes. First, the MJO is the largest mode of subseasonal variability in the tropics and offers a significant source of predictability on these temporal scales, both in the tropics and extratropics, and so these studies can inform the design of operational prediction systems. Secondly, investigating the role of air-sea interaction in the MJO as a process study within a prediction framework offers a number of benefits over more traditional coupled-versus-uncoupled climate-model simulations.

The use of a forecasting framework means that the state of the model system is close to the observed system, which allows the following: a clear separation between the role of air-sea coupling and the differences in basic state between coupled and uncoupled climate models; investigation of the role of coupling in a less biased basic state, which is important given the relationship between the intraseasonal flux anomalies and the basic state; and an assessment of the role of air-sea interaction in the maintenance and propagation of the MJO in different phases without a reliance on the ability of the GCM to generate an MJO through its own internal variability. Furthermore, a prediction framework allows a direct comparison against observations through measures of forecast skill rather than comparison of statistical measures of MJO behavior.

These simulations studies fall into two broad categories: comparisons of AGCM hindcasts with differing temporal resolution of time-evolving observed SST boundary conditions and comparisons of CGCM hindcasts with a parallel set of AGCM hindcasts.

The first of these suffer from the same weaknesses as their "climate" simulation counterparts in relation to the inconsistency between the surface fluxes and the evolution of the SST (section 5.4). However, this inconsistency is perhaps slightly ameliorated by the fact that while the atmosphere remains close to the observed state (i.e., the hindcast has skill), there should be some agreement between the modeled surface fluxes and the surface fluxes that drove the SST variability. Furthermore, these configurations do not compare potential operational configurations and hence provide no information on the design of operational systems. Despite these weaknesses in the experimental design, for completeness, we will discuss these briefly below.

*Kim et al.* [2008] and *de Boisséson et al.* [2012] examine the influence of intraseasonal SST anomalies on hindcast skill in versions of the Seoul National University (SNU) and the ECMWF AGCMs, respectively. They force the AGCM with prescribed SSTs taken from observations at daily, weekly, and monthly resolution.

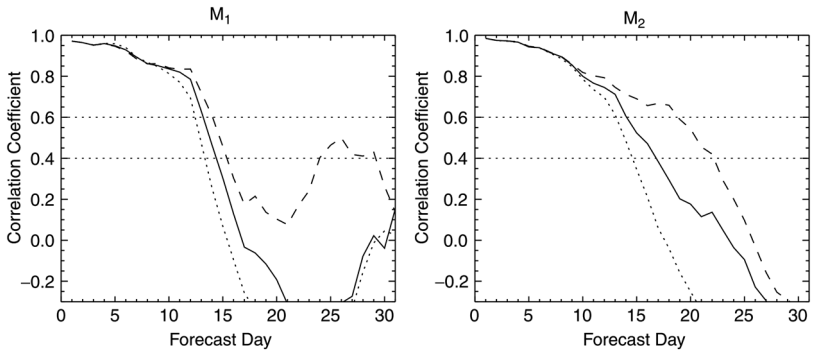


**Figure 16.** Correlation of the observed $M_1$ and $M_2$ time series with the ensemble mean forecast time series, based on 47 start dates, for the control experiment CONT (solid line), the mixed layer experiment ML (dashed line), and the persisted SST experiment PERS (dotted line). $M_1$ and $M_2$ are essentially equivalent to *Wheeler and Hendon* [2004] RMM1 and RMM2, but replace 200 hPa zonal wind with 200 hPa velocity potential. The horizontal dotted lines highlight threshold correlation values of 0.6 and 0.4 (reprinted from *Woolnough et al.* [2007, Figure 5], copyright 2007, with permission from Royal Meteorological Society).

In *Kim et al.* [2008], they consider hindcasts initialized at 5 day intervals for eight winter seasons, while *de Boisséson et al.* [2012] consider hindcasts initialized each day for 48 consecutive days during the TOGA COARE Intensive Observing Period (IOP). Both studies find improved hindcast skill with high-frequency SST forcing compared to monthly varying SSTs, in particular at extended lead times (>10 days), although the skill of the SNU-AGCM is low compared to the operational forecast model of ECMWF and the sensitivity to temporal resolution of the SST is smaller. *Kim et al.* [2008] find a degradation of the phase relationship between SST and convection, with a shortened lag between SST maximum and convection maximum for lead times >4 days, consistent with climate simulations with prescribed daily SSTs. However, in an extended set of hindcasts over 21 winters, *de Boisséson et al.* [2012] notice this change in phase at short lead times (week 1), but it is less apparent at longer lead times (weeks 2 and 3), perhaps related to the higher inherent skill of the ECMWF model. *de Boisséson et al.* [2012] go on to compare these daily forced SST experiments with fully coupled simulations over this extended period. They find similar skill for the coupled simulations and daily forced simulations out to day 20, with enhanced skill at lead times greater than 20 days for the coupled simulations.

*Woolnough et al.* [2007], *Vitart et al.* [2007], *Seo et al.* [2009], *Kim et al.* [2010], *Fu et al.* [2013], and *Shelly et al.* [2014] compare hindcasts with CGCMs to those with AGCMs. These studies differ in their experimental design. *Kim et al.* [2010] consider hindcasts over a multiyear period and compare to simulations with pentad mean forecasted SST from the coupled integration. This approach allows for a direct assessment of the role of air-sea interaction independent of the role of intraseasonal SST variability but, again, does not compare practical operational approaches. The other studies use much shorter hindcast data sets often centered around major field campaigns [*Woolnough et al.*, 2007; *Vitart et al.*, 2007; *Fu et al.*, 2013] but compare to possible operational configurations of an atmosphere-only forecasting system with persisted SSTs from the initial conditions.

*Woolnough et al.* [2007] and *Vitart et al.* [2007] examine the role of air-sea interaction in MJO prediction for 48 hindcasts initialized during the TOGA COARE IOP in the ECMWF model. In *Woolnough et al.* [2007] they compare forecasts with (a) an AGCM with persisted SSTs, (b) a CGCM with a full dynamical ocean, and (c) the same AGCM with tropics-wide coupling to a 1-D mixed layer model. They show that although the skill is similar between all configurations until about day 10, the models then start to diverge (Figure 16). Coupling to the full dynamical ocean provides about 1 day of additional skill over the uncoupled configuration, while coupling to the mixed layer model increases this by an extra day for active and suppressed MJO phases over the Maritime Continent, but an additional 7 days skill for phases of the MJO associated with active convection over the Indian Ocean or West Pacific. In further sensitivity experiments, they demonstrate that this improved skill can be attributed to the higher vertical resolution near the surface in the mixed layer model, allowing an improved representation of the diurnal cycle of SST during the suppressed phase of the MJO (cf. section 5.1). *Vitart et al.* [2007] examine the sensitivity of the improved skill with the mixed layer model to changes in the atmospheric physics which improve MJO prediction in the operational forecast configuration with a fully dynamical ocean. They find that the coupling to the mixed layer ocean improves the simulation over the operational configuration, i.e., that the impact of the coupling and the improved physics is additive to a lead

time of at least 18 days. Beyond this the additive nature of the impact is sensitive to the physics change, but the mixed layer model continues to outperform the fully dynamical ocean.

*Seo et al.* [2009] compare the National Centers for Environmental Prediction (NCEP) coupled Climate Forecast System (CFS) to an AGCM configuration of the same model at the same resolution for the period January 2005 to February 2006. They find improved skill of 2–4 days for winter MJO in the CGCM compared to the AGCM, with the largest improvements for the phases associated with active convection over the Indian Ocean and West Pacific. For these phases the skill at extended lead times exceeds that of the high-resolution operational configuration of the AGCM. For the phase associated with convection over the Maritime Continent, the high-resolution configuration has higher skill at all lead times. *Fu et al.* [2013] compare a later version of the NCEP system (CFSv2) to the operational AGCM forecasts during the CINDY/DYNAMO field campaign. They find a similar improvement in skill for the coupled configuration. To further examine the role of air-sea interaction, they perform a number of hindcasts during the CINDY/DYNAMO period in a version of the ECHAM AGCM coupled to an intermediate complexity upper ocean model and in the AGCM with a variety of prescribed SSTs including persisted SSTs and forecast SSTs from the CGCM. They find similar skill for the fully coupled forecasts and those with SSTs from the CGCM, with reduced skill in the persisted SST experiments. In a subsequent study with their intermediate complexity upper ocean model framework *Fu et al.* [2015] found that the sensitivity to coupling was event dependent, with a greater (lesser) sensitivity to ocean coupling for the November (October) case.

*Shelly et al.* [2014] compare coupled and uncoupled forecasts in the Met Office Unified Model for a 3 month period during the Year of Tropical Convection including two MJO events (E and F of *Waliser et al.* [2012]). Similar to other studies they find improved skill of 3–5 days for the phases of the MJO with active convection over the Indian Ocean and West Pacific, with more marginal improvement for the active phase over the Maritime Continent. This improvement in skill largely comes from improved prediction of the convective signal and low-level winds. They also show some skill in prediction of the Indian Ocean downwelling Kelvin wave associated with the westerly wind burst of the first of these MJO events and a number of downwelling Rossby waves and their associated SST, which *Webber et al.* [2012] argue may be important for triggering MJO events (cf. section 3.3.4).

*Kim et al.* [2010] compare hindcasts with a coupled version of the SNU-AGCM with its atmosphere-only counterpart over 26 winter seasons. In contrast to the above, they use pentad mean SSTs from the coupled forecasts to isolate the role of coupling from intraseasonal SST variability. They find again that coupling improves the MJO prediction skill by about 1 day compared to the AGCM, with particular improvements for phases where the MJO is active over the Indian Ocean and West Pacific. They also show that coupling leads to an improvement in the phase relationship between SST and convection compared to the AGCM.

*Pegion and Kirtman* [2008a] examine the role of air-sea coupling in a perfect-model scenario using the NCEP CFS. They select ten strong MJO events from a coupled control simulation of the model and then perform coupled and uncoupled "forecasts" of these events. The initialization time is chosen such that the MJO is active in the Indian Ocean. The atmospheric initial conditions come from perturbing the state of the control simulation using states from nine times at hourly intervals either side of the initial time. In the coupled forecasts the initial ocean state is taken from the ocean state at the initial time of the control integration (i.e., perfect ocean initial state) but develops freely due to the perturbed atmospheric conditions. The uncoupled simulations use a range of prescribed SSTs: the daily SSTs from the control integration (i.e., "observed" SSTs); SSTs from each of the coupled forecasts but randomized so the atmosphere and ocean are mismatched; persisted initial SST anomalies; monthly "observed" SSTs; and climatological SSTs. They find that for dynamical variables the coupled SST experiments and those forced with either of the daily varying SST data sets produce largely similar skill; however, these tend to separate from the persisted or monthly varying SST experiments after about 10 days. The climatological SST experiments lose skill very quickly. For precipitation the coupled forecasts diverge from the daily varying prescribed SST simulations.

### 5.6. Summary and Outstanding Questions

Many studies, using models of varying resolution and complexity, have demonstrated that including air-sea feedbacks improves some combination of the amplitude, period, and propagation of the MJO. These improvements hold for both free-running climate simulations and initialized hindcasts. Coupling is often more beneficial for MJO phases with active convection over the Indian Ocean or West Pacific than for phases with active convection over the Maritime Continent. However, a minority of investigations have concluded that

coupling either degrades or does not affect the representation of the MJO in coupled climate simulations [e.g., *Hendon*, 2000; *Liess et al.*, 2004; *Zheng et al.*, 2004; *Sperber et al.*, 2005; *Pegion and Kirtman*, 2008b]. Where air-sea feedbacks have enhanced the MJO, authors have commonly attributed the improvements to more realistic phase relationships between SSTs, rainfall, and surface fluxes and associated stronger low-level moisture convergence leading the MJO active convection. Beyond this "first-order" effect of coupling, studies have shown that increasing subseasonal SST variability in CGCMs, by resolving the diurnal cycle at the air-sea interface and refining upper ocean vertical resolution, can help to maintain and propagate the simulated MJO [e.g., *Bernie et al.*, 2008; *Tseng et al.*, 2015]. These processes are most important in the MJO suppressed phase [e.g., *Woolnough et al.*, 2007]. The broad range of atmospheric horizontal and vertical resolutions employed in climate-model studies demonstrates that in models with parameterized convection, atmospheric resolution does not systematically affect the role of air-sea coupling on the MJO or indeed overall MJO fidelity.

Despite the wealth of studies conducted, three key questions on the role of air-sea interactions are still unanswered. First and foremost, the mechanisms by which the atmosphere responds to SST variability remain unclear. Recently, *DeMott et al.* [2014] analyzed CGCM and AGCM experiments of SPCAM, with the AGCM driven by the monthly mean CGCM SSTs. The CGCM produced a stronger MJO with more coherent propagation, which the authors hypothesized was due to air-sea interactions strengthening convection and the associated zonal overturning circulation in the Warm Pool. The enhanced circulation then increased horizontal moisture advection downstream, encouraging MJO propagation. While *DeMott et al.* [2014] and many other studies have put forward a variety of potential mechanisms for how the atmospheric MJO responds to SST variability, these mechanisms are largely untested and often based on the results of experiments with a single GCM with a biased representation of the MJO. Further, improvements to the representation of the MJO in GCMs—whether from air-sea coupling or otherwise—often enhance many processes that are central to MJO theories, particularly since most involve positive feedbacks. This makes it easy to identify one or several mechanisms for the improved MJO but difficult to interpret which of them is critical. The wide variety of experiment designs and the strong links between GCM mean state errors and biases in subseasonal variability make it extremely difficult to compare results and conclusions among these studies. Authors have compared CGCMs to AGCMs with climatological, monthly mean, pentad mean, or daily mean SSTs drawn from either observations or CGCMs. Even investigations of the same CGCM have disagreed over whether air-sea coupling affects the MJO, perhaps due to differences in the diagnostics applied [*Liess et al.*, 2004; *Sperber et al.*, 2005].

Second, regional variations in the effects of air-sea coupling throughout the MJO domain have not been rigorously explored; only two relatively recent studies have employed CGCMs with regional coupling to examine these effects. *Weng and Yu* [2010] employed the University of California, Los Angeles, model ($4^\circ \times 5^\circ$, L15) coupled to a full OGCM; outside the coupled region, they prescribed a repeating annual cycle of observed climatological monthly mean SSTs. *Klingaman and Woolnough* [2014b] used the MetUM coupled to the KPP 1-D ocean, with observed climatological daily SSTs outside the coupling region. In both studies, the CGCM simulation with coupling in both the tropical Indian and Pacific Oceans produced the strongest MJO with the most coherent eastward propagation. Coupling only in the Indian Ocean terminated MJO propagation west of the Maritime Continent in both models, stressing the importance of air-sea feedbacks in the Maritime Continent and West Pacific for MJO propagation. While *Klingaman and Woolnough* [2014b] did not perform a Pacific Ocean-only experiment, *Weng and Yu* [2010] found that coupling in the Pacific Ocean only modestly reduced MJO propagation from the Indian Ocean to the Maritime Continent, with little change in amplitude or propagation in the Pacific. The authors hypothesized that the greater importance of Pacific coupling was due to the stronger SST intraseasonal variability in that basin in their model. However, the AGCM in *Weng and Yu* [2010] suffered from several issues, particularly the use of a binary cloudiness variable (i.e., the sky was always either completely cloud covered or completely cloud free) that limited the role of cloud radiative feedbacks in favor of strong wind evaporation feedbacks. Further, the OGCM used a coarse 10 m near-surface vertical resolution, known to inhibit subseasonal variability, although *Klingaman and Woolnough* [2014b] found broadly similar results using a 1 m near-surface resolution and an AGCM capable of simulating the full dynamic range of cloudiness.

Finally, the sensitivity of GCM representations of the MJO to air-sea coupling has not been quantitatively compared with the sensitivities to other aspects of the GCM configuration, such as the treatment of cumulus convection or horizontal resolution (section 2.3). Further, there have been few investigations of how

these other aspects of the GCM configuration affect the response of the MJO to air-sea interactions; far more attention has been paid to inter-GCM variations in the effects of coupling than to intra-GCM variations. Two recent studies have demonstrated that the latter can be as strong, if not stronger, than the former. In MetUM AGCM and KPP-coupled simulations, *Klingaman and Woolnough* [2014b] demonstrated that the effect of coupling depends strongly on model formulation. When the rates of mixing entrainment and detrainment in the atmospheric convective parameterization were increased, the MetUM AGCM produced a stronger intraseasonal oscillation but no propagation through the Maritime Continent (Figure 15f). Coupling this AGCM to KPP improved this propagation but not did not change MJO amplitude (Figure 15g); in the standard AGCM, coupling to KPP mainly improved MJO amplitude and not propagation. *Crueger et al.* [2013] compared CGCM and AGCM simulations of ECHAM6 at lower (1.9° × 1.9°, L47) and higher (1.0° × 1.0°, L95) resolutions, having first implemented a modification to the convection parameterization that improved the MJO amplitude, similar to *Klingaman and Woolnough* [2014b] and others [e.g., *Bechtold et al.*, 2008; *Hannah and Maloney*, 2011; *Kim et al.*, 2012]. Unlike *Klingaman and Woolnough* [2014b], however, *Crueger et al.* [2013] concluded that coupling primarily increased MJO amplitude, while increasing spatial resolution improved eastward propagation. The controlled nature of these sensitivity experiments offers considerable potential to further our understanding of how air-sea feedbacks affect the MJO in GCMs.

## 6. Recommendations

Fifteen years of modeling experiments have confirmed that including atmosphere-ocean interactions improves the representation of the MJO in most GCMs, in both free-running and initialized simulations. Therefore, there is little need for further studies to demonstrate that the "gross properties" of the simulated MJO (e.g., its amplitude, period, and propagation) are sensitive to the presence of coupled interactions. We propose that future research should focus on the mechanisms by which air-sea feedbacks maintain and enhance the MJO and organized tropical convection generally. New and ongoing observations are needed to confirm theories, verify model results, and reveal processes of air-sea interaction. Decomposing the effects of coupled feedbacks entails the careful design of targeted modeling experiments that extend beyond comparisons of companion CGCM and AGCM integrations. Understanding the effects of coupling in GCMs requires development of novel diagnostics to untangle feedbacks at the air-sea interface.

### 6.1. The Need for New and Ongoing Observations

Continued progress in understanding the MJO requires ongoing support of existing observing systems and new or improved measurements that target specific processes or geographic regions. Substantial progress continues to be made in understanding the ocean response to MJO forcing, although observations that allow tighter closure of mixed layer temperature and salinity budgets are still needed. Understanding ocean feedbacks to the atmosphere remains the missing piece of the puzzle. The SST modulates sensible and latent heat fluxes, each of which can influence moistening associated with the MJO, as we discuss in section 6.3. Observations that focus on boundary layer moistening and subsequent detrainment to the free troposphere will help clarify how the fluxes impact the MJO. Observations that reduce uncertainties in low-level winds, temperature, and moisture are particularly relevant to this problem.

Regionally, the Indian Ocean remains undersampled in terms of in situ observations of surface fluxes or ocean profiles. Continued expansion of the RAMA buoy array and time to accumulate observations will partly remedy this issue. Recent observations made during the CINDY/DYNAMO field campaign provided detailed information on a limited number of MJO events. The need for additional or new observations in the Indian Ocean may arise as these observations are tested against and incorporated into MJO theories.

Elsewhere, little is known about intraseasonal air-sea interactions in the Maritime Continent region, including both the surrounding oceans and the Indonesian Seas. Whether air-sea interactions on diurnal time scales are important and how they might be rectified onto the MJO [e.g., *Peatman et al.*, 2014] are questions whose answers require a variety of spatially and temporally comprehensive observations. The upcoming Bay of Bengal Boundary Layer Experiment (summer 2016) and Years of the Maritime Continent field campaigns (2017–2019) will mitigate some of the observational shortcomings specific to these regions.

Finally, the growing collection of in situ and remotely sensed oceanic and atmospheric observations can be applied to progressively more sophisticated data assimilation schemes to produce high-quality oceanic and atmospheric reanalysis data sets.

### 6.2. Modeling Experiments

The MJO is a mode of atmospheric variability. Its gross properties may be enhanced or otherwise modified by coupling with the underlying ocean, but it is unlikely that this coupling is critical to the very existence of the MJO. Therefore, experiments that show an ex nihilo emergence of the MJO with air-sea coupling (i.e., the presence of a strong MJO in the CGCM where none exists in the AGCM) must be treated with suspicion. Coupling or high-frequency SST variability must not be used as a crutch to correct for deficiencies in the AGCM representation of the MJO, which likely involve errors in subgrid-scale parameterizations and their interactions with the large-scale atmospheric dynamics [e.g., *Jiang et al.*, 2015; *Xavier et al.*, 2015; *Klingaman et al.*, 2015a, 2015b].

GCM representations of the MJO are highly sensitive to the simulated mean climate (section 5.3). Experiments to isolate the effects of air-sea feedbacks on the MJO must ensure that the mean states of the CGCM and AGCM integrations are as similar as possible. AMIP-type AGCM integrations cannot be compared to free-running CGCM integrations. The simplest experiment design to achieve a comparable mean state is to prescribe the monthly mean SST and sea ice from the CGCM in the AGCM, effectively replacing the AMIP SST and sea ice forcing with that from the CGCM. While prescribing SSTs at frequencies higher than monthly means (e.g., daily or pentad means) has been shown to increase MJO activity in AGCMs (section 5.4), it is likely that this arises from incorrect phase relationships between SSTs, surface fluxes, and rainfall. Comparing CGCMs to AGCMs with high-frequency CGCM SSTs will conflate the impact of coupling with the erroneous SST-surface flux relationships in the AGCM.

Prescribing CGCM SSTs at any temporal resolution is less than ideal, however, because many CGCMs have substantial cold biases in tropical mean SST, which can affect the representation of the MJO [e.g., *Inness et al.*, 2003] and the impact of coupling [e.g., *Klingaman and Woolnough*, 2014b]. Simulated air-sea feedbacks under a biased CGCM mean climate likely differ from such feedbacks in the observed mean climate, although further research is needed to confirm these differences and their magnitudes. Studies of air-sea coupling in the MJO should use a CGCM in which the mean state biases can be controlled and limited. Flux corrections can strongly reduce CGCM biases, bringing the mean SST closer to observations. Care must be taken when applying flux corrections in a CGCM with ocean dynamics, because the dynamics can respond to the corrections to produce a different ocean mean state to the one intended.

CGCMs comprising an AGCM coupled to a 1-D mixed layer ocean offer a flexible framework for targeted experiments to identify the mechanisms by which air-sea interactions influence the MJO. Unlike single-layer slab models, a mixed layer model with fine vertical resolution can accurately represent the diurnal cycle at the air-sea interface that is critical during the MJO suppressed phase [e.g., *Bernie et al.*, 2005; *Woolnough et al.*, 2007; *Tseng et al.*, 2015]. The lack of ocean dynamics means that flux corrections can be applied more effectively in CGCMs with mixed layer oceans than in CGCMs with 3-D OGCMs. CGCMs with mixed layer oceans and flux corrections produce minimal SST biases in multidecadal simulations [e.g., *Hirons et al.*, 2015]. These corrections can be used to maintain any preferred mean state, including that of a CGCM or of particular phases of modes of variability, such as the ENSO and the IOD. Constraining the 1-D ocean toward the CGCM ocean climatology allows diagnosing the effects of mean state errors within a coupled framework. Further, since the 1-D ocean columns do not communicate, these models allow considerable flexibility in when and where the atmosphere and ocean are coupled, permitting sensitivity tests of the presence of coupling in individual regions [e.g., *Klingaman and Woolnough*, 2014b] or during particular MJO phases. Isolating the impact of coupling can be achieved with a similar experiment design to that with a full CGCM: by comparing a coupled simulation to the AGCM with prescribed monthly mean coupled model SSTs.

The drawback of CGCMs with mixed layer oceans is that they lack interactive ocean dynamics, which may be important to subseasonal mixed layer variability in the tropics, particularly near the equator [e.g., *Halkides et al.*, 2015] where upper ocean mixing induced by current shear can be important [*Moum et al.*, 2013]. This makes these models imperfect tools for experiments that require capturing the complete response of the ocean to atmospheric forcing. However, the key remaining challenge in understanding the role of air-sea coupling in the MJO is identifying the response of the atmosphere to SST variations. Mixed layer ocean models are capable of simulating near-observed levels of subseasonal SST variability in forced [e.g., *Bernie et al.*, 2005; *Shinoda*, 2005] and coupled configurations [e.g., *Klingaman and Woolnough*, 2014b]. While CGCMs with 3-D oceans remain essential for understanding the contributions from ocean dynamical processes, CGCMs with mixed layer oceans are highly practical tools for studying the role of air-sea feedbacks in the MJO.

### 6.3. Analyzing Air-Sea Interactions in Models

Understanding air-sea interactions within the MJO requires process-level analyses of how intraseasonal atmospheric and oceanic variations impact the magnitude and phasing of surface fluxes, their impact on boundary layer moisture and temperature, and the large-scale atmospheric response to these changes. These coupled processes can be studied using the conceptual framework employed elsewhere in this review: by analyzing MJO forcing to the ocean, the ocean response to MJO forcing, and ocean feedbacks to the MJO. Such analyses should characterize air-sea interactions in terms of both the atmospheric forcing and the ocean response and provide insight into whether SST-modulated surface fluxes support existing MJO theories (section 2.2) or motivate new theories for their role in the MJO life cycle. They should highlight model-to-model or model-to-observations differences and motivate process-oriented analyses and modeling studies.

Some elements of this diagnostic framework are routinely practiced. For example, MJO forcing of the ocean is typically (and sufficiently) assessed by comparing mean and intraseasonal variations of the surface energy budget, wind speed or stress, and rainfall. For most studies of the MJO in coupled ocean-atmosphere simulations, assessment of the ocean response to MJO forcing is limited to the SST response, presumably because high-frequency, vertically resolved ocean output is not always saved. In the absence of such output, the relative contributions of ocean dynamics and surface heating to the SST response can be only qualitatively assessed through the relationship between dSST/d$t$ and $Q_{net}$ [e.g., *Hendon and Glick*, 1997; *Duvel and Vialard*, 2007]. Saving daily (or finer) time series of mixed layer depth, temperature, salinity, sea surface height, and currents will allow greater insight into the role of ocean processes within the MJO. The methods presented in *Halkides et al.* [2015], for example, can be applied to ocean model output to assess the ocean response to MJO forcing.

Intraseasonal SST variations are communicated to the atmosphere primarily through surface turbulent fluxes. The SST feedback is modulated by the atmosphere, since both ocean and atmosphere determine $\Delta q$ and $\Delta T$. This is demonstrated in Figure 17 using 2 years of latent heat flux data from the 0°N, 90°E RAMA buoy and methodologies of *Hendon and Glick* [1997], *Shinoda et al.* [1998], *Maloney and Sobel* [2004], *Araligidad and Maloney* [2008], *Andersen and Kuang* [2012], *Riley Dellaripa and Maloney* [2015], and others. Flux-related variables and rainfall are lag regressed onto SST anomalies. In Figure 17a, $q_{air}$ and $q^*_{SST}$ amplitude and phase differences induce a large-amplitude (compared to either $q_{air}$ or $q^*_{SST}$) $\Delta q$ that maximizes prior to the warmest SSTs. $\Delta q$ influences the magnitude and phasing of the thermodynamic part of the flux ($\Delta q' \overline{|V|}$; dashed gray line in Figure 17b) relative to the wind-driven part ($\overline{\Delta q |V|}'$; solid gray line). Although the wind-driven part is much larger than the thermodynamic part, when combined with $\overline{\Delta q |V|}'$, $\Delta q' \overline{|V|}$ shifts the peak total flux (black line) closer to peak rainfall (green line) and enhances the wind-driven flux by 10∼15 W m$^{-2}$ during convective development (lags −5 through +5 days). The impact of variable SSTs on the thermodynamic flux can be estimated by recomputing $\Delta q' \overline{|V|}$ with a heavily smoothed SST time series (a 51 day running mean was used here; Figure 17c). When only $q_{air}$ varies, the $\Delta q' \overline{|V|}$ amplitude is reduced and shifted so that it opposes, rather than enhances, total evaporation during convective development.

In both observations and CGCMs, the amplitude and phasing of $q_{air}$ and $T_{air}$ may be sensitive to downdraft saturation, cloud entrainment/detrainment, and convective organization, while those of $q^*_{SST}$ and SST depend on the upper ocean adjustment to MJO forcing. Biases in these processes—whether in the atmosphere, ocean, or both—can have important impacts on the phasing and amplitude of $\Delta q$ and $\Delta T$, which are conduits for the ocean feedback. Evaluation of intraseasonal air-sea interactions and their biases in models may be clarified with these types of analyses that first shaped our understanding of how the ocean and atmosphere cooperatively yield fluxes of heat and moisture to the atmosphere.

Analyzing what controls the surface fluxes, however, is only the first step toward understanding ocean feedbacks to the MJO. Conceptually, these feedbacks may be considered in terms of MJO theory (section 4.1), as illustrated in Figure 18. Latent heat flux anomalies maximize in the vicinity of mature MJO convection, where they may help maintain the convective anomaly via the modified WISHE arguments of *Maloney and Sobel* [2004] and *Sobel et al.* [2010]. Here latent heat flux enhancement by warm SSTs is 10∼15 W m$^{-2}$, or about 10% of the total flux. This modest increase in the latent heat flux may nevertheless be important for maintaining the MJO column moist static energy anomaly, as the anomaly is depleted by convection at a rate of 10∼20% d$^{-1}$ [e.g., *Riley Dellaripa and Maloney*, 2015, and references therein]. By maintaining MJO convection, the ocean feedbacks may indirectly supplement longwave heating and moistening associated with stratiform cloud feedbacks [*Chikira*, 2014]. To the east of the active convection, large diurnal SST variations can force

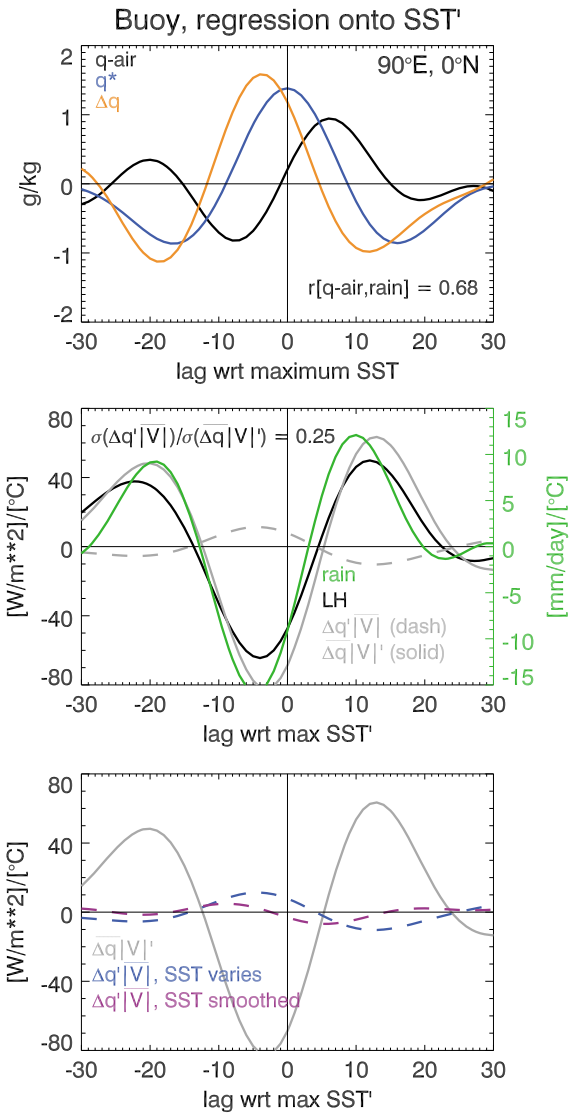


**Figure 17.** (a) Lag regression of $q_{air}$ (q-air, black), $q^*_{SST}$ (q*, blue), and $\Delta q$ (orange) onto DJF SST anomalies from the 90°E, 0°N RAMA buoy. The correlation of rainfall to $q_{air}$ is shown. (b) Lag regression of rainfall (green), total latent heat flux (black), and thermodynamic ($\Delta q'|\overline{V}|$; gray dashed) and wind driven ($\overline{\Delta q}|V|'$; gray solid) onto SST. The amplitude ratio of $\Delta q'|\overline{V}|$ to $\overline{\Delta q}|V|'$ is shown. See text for details on computation of $\Delta q'|\overline{V}|$ and $\overline{\Delta q}|V|'$. (c) Lag regression of wind-driven ($\overline{\Delta q}|V|'$; gray solid) and thermodynamic ($\Delta q'|\overline{V}|$; blue dashed) onto SST (repeated from Figure 17b), and $\Delta q'|\overline{V}|$ calculated using 51 day smoothed SSTs (magenta). A 20–100 day bandpass filter is first applied to all time series. Curves in Figures 17a–17c are scaled for a positive 1°C anomaly.

diurnal convection that may supplement low-level moistening [*Ruppert and Johnson*, 2015] either directly through enhanced turbulent transfer between the boundary layer and free troposphere or through dynamical moisture convergence driven by the shallow heating [e.g., *Wu*, 2003]. The spatially extensive warm SST anomaly can promote low-level moisture convergence [*Lindzen and Nigam*, 1987; *Back and Bretherton*, 2009; *Hsu and Li*, 2012], encouraging the eastward propagation of the MJO by supplementing the atmospheric frictional wave-CISK convergence.

The interaction between the ocean-atmosphere coupled feedbacks and the MJO and the possibility that these feedbacks may lead to changes in MJO amplitude, structure, or propagation characteristics will make diagnosing the processes by which air-sea interaction modifies the MJO a particular challenge. One avenue for assessing air-sea interactions within the MJO would be to combine the analyses presented in Figure 17 with process-oriented diagnostics developed for the atmospheric component of the MJO. Examples are the relationship of convection to the environmental moisture profile [*Thayer-Calder and Randall*, 2009; *Kim et al.*, 2009]

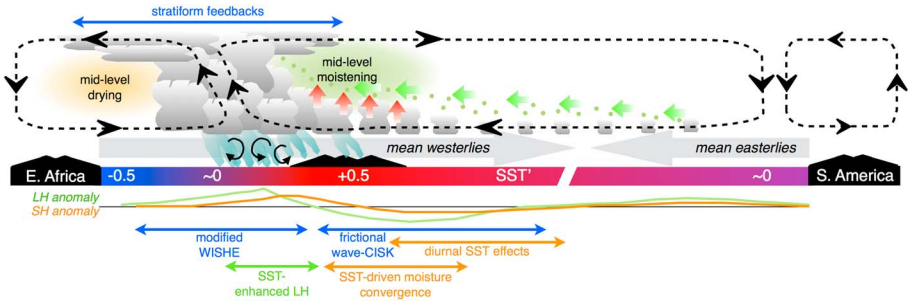


**Figure 18.** Schematic depiction of Indian and Pacific Ocean feedbacks to the MJO when convection (gray cloud elements) is maximized in the eastern Indian Ocean. Rainfall (aquamarine), circulation anomalies (black dashed cells), convective downdrafts (black rotor arrows), mean winds (faint gray arrows), and moistening by convective detrainment (small green dots) and horizontal and vertical advection (thick green and red arrows, respectively) are overlaid. Net moistening (drying) is shaded green (orange). Positive (red) and negative (blue) SST anomalies for a strong event are shaded, while latent (sensible) heat flux anomalies are shown with green (orange) curves. Feedback mechanisms associated with latent (sensible) heat are labeled with green (orange) arrows and text. Maintenance or propagation processes not directly linked to SST variations are labeled with blue arrows and text. Central and East Pacific spatial scale is compressed relative to the Warm Pool.

and the moisture (or moist static energy) budget of the MJO [*Maloney*, 2009; *Kiranmayi and Maloney*, 2011; *Andersen and Kuang*, 2012; *DeMott et al.*, 2014; *Chikira*, 2014], which is particularly well suited to quantifying processes relevant to MJO initiation, maintenance, and propagation within the context of current theories.

## 7. Summary

Air-sea interactions within the MJO life cycle are governed by a complex series of heat and momentum exchanges at the atmosphere-ocean interface. During the MJO suppressed phase, the ocean surface gains energy through enhanced shortwave heating and the reduced surface turbulent fluxes via decreased wind speeds. In the presence of light winds, reduced mixing allows the heating to accumulate in the upper few meters of the ocean, leading to a shallow, warm, stably stratified ocean mixed layer. Such shallow, warm mixed layers experience large diurnal SST amplitudes, which can further stratify the upper ocean and help maintain the SST anomaly against the generally weaker cooling effects of ocean mixing. During the developing phase of the MJO, convection gradually becomes deeper and more widespread. The increase in convective activity generates locally windy conditions, which effectively transfer energy stored in the upper ocean to the atmosphere. As the disturbance propagates eastward, active phase large-scale westerly wind anomalies perturb the upper ocean for several days. The westerly phase of the MJO is associated with continued evaporative surface cooling, mixing, and atmosphere-ocean momentum transfer. The enhanced evaporation and mixing destroys the upper ocean vertical stratification, while the momentum transfer can drive upper ocean surface currents and, for particularly strong and long-lived westerly wind events, excite oceanic Kelvin waves. In the Indian Ocean, the oceanic Kelvin wave can reflect off of the eastern coastlines as a downwelling oceanic Rossby wave, while Kelvin waves excited in the West Pacific are sometimes associated with ENSO initiation. The weakening of strong surface winds marks the transition from the MJO active to suppressed phase.

The ocean feedbacks to the MJO are communicated through their effect on surface fluxes. The effect of intraseasonal SST variations on surface fluxes is to shift their moistening and heating of the boundary layer slightly earlier in the MJO life cycle than would otherwise occur. How this subtle shift impacts the MJO is not yet fully understood. In the decade since the MJO and its air-sea interactions were reviewed by *Zhang* [2005], *Hendon* [2005], and *Kessler* [2005], new in situ and satellite observations have provided a clearer picture of the structure of MJO convection and the ocean response to intraseasonal atmospheric forcing. At the same time, the inability of existing theories to fully explain MJO existence or behavior spurred new thinking regarding the interactions of convection with environmental moisture [e.g., *Raymond and Fuchs*, 2009]. The concept of the MJO as a "moisture mode," where the disturbance growth and propagation are chiefly governed by environmental moisture availability, has refocused the assessment of MJO theories such as WISHE, frictional wave-CISK, and stratiform instability from their impacts on convective heating to their impacts on environmental moistening. Within this context, the impact of variable SSTs on the MJO should be considered from observational, theoretical, and experimental viewpoints.

During the past 15 years, numerous modeling studies have demonstrated improved MJO simulation when AGCMs are coupled to interactive ocean models. Differences in experimental design, mean state biases, and potentially different sensitivities to ocean coupling have thus far hindered a clear understanding of how air-sea interaction impacts the MJO in these simulations. The use of high-resolution mixed layer ocean models is one solution to reducing the complications that arise from model-dependent mean state biases, particularly where the mixed layer energy budget is dominated by a combination of surface fluxes and vertical mixing processes. The impact of air-sea interactions on the MJO in coupled simulations (whether they use fully dynamic or mixed layer ocean models) may be better understood if subjected to a uniform set of air-sea interaction diagnostics and if rigorously evaluated in terms of the relationship of convection to SST-modulated surface fluxes, vertical moisture profiles, and environmental moistening processes. These practices can be applied to a wide subset of problems associated with the MJO, such as propagating versus nonpropagating intraseasonal events and primary versus successive events, and should lead to a clearer understanding of the MJO and its interactions with the ocean.

**Acknowledgments**

The authors are grateful to four anonymous and patient reviewers for their comments and guidance, which greatly improved this manuscript. C.A.D. received support from National Science Foundation grant AGS-1119999 and by the National Science Foundation Science and Technology Center for Multi-Scale Modeling of Atmospheric Processes, managed by Colorado State University under cooperative agreement ATM-0425247. N.P.K. and S.J.W. were supported by the National Centre for Atmospheric Research, a Natural Environment Research Council collaborative center, under contract R8/H12/83/001. We thank Emily Riley-Dellaripa for providing RAMA buoy surface flux estimates and Simon de Szoeke for input on Figure 4. Eric Maloney, Daehyun Kim, Matthew Wheeler, and Duane Waliser provided valuable feedback on early versions of this review. RAMA buoy data were provided by the National Center for Atmospheric Research staff and retrieved from https://climatedataguide.ucar.edu/climate-data/tropical-moored-buoy-system-tao-triton-pirata-rama-toga.

## References

Abraham, J. P., et al. (2013), A review of global ocean temperature observations: Implications for ocean heat content estimates and climate change, *Rev. Geophys.*, *51*, 450–483, doi:10.1002/rog.20022.

Alverson, K., and D. J. Baker (2006), Taking the pulse of the oceans, *Science*, *314*, 1657, doi:10.1126/science.1135358.

Andersen, J. A., and Z. Kuang (2012), Moist static energy budget of MJO-like disturbances in the atmosphere of a zonally symmetric aquaplanet, *J. Clim.*, *25*, 2782–2804.

Anderson, J. E., and S. C. Riser (2014), Near-surface variability of temperature and salinity in the near-tropical ocean: Observations from profiling floats, *J. Geophys. Res. Oceans*, *119*, 7433–7448, doi:10.1002/2014JC010112.

Anderson, S. P., R. A. Weller, and R. B. Lukas (1996), Surface buoyancy forcing and the mixed layer of the western pacific warm pool: Observations and 1D model results, *J. Clim.*, *9*, 3056–3085.

Andersson, A., C. Klepp, K. Fennig, S. Bakan, H. Grassl, and J. Schulz (2011), Evaluation of HOAPS-3 ocean surface freshwater flux components, *J. Appl. Meteorol. Climatol.*, *50*, 379–398.

Araligidad, N. M., and E. D. Maloney (2008), Wind-driven latent heat flux and the intraseasonal oscillation, *Geophys. Res. Lett.*, *35*, L04815, doi:10.1029/2007GL032746.

Aziz, M. A., S. C. Reising, W. E. Asher, L. A. Rose, P. W. Gaiser, and K. A. Horgan (2005), Effects of air-sea interaction parameters on ocean surface microwave emission at 10 and 37 GHz, *IEEE Trans. Geosci. Remote Sens.*, *43*, 1763–1774.

Back, L. E., and C. S. Bretherton (2009), On the relationship between SST gradients, boundary layer winds, and convergence over the tropical oceans, *J. Clim.*, *22*, 4182–4196.

Bailey, S. W., and P. J. Werdell (2006), A multi-sensor approach for the on-orbit validation of ocean color satellite data products, *Remote Sens. Env.*, *102*, 12–23.

Barsugli, J. J., and D. A. Battisti (1998), The basic effects of atmosphere-ocean thermal coupling on midlatitude variability, *J. Atmos. Sci.*, *55*, 477–493.

Bechtold, P., M. Köhler, T. Jung, F. Doblas-Reyes, M. Leutbecher, M. J. Rodwell, F. Vitart, and G. Balsamo (2008), Advances in simulating atmospheric variability with the ECMWF model: From synoptic to decadal timescales, *Q. J. R. Meteorol. Soc.*, *137*, 553–597.

Bellenger, H., and J.-P. Duvel (2009), An analysis of tropical ocean diurnal warm layers, *J. Clim.*, *22*, 3629–3646.

Bellenger, H., Y. N. Takayabu, T. Ushiyama, and K. Yoneyama (2010), Role of diurnal warm layers in the diurnal cycle of convection over the tropical Indian ocean during MISMO, *Mon. Weather Rev.*, *138*, 2426–2433.

Benedict, J. J., and D. A. Randall (2007), Observed characteristics of the MJO relative to maximum rainfall, *J. Atmos. Sci.*, *64*, 2332–2354.

Benedict, J. J., and D. A. Randall (2009), Structure of the Madden-Julian oscillation in the superparameterized CAM, *J. Clim.*, *66*, 3277–3296.

Benedict, J. J., and D. A. Randall (2011), Impacts of idealized air-sea coupling on Madden-Julian oscillation structure in the superparameterized CAM, *J. Atmos. Sci.*, *68*, 1990–2008.

Benedict, J. J., E. D. Maloney, A. H. Sobel, D. M. Frierson, and L. J. Donner (2013), Tropical intraseasonal variability in version 3 of the GFDL Atmosphere Model, *J. Clim.*, *26*, 426–449.

Bentamy, A., K. B. Katsaros, A. M. Mestas-Nuñez, W. M. Drennan, E. B. Forde, and H. Roquet (2003), Satellite estimates of wind speed and latent heat flux over the global oceans, *J. Clim.*, *16*, 637–656.

Bergman, J. W., H. H. Hendon, and K. M. Weickmann (2001), Intraseasonal air-sea interactions at the onset of El Niño, *J. Clim.*, *14*, 1702–1719.

Bernie, D. J., S. J. Woolnough, and J. M. Slingo (2005), Modeling diurnal and intraseasonal variability of the ocean mixed layer, *J. Clim.*, *18*, 1190–1202.

Bernie, D. J., E. Guilyardi, G. Madec, J. M. Slingo, and S. J. Woolnough (2007), Impact of resolving the diurnal cycle in an ocean-atmosphere GCM. Part 1: A diurnally forced OGCM, *Clim. Dyn.*, *29*, 575–590.

Bernie, D. J., E. Guilyardi, G. Madec, J. M. Slingo, S. J. Woolnough, and J. Cole (2008), Impact of resolving the diurnal cycle in an ocean-atmosphere GCM. Part 2: A diurnally coupled CGCM, *Clim. Dyn.*, *31*, 909–925.

Biello, J. A., and A. J. Majda (2005), A new multiscale model for the Madden-Julian oscillation, *J. Atmos. Sci.*, *62*, 1694–1721.

Bourras, D., L. Eymard, and W. T. Liu (2002), A neural network to estimate the latent heat flux over oceans from satellite observations, *Int. J. Remote Sens.*, *23*, 2405–2423, doi:10.1080/01431160110070825.

Brunke, M. A., Z. Wang, X. Zeng, M. Bosilovich, and C.-L. Shie (2011), An assessment of the uncertainties in ocean surface turbulent fluxes in 11 reanalysis, satellite-derived and combined global datasets, *J. Clim.*, *24*, 5469–5493.

Bush, S. J., A. G. Turner, S. J. Woolnough, G. M. Martin, and N. P. Klingaman (2015), The effect of increased convective entrainment on Asian monsoon biases in the MetUM general circulation model, *Q. J. R. Meteorol. Soc.*, *141*, 311–326.

Cabrera, O. C., C. L. Villanoy, L. T. David, and A. L. Gordon (2011), Barrier layer control of entrainment and upwelling in the Bohol Sea, Philippines, *Oceanography*, *24*, 130–141.

Camargo, S. J., A. W. Robertson, A. G. Barnston, and M. Ghil (2008), Clustering of eastern North Pacific tropical cyclone tracks: ENSO and MJO effects, *Geochem. Geophys. Geosyst.*, *9*, Q06V05, doi:10.1029/2007GC001861.

Carbone, R. E., and Y. Li (2015), Tropical oceanic rainfall and sea surface temperature structure: Parsing causation from correlation in the MJO, *J. Atmos. Sci.*, *72*, 2703–2718.
Carvalho, L. M. V., C. Jones, and B. Liebmann (2004), The South Atlantic Convergence Zone: Intensity, form, persistence, and relationships with intraseasonal to interannual activity and extreme rainfall, *J. Clim.*, *17*, 88–108, doi:10.1175/1520-0442(2004)017<0088:tsaczi>2.0.co;2.
Cassou, C. (2008), Intraseasonal interaction between the Madden-Julian oscillation and the North Atlantic oscillation, *Nature*, *455*, 523–527.
Chang, H.-R., and R. L. Grossman (1999), Evaluation of bulk surface flux algorithms for light wind conditions using data from the Coupled Ocean-Atmosphere Response Experiment (COARE), *Q. J. R. Meteorol. Soc.*, *125*, 1551–1588, doi:10.1002/qj.49712555705.
Chelton, D. B., and M. H. Freilich (2005), Scatterometer-based assessment of 10-m wind analyses from the operational ECMWF and NCEP numerical weather prediction models, *Mon. Weather Rev.*, *133*, 409–429.
Chen, S., et al. (2015), A study of CINDY/DYNAMO MJO suppressed phase, *J. Atmos. Sci.*, *72*, 3755–3779, doi:10.1175/JAS-D-13-0348.1.
Chen, S. S., and R. A. Houze (1997), Diurnal variation and life-cycle of deep convective systems over the tropical Pacific Warm Pool, *Q. J. R. Meteorol. Soc.*, *123*, 357–388.
Chi, N.-H., R.-C. Lien, E. A. D'Asaro, and B. B. Ma (2014), The surface mixed layer heat budget from mooring observations in the central Indian Ocean during Madden-Julian oscillation events, *J. Geophys. Res. Oceans*, *119*, 4638–4652, doi:10.1002/2014JC010192.
Chikira, M. (2014), Eastward-propagating intraseasonal oscillation represented by Chikira-Sugiyama cumulus parameterization. Part II: Understanding moisture variation under weak temperature gradient balance, *J. Atmos. Sci.*, *71*, 615–639.
Chikira, M., and M. Sugiyama (2010), A cumulus parameterization with state-dependent entrainment rate. Part I: Description and sensitivity to temperature and humidity profiles, *J. Atmos. Sci.*, *67*, 2171–2193.
Chou, S.-H., R. M. Atlas, C.-L. Shie, and J. Ardizzone (1995), Estimates of surface humidity and latent heat fluxes over oceans from SSM/I data, *Mon. Weather Rev.*, *123*, 2405–2425.
Chou, S.-H., E. Nelkin, J. Ardizzone, R. M. Atlas, and C.-L. Shie (2003), Surface turbulent heat and momentum fluxes over global oceans based on the Goddard Satellite Retrivals, version 2 (GSSTF2), *J. Clim.*, *16*, 3256–3273.
Clayson, C. A., and D. Weitlich (2005), Diurnal warming in the tropical Pacific and its interannual variability, *Geophys. Res. Lett.*, *32*, L21604, doi:10.1029/2005GL023786.
Cronin, M. F., and M. J. McPhaden (1997), The upper ocean heat balance in the western equatorial Pacific warm pool during September–December 1992, *J. Geophys. Res*, *102*, 8533–8553.
Cronin, M. F., and M. J. McPhaden (2002), Barrier layer formation during westerly wind bursts, *J. Geophys. Res.*, *107*, 8020, doi:10.1029/2001JC001171.
Crueger, T., B. Stevens, and R. Brokopf (2013), The Madden-Julian oscillation in ECHAM6 and the introduction of an objective MJO metric, *J. Clim.*, *26*, 3241–3257.
Curry, J. A., C. A. Clayson, W. B. Rossow, R. Reeder, Y.-C. Zhang, P. J. Webster, G. Liu, and R.-S. Sheu (1999), High-resolution satellite-derived dataset of the surface fluxes of heat, freshwater and momentum for the TOGA COARE IOP, *Bull. Am. Meteorol. Soc.*, *80*, 2059–2080.
Curry, J. A., et al. (2004), SEAFLUX, *85*, 409–424, doi:10.1175/bams-85-3-409.
Danbasoglu, G., W. G. Large, J. J. Tribbia, P. R. Gent, B. P. Briegleb, and J. McWilliams (2006), Diurnal coupling in the tropical oceans of CCSM3, *J. Clim.*, *19*, 2347–2365.
de Boisséson, E., M. A. Balmaseda, F. Vitart, and K. Mogensen (2012), Impact of the sea surface temperature forcing on hindcasts of Madden-Julian oscillation events using the ECMWF model, *Ocean Sci.*, *8*, 1071–1084.
de Boyer Montégut, C., G. Madec, A. S. Fischer, A. Lazar, and D. Iudicone (2004), Mixed layer depth over the global ocean: An examination of profile data and a profile-based climatology, *J. Geophys. Res.*, *109*, C12003, doi:10.1029/2004JC002378.
de Leeuw, G., E. L. Andreas, M. D. Anguelove, C. W. Fairall, E. R. Lewise, C. O'Dowd, M. Schulz, and S. E. Schwartz (2011), Production flux of sea spray aerosol, *Rev. Geophys.*, *49*, RG2001, doi:10.1029/2010RG000349.
de Szoeke, S. P., J. B. Edson, J. R. Marion, C. W. Fairall, and L. Bariteau (2015), The MJO and air-sea interaction in TOGA COARE and DYNAMO, *J. Clim.*, *28*, 597–622.
Dee, D. P., et al. (2011), The ERA-Interim reanalysis: Configuration and performance of the data assimilation system, *Q. J. R. Meteorol. Soc.*, *137*, 553–597.
Delcroix, T., J. Picaut, and G. Eldin (1991), Equatorial Kelvin and Rossby waves evidenced in the Pacific Ocean through Teosat sea level and surface current anomalies, *J. Geophys. Res.*, *96*, 3249–3262.
DeMott, C. A., C. Stan, D. A. Randall, and M. D. Branson (2014), Intraseasonal variability in Coupled GCMs: The roles of ocean feedbacks and model physics, *J. Clim.*, *27*(13), 4970–4995, doi:10.1175/jcli-d-13-00760.1.
DeWitt, H. L., D. J. Coffman, K. J. Schulz, W. A. Brewer, T. S. Bates, and P. K. Quinn (2013), Atmospheric aerosol properties over the equatorial Indian Ocean and the impact of the Madden-Julian oscillation, *J. Geophys. Res. Atmos.*, *118*, 5736–5749, doi:10.1002/jgrd.50419.
Donald, A., H. Meinke, B. Power, A. H. N. de Maia, M. C. Wheeler, N. White, R. C. Stone, and J. Ribbe (2006), Near-global impact of the Madden-Julian oscillation on rainfall, *Geophys. Res. Lett.*, *33*, L09704, doi:10.1029/2005GL025155.
Drushka, K., J. Sprintall, and S. T. Gille (2010), Vertical structure of Kelvin Waves in the Indonesian Throughflow exit passages, *J. Phys. Oceanogr.*, *40*, 1965–1987.
Drushka, K., J. Sprintall, and S. T. Gille (2012), In situ observations of Madden-Julian oscillation mixed layer dynamics in the Indian and western Pacific Oceans, *J. Clim.*, *25*, 2306–2328.
Drushka, K., J. Sprintall, and S. T. Gille (2014), Subseasonal variations in salinity and barrier-layer thickness in the eastern equatorial Indian Ocean, *J. Geophys. Res. Oceans*, *119*, 805–823, doi:10.1002/2013JC009422.
Duvel, J. P. (2012), Oceans and air-sea interaction, in *Intraseasonal Variability in the Atmosphere-Ocean Climate System, Springer Praxis Books*, edited by J. P. Duvel, pp. 513–536, Springer, Berlin.
Duvel, J. P., and J. Vialard (2007), Indo-Pacific sea surface temperature perturbations associated with intraseasonal oscillations of tropical convection, *J. Clim.*, *20*(13), 3056–3082, doi:10.1175/jcli4144.1.
Duvel, J. P., R. Roca, and J. Vialard (2004), Ocean mixed layer temperature variations induced by intraseasonal convective perturbations over the Indian Ocean, *J. Atmos. Sci.*, *61*, 1004–1022.
Emanuel, K. A. (1987), An air-sea interaction model of intraseasonal oscillations in the tropics, *J. Atmos. Sci.*, *44*, 2324–2340.
Fairall, C. W., E. F. Bradley, D. P. Rogers, J. B. Edson, and G. S. Young (1996a), Bulk parameterization of air-sea fluxes for Tropical Ocean-Global Atmosphere Coupled-Ocean Atmosphere Response Experiment, *J. Geophys. Res.*, *101*(C2), 3747–3764, doi:10.1029/95JC03205.
Fairall, C. W., E. F. Bradley, J. S. Godfrey, G. A. Wick, J. B. Edson, and G. S. Young (1996b), Cool-skin and warm-layer effects on sea-surface temperature, *J. Geophys. Res.*, *101*, 1295–1308.
Fairall, C. W., E. F. Bradley, J. E. Hare, A. A. Grachev, and J. B. Edson (2003), Bulk parameterization of air-sea fluxes: Updates and verifications for the COARE algorithm, *J. Clim.*, *16*, 571–591.

Fairall, C. W., M. Yang, L. Bariteau, J. B. Edson, D. Helmig, W. McGillis, S. Pezoa, J. E.Hare, B. Huebert, and B. Blomquist (2011), Implementation of the Coupled Ocean-Atmosphere Response Experiment flux algorithm with $CO_2$, dimethyl sulfide, and $O_3$, *J. Geophys. Res.*, *116*, C00F09, doi:10.1029/2010JC006884.
Fink, A., and P. Speth (1997), Some potential forcing mechanisms of the year-to-year variability of the tropical convection and its intraseasonal (25–70 day) variability, *Int. J. Climatol.*, *17*, 1513–1534.
Flatau, M., P. J. Flatau, P. Phoebus, and P. P. Niler (1997), The feedback between equatorial convection and local radiative and evaporative processes: The implications for intraseasonal oscillations, *J. Atmos. Sci.*, *54*, 2373–2386.
Foltz, G. R., and M. J. McPhaden (2004), The 30–70 day oscillations in the tropical Atlantic, *Geophys. Res. Lett.*, *31*, L15205, doi:10.1029/2004GL020023.
Franz, B. A., et al. (2005), The continuity of ocean color measurements from SeaWiFS to MODIS, in *Earth Observing Systems X*, vol. 5882, edited by J. J. Butler, pp. 304–316, SPIE, Bellingham, Wash.
Fu, X., and B. Wang (2009), Critical roles of the stratiform rainfall in sustaining the Madden-Julian oscillation: GCM experiments, *J. Clim.*, *22*, 3939–3959.
Fu, X., J. Lee, P.-C. Hsu, H. Taniguchi, B. Wang, and W. Wng (2013), Multi-model MJO forecasting during DYNAMO/CINDY period, *Clim. Dyn.*, *41*, 1067–1081.
Fu, X., W. Wang, J.-Y. Lee, B. Wang, K. Kikuchi, J. Xu, J. Li, and S. Weaver (2015), Distinctive roles of air-sea coupling on different MJO events: A new perspective revealed from the DYNAMO/CINDY field campaign, *Mon. Weather Rev.*, *143*, 794–812.
Fuchs, Z., S. Gjorgjievska, and D. Raymond (2012), Effects of varying the shape of the convective heating profile on convectively coupled gravity waves and moisture modes, *J. Atmos. Sci.*, *69*, 2505–2519.
Gantt, B., and N. Meskhidze (2013), The physical and chemical characteristics of marine primary organic aerosol: A review, *Atmos. Chem. Phys.*, *13*, 3979–3996.
Gaspar, P., F. Ogor, P. Y. L. Traon, and O. Z. Zanife (1994), Joint estimation of the TOPEX and POSEIDON sea-state biases, *J. Geophys. Res.*, *99*, 24,981–24,994.
Gebbie, G., I. Eisenman, A. Wittenberg, and E. Tzipermann (2007), Modulation of westerly wind bursts by sea surface temperature: A semistochastic feedback for ENSO, *J. Atmos. Sci.*, *64*, 3281–3295.
Gill, A. E. (1980), Some simple solutions for heat-induced tropical circulation, *Q. J. R. Meteorol. Soc.*, *106*, 447–462.
Girishkumar, M. S., M. Ravichandran, and V. Pant (2012), Observed chlorophyll-a bloom in the southern Bay of Bengal during winter 2006–2007, *Int. J. Remote Sens.*, *33*(4), 1264–1275, doi:10.1080/01431161.2011.563251.
Godfrey, J. S., and E. Lindstrom (1989), The heat budget of the equatorial West Pacific surface mixed layer, *J. Geophys. Res.*, *94*(C6), 8007–8017.
Gordon, A. L. (2005), Oceanography of the Indonesian Seas and their throughflow, *Oceanography*, *18*, 14–27.
Gordon, A. L., J. Sprintall, H. M. Van Aken, D. Susanto, S. Wijffels, R. Molcard, A. Ffield, W. Pranowo, and S. Wirasantosa (2010), The Indonesian throughflow during 2004–2006 as observed by the INSTANT program, *Dyn. Atmos. Oceans*, *50*, 115–128.
Gottschalck, J., P. E. Roundy, C. J. Schreck III, A. Vintzileos, and C. Zhang (2013), Large-scale atmospheric and oceanic conditions during the 2011-12 DYNAMO field campaign, *Mon. Weather Rev.*, *141*, 4173–4196.
Gould, J., et al. (2004), Aro profiling floats bring new era of in situ ocean observations, *Eos*, *85*, 179,190–179,191.
Grabowski, W. W. (2006), Impact of explicit atmosphere-ocean coupling on MJO-like coherent structures in idealized aquaplanet simulations, *J. Atmos. Sci.*, *63*, 2289–2306.
Gray, W. M., and R. W. Jacobson (1977), Diurnal variation of deep cumulus convection, *Mon. Weather Rev.*, *105*, 1171–1188.
Grunseich, G., B. Subrahmanyam, and B. Wang (2013), The Madden-Julian oscillation detected in Aquarius salinity observations, *Geophys. Res. Lett.*, *40*, 5461–5466, doi:10.1002/2013GL058173.
Guan, B., T. Lee, D. J. Halkides, and D. E. Waliser (2014), Aquarius surface salinity and the Madden-Julian oscillation: The role of salinity in surface layer density and potential energy, *Geophys. Res. Lett.*, *41*, 2858–2869, doi:10.1002/2014GL059704.
Gushchina, D., and B. Dewitte (2012), Intraseasonal tropical atmospheric variability associated with the two flavors of El Niño, *Mon. Weather Rev.*, *140*, 3669–3681.
Haertel, P., K. Straub, and A. Budsock (2015), Transforming circumnavigating Kelvin waves that initiate and dissipate the Madden-Julian oscillation, *Q. J. R. Meteorol. Soc.*, *141*, 1586–1602.
Halkides, D. J., L. E. Lucas, D. E. Waliser, T. Lee, and R. Murtugudde (2011), Mechanisms controlling mixed-layer temperature variability in the eastern tropical Pacific on the intraseasonal timescale, *Geophys. Res. Lett.*, *38*, L17602, doi:10.1029/2011GL048545.
Halkides, D. J., D. E. Waliser, T. Lee, D. Menemenlis, and B. Guan (2015), Quantifying the processing controlling intraseasonal mixed-layer temperature variability in the tropical Indian Ocean, *J. Geophys. Res. Oceans*, *120*, 692–715, doi:10.1002/2014JC010139.
Ham, S., S.-Y. Hong, and S. Park (2014), A study on air-sea interaction on the simulated seasonal climate in an ocean-atmosphere coupled model, *Clim. Dyn.*, *42*, 1175–1187.
Ham, Y.-G., J.-S. Kug, I.-S. Kang, F.-F. Jin, and A. Timmerman (2010), Impact of diurnal atmosphere-ocean coupling on tropical climate simulations using a coupled GCM, *Clim. Dyn.*, *34*, 905–917.
Han, W. (2005), Origins and dynamics of the 90 day and 30–60 day variations in the equatorial Indian Ocean, *J. Phys. Oceanogr.*, *35*, 708–728.
Han, W., D. M. Lawrence, and P. J. Webster (2001), Dynamical response of equatorial Indian Ocean to intraseasonal winds: Zonal flow, *Geophys. Res. Lett.*, *28*, 4215–4218, doi:10.1029/2001GL013701.
Hannah, W. M., and E. D. Maloney (2011), The role of moisture-convection feedbacks in simulating the Madden-Julian oscillation, *J. Clim.*, *24*, 2754–2770.
Harrison, D. E., and G. A. Vecchi (2001), January 1999 Indian Ocean cooling event, *Geophys. Res. Lett.*, *28*(19), 3717–3720.
Henderson, G. R., B. S. Barrett, and D. M. Lafleur (2014), Arctic sea ice and the Madden-Julian oscillation (MJO), *Clim. Dyn.*, *43*, 2185–2196.
Hendon, H. H. (2000), Impact of air-sea coupling on the Madden-Julian oscillation in a general circulation model, *J. Atmos. Sci.*, *57*, 3939–3952.
Hendon, H. H. (2005), Air-sea interaction, in *Intraseasonal Variability in the Atmosphere-Ocean Climate System, Springer Praxis*, pp. 223–246, Springer, Berlin.
Hendon, H. H., and J. Glick (1997), Intraseasonal air-sea interaction in the tropical Indian and Pacific Oceans, *J. Clim.*, *10*, 647–661.
Hendon, H. H., and M. L. Salby (1994), The life cycle of the Madden-Julian oscillation, *J. Atmos. Sci.*, *51*, 2225–2237.
Hendon, H. H., B. Liebmann, and J. D. Glick (1998), Oceanic Kelvin waves and the Madden-Julian oscillation, *J. Atmos. Sci.*, *55*, 88–101.
Hendon, H. H., C. Zhang, and J. D. Glick (1999), Interannual variation of the Madden-Julian oscillation during austral summer, *J. Clim.*, *12*, 2538–2550.

Higgins, R. W., and W. Shi (2001), Intercomparison of the principal modes of interannual and intraseasonal variability of the North American monsoon system, *J. Clim.*, *14*, 403–417.
Higgins, R. W., J.-K. E. Schemm, W. Shi, and A. Leetmaa (2000), Extreme precipitation events in the Western United States related to tropical forcing, *J. Clim.*, *13*, 793–820.
Hirata, F. E., P. J. Webster, and V. E. Toma (2013), Distinct manifestations of austral summer tropical intraseasonal oscillations, *Geophys. Res. Lett.*, *40*, 3337–3341, doi:10.1002/grl.50632.
Hirons, L. C., P. Inness, F. Vitart, and P. Bechtold (2013), Understanding advances in the simulation of intraseasonal variability in the ECMWF model. Part II: The application of process-based diagnostics, *Q. J. R. Meteorol. Soc.*, *139*, 1417–1426.
Hirons, L. C., N. P. Klingaman, and S. J. Woolnough (2015), MetUM-GOML: A near-globally coupled atmosphere-ocean-mixed-layer model, *Geosci. Model Dev.*, *8*, 363–379.
Holloway, C. E., S. J. Woolnough, and G. M. S. Lister (2013), The effects of explicit versus parameterized convection on the MJO in a large-domain high-resolution tropical case study. Part I: Characterization of large-scale organization and propagation, *J. Atmos. Sci.*, *70*, 1342–1369.
Horii, T., Y. Masumoto, I. Ueki, S. P. Kumar, and K. Mizuno (2011), Intraseasonal vertical velocity variation caused by the equatorial wave in the central equatorial Indian Ocean, *J. Geophys. Res.*, *116*, C09005, doi:10.1029/2011JC007081.
Hsu, P.-C., and T. Li (2012), Role of the boundary layer moisture asymmetry in causing the eastward propagation of the Madden-Julian oscillation, *J. Clim.*, *25*, 4914–4931.
Hung, M.-P., J.-L. Lin, W. Wang, D. Kim, T. Shinoda, and S. J. Weaver (2013), MJO and convectively coupled equatorial waves simulated by CMIP5 climate models, *J. Clim.*, *26*(17), 6185–6214, doi:10.1175/jcli-d-12-00541.1.
Inness, P. M., and J. M. Slingo (2003), Simulation of the Madden-Julian oscillation in a coupled general circulation model. Part I: Comparison with observations and an atmosphere-only GCM, *J. Clim.*, *16*, 345–364.
Inness, P. M., and J. M. Slingo (2006), The interaction of the Madden-Julian oscillation with the Maritime Continent in a GCM, *Q. J. R. Meteorol. Soc.*, *132*, 1645–1667.
Inness, P. M., J. M. Slingo, E. Guilyardi, and J. Cole (2001), Organization of tropical convection in a GCM with varying vertical resolution: Implications for the simulation of the Madden-Julian oscillation., *Clim. Dyn.*, *17*, 777–793.
Inness, P. M., J. M. Slingo, E. Guilyardi, and J. Cole (2003), Simulation of the Madden-Julian oscillation in a coupled general circulation model. Part II: The role of the basic state, *J. Clim.*, *17*, 365–382.
Iskandar, I., Y. Masumoto, K. Mizuno, H. Sasaki, A. K. Affandi, D. Setiabudidaya, and F. Syamsuddin (2014), Coherent intraseasonal oceanic variations in the eastern equatorial Indian Ocean and in the Lombok and Ombai Straits from observations and a high-resolution OGCM, *J. Geophys. Res. Oceans*, *119*, 615–630, doi:10.1002/2013JC009592.
Isobe, A., S. Kako, and S. Iwasaki (2014), Synoptic-scale atmospheric motions modulated by spring phytoplankton bloom in the Sea of Japan, *J. Clim.*, *27*, 7587–7602, doi:10.1175/jcli-d-14-00277.1.
Isoguchi, O., and H. Kawamura (2006), MJO-related summer cooling and phytoplankton blooms in the South China Sea in recent years, *Geophys. Res. Lett.*, *33*, L16615, doi:10.1029/2006GL027046.
Izumo, T., S. Masson, J. Vialard, C. de Boyer Montegut, S. K. Behera, G. Madec, K. Takahashi, and T. Yamagata (2010), Low and high frequency Madden-Julian oscillations in austral summer: Interannual variations, *Clim. Dyn.*, *35*, 669–683.
Jackson, D. L., and G. A. Wick (2010), Near-surface air temperature retrieval derived from AMSU-A and sea surface temperature observations, *J. Atmos. Oceanic Technol.*, *27*, 1769–1776.
Jackson, D. L., G. A. Wick, and J. J. Bates (2006), Near-surface retrieval of air temperature and specific humidity using multisensor microwave satellite observations, *J. Geophys. Res.*, *111*, D10306, doi:10.1029/2005JD006431.
Jahne, B., and H. Haussecker (1998), Air-water gas exchange, *Annu. Rev. Fluid Mech.*, *30*, 443–468.
Janowiak, J. E., P. A. Arkin, and M. Morrissey (1994), An examination of the diurnal cycle in oceanic tropical rainfall using satellite and in situ data, *Mon. Weather Rev.*, *122*, 2296–2311.
Janssen, P. A. E. M. (1991), Quasi-linear theory of wind-wave generation applied to wave forecasting, *J. Phys. Oceanogr.*, *21*, 1631–1642.
Jayakumar, A., J. Vialard, M. Lengaigne, C. Gnanaseelan, J. P. McCreary, and B. P. Kumar (2011), Processes controlling the surface temperature signature of the Madden-Julian oscillation in the thermocline ridge of the Indian Ocean, *Clim. Dyn.*, *37*, 2217–2234.
Jerlov, N. G. (1968), *Optical Oceanography*, Elsevier, New York.
Jia, X., C. Li, J. Ling, and C. Zhang (2008), Impacts of a GCM's resolution on MJO simulation, *Adv. Atmos. Sci.*, *25*, 139–156.
Jiang, X., et al. (2015), Vertical structure and physical processes of the Madden-Julian oscillation: Exploring key model physics in climate simulations, *J. Geophys. Res. Atmos.*, *120*, 4718–4748, doi:10.1002/2014JD022374.
Jin, D., R. Murtugudde, and D. E. Waliser (2012), Tropical Indo-Pacific ocean chlorophyll response to MJO forcing, *J. Geophys. Res.*, *117*, C11008, doi:10.1029/2012JC008015.
Jin, D., D. E. Waliser, C. Jones, and R. Murtugudde (2013), Modulation of tropical ocean surface chlorophyll by the Madden-Julian oscillation, *Clim. Dyn.*, *40*, 39–58, doi:10.1007/s00382-012-1321-4.
Jin, X., and L. Yu (2015), An improved near-surface specific humidity and air temperature climatology for the SSM/I satellite period, *J. Atmos. Oceanic Technol.*, *32*, 412–433.
Johnson, R. H., P. E. Ciesielski, and J. H. Ruppert Jr. (2015), Sounding-based thermodynamic budgets for DYNAMO, *J. Atmos. Sci.*, *72*, 598–622.
Jones, C., and B. C. Weare (1996), The role of low-level moisture convergence and ocean latent heat fluxes in the Madden and Julian oscillation: An observational analysis using ISCCP data and ECMWF analyses, *J. Clim.*, *9*, 3086–3104.
Jones, C., D. E. Waliser, and C. Gautier (1998), The influence of the Madden-Julian oscillation on ocean surface heat fluxes and sea surface temperature, *J. Clim.*, *11*, 1057–1072.
Jones, C., D. E. Waliser, K. M. Lau, and W. Stern (2004a), Global occurrences of extreme precipitation and the Madden-Julian oscillation: Observations and predictability, *J. Clim.*, *17*, 4575–4589, doi:10.1175/3238.1.
Jones, C., L. M. V. Carvalho, R. W. Higgins, D. E. Waliser, and J.-K. E. Schemm (2004b), Climatology of tropical intraseasonal convective anomalies: 1979–2002, *J. Clim.*, *17*, 523–539.
Kalnay, E., et al. (1996), The NCEP/NCAR 40-year reanalysis project, *Bull. Am. Meteorol. Soc.*, *77*, 437–471, doi:10.1175/1520-0477(1996)077<0437:tnyrp>2.0.co;2.
Kapur, A., and C. Zhang (2012), Multiplicative MJO forcing of ENSO, *J. Clim.*, *25*, 8132–8147.
Katsaros, K. B. (1980), The aqueous thermal boundary layer, *Boundary Layer Meteorol.*, *18*, 107–127.
Kawai, Y., and A. Wada (2007), Diurnal sea surface temperature variation and its impact on the atmosphere and ocean: A review, *J. Oceanogr.*, *63*, 721–744.
Kayano, M. T., and V. E. Kousky (1999), Intraseasonal (30–60 day) variability in the global tropics: Principal modes and their evolution, *Tellus A*, *51*, 373–386, doi:10.1034/j.1600-0870.1999.t01-3-00003.x.

Keerthi, M. G., M. Lengaigne, J. Vialard, C. de Boyer Montegut, and P. M. Muraleedharan (2013), Interannual variability of the tropical Indian Ocean mixed layer depth, *Clim. Dyn.*, *40*, 743–759.
Kemball-Cook, S., B. Wang, and X. Fu (2002), Simulation of the ISO in the ECHAM4 model: The impact of coupling with an ocean model, *J. Atmos. Sci.*, *59*, 1433–1453.
Kennedy, J. J. (2014), A review of uncertainty in in situ measurements and data sets of sea surface temperature, *Rev. Geophys.*, *52*, 1–32, doi:10.1002/2013RG000434.
Kessler, W. S. (2001), EOF representations of the Madden-Julian oscillation and its connection with ENSO, *J. Clim.*, *14*, 3055–3061.
Kessler, W. S. (2005), The oceans, in *Intraseasonal Variability in the Atmosphere-Ocean Climate System, Springer Praxis*, pp. 175–222, Springer, Berlin.
Kessler, W. S., and R. Kleeman (2000), Rectification of the Madden-Julian oscillation into the ENSO cycle, *J. Clim.*, *13*, 3560–3575.
Kessler, W. S., M. J. McPhaden, and K. M. Weickmann (1995), Forcing of intraseasonal Kelvin waves in the equatorial Pacific, *J. Geophys. Res.*, *100*, 10,613–10,631.
Kim, D., et al. (2009), Application of MJO simulation diagnostics to climate models, *J. Clim.*, *22*, 6413–6436.
Kim, D., A. H. Sobel, D. M. W. Frierson, E. D. Maloney, and I.-S. Kang (2011), A systematic relationship between intraseasonal variability and mean state bias in AGCM simulations, *J. Clim.*, *24*, 5506–5520.
Kim, D., A. H. Sobel, A. D. Del Genio, Y. Chen, S. J. Camargo, M.-S. Yao, M. Kelley, and L. Nazarenko (2012), The tropical subseasonal variability simulated in the NASA GISS general circulation model, *J. Clim.*, *25*, 4641–4659.
Kim, H.-M., C. D. Hoyos, P. J. Webster, and I.-S. Kang (2008), Sensitivity of MJO simulation and predictability to sea surface temperature variability, *J. Clim.*, *21*, 5304–5317.
Kim, H.-M., C. D. Hoyos, P. J. Webster, and I.-S. Kang (2010), Ocean-atmosphere coupling and the boreal winter MJO, *Clim. Dyn.*, *35*, 771–784.
Kiranmayi, L., and E. D. Maloney (2011), Intraseasonal moist static energy budget in reanalysis data, *J. Geophys. Res.*, *116*, D21117, doi:10.1029/2011JD016031.
Klingaman, N. P., and S. J. Woolnough (2014a), Using a case-study approach to improve the Madden-Julian oscillation in the Hadley Centre model, *Q. J. R. Meteorol. Soc.*, *140*, 2491–2505.
Klingaman, N. P., and S. J. Woolnough (2014b), The role of air-sea coupling in the simulation of the Madden-Julian oscillation in the Hadley Centre model, *Q. J. R. Meteorol. Soc.*, *140*, 2272–2286.
Klingaman, N. P., P. M. Inness, H. Weller, and J. M. Slingo (2008), The importance of high-frequency sea-surface temperature variability to the intraseasonal oscillation of Indian monsoon rainfall, *J. Clim.*, *21*, 6119–6140.
Klingaman, N. P., S. J. Woolnough, H. Weller, and J. M. Slingo (2011), The impact of finer-resolution air-sea coupling on the intraseasonal oscillation of the Indian summer monsoon, *J. Clim.*, *24*, 2451–2468.
Klingaman, N. P., et al. (2015a), Vertical structure and physical processes of the Madden-Julian oscillation: Linking hindcast fidelity to simulated diabatic heating and moistening, *J. Geophys. Res. Atmos.*, *120*, 4690–4717, doi:10.1002/2014JD022374.
Klingaman, N. P., X. Jiang, P. K. Xavier, J. Petch, D. Waliser, and S. J. Woolnough (2015b), Vertical structure and physical processes of the Madden-Julian oscillation: Synthesis and summary, *J. Geophys. Res. Atmos.*, *120*, 4671–4689, doi:10.1002/2014JD022374.
Klotzbach, P. J. (2010), On the Madden-Julian oscillation-Atlantic hurricane relationship, *J. Clim.*, *23*, 282–293.
Koch-Larrouy, A., M. Lengaigne, P. Terray, G. Madec, and S. Masson (2011), Tidal mixing in the Indonesian Seas and its effect on the tropical climate system, *Clim. Dyn.*, *34*, 891–904.
Krishnamurti, T. N., and D. Subrahmanyam (1982), The 30–50 day mode at 850 mb during MONEX, *J. Atmos. Sci.*, *39*, 2088–2095.
Krishnamurti, T. N., D. K. Oosterhof, and A. V. Metha (1988), Air-sea interaction on the timescale of 30–50 days, *J. Atmos. Sci.*, *45*, 1304–1322.
Kuang, Z. (2008), A moisture-stratiform instability for convectively coupled waves, *J. Atmos. Sci.*, *65*, 834–854.
Kubota, M., N. Iwasaka, S. Kizu, M. Konda, and K. Kutsuwada (2002), Japanese ocean flux data sets with use of remote sensing observations (J-OFURO), *J. Oceanogr.*, *58*, 213–225.
Kumar, B. P., J. Vialard, M. Lengaigne, V. S. N. Murty, and M. J. McPhaden (2012), TropFlux: Air-sea fluxes for the global tropical oceans—Description and evaluation, *Clim. Dyn.*, *38*, 1521–1543.
Kummerow, C., W. Barnes, T. Kozu, J. Shiue, and J. Simpson (1998), The Tropical Rainfall Measuring Mission (TRMM) sensor package, *J. Oceanic. Technol.*, *15*, 809–817.
Lagerloef, G., et al. (2008), The Aquarius/SAC-D mission: Designed to meet the salinity remote-sensing challenge, *Oceanography*, *21*, 68–81, doi:10.5670/oceanog.2008.68.
Lagerloef, G. S. E., G. Mitchum, R. Lukas, and P. Niller (1999), Tropical Pacific near-surface currents estimated from altimeter, wind and drifter data, *J. Geophys. Res.*, *104*, 23,313–23,326.
Lagerloef, G. S. E., et al. (2010), Aquarius/SAC-D mission: Designed to meet the salinity remote-sensing challenge, *Oceanography*, *21*, 68–81.
Lappen, C.-L., and C. Schumacher (2012), Heating in the tropical atmosphere: What level of detail is critical for accurate MJO simulations in GCMs?, *Clim. Dyn.*, *39*, 2547–2568.
Lappen, C.-L., and C. Schumacher (2014), The role of tilted heating in the evolution of the MJO, *J. Geophys. Res. Atmos.*, *119*, 2966–2989, doi:10.1002/2013JD020638.
Lau, K. M., and L. Peng (1987), Origin of low-frequency (intraseasonal) oscillations in the tropical atmosphere. Part I: Basic theory, *J. Atmos. Sci.*, *44*, 950–972.
Lau, K.-M., and C.-H. Sui (1997), Mechanisms of short-term sea surface temperature regulation: Observations during TOGA COARE, *J. Clim.*, *10*, 465–472.
Lau, W. K.-M., and D. E. Waliser (2005), *Intraseasonal Variability in the Atmosphere-Ocean Climate System*, 474 pp., Springer, Berlin.
Li, C., X. Jia, W. Ling, W. Zhou, and C. Zhang (2009), Sensitivity of MJO simulations to convective heating profiles, *Clim. Dyn.*, *32*, 167–187.
Li, K.-F., B. Tian, D. E. Waliser, and Y. L. Yung (2010), Tropical mid-tropospheric $CO_2$ variability driven by the Madden-Julian oscillation, *Proc. Natl. Acad. Sci.*, *107*, 19,171–19,175, doi:10.1073/pnas.1008222107.
Li, Y., and R. E. Carbone (2012), Excitation of rainfall over the tropical Western Pacific, *J. Atmos. Sci.*, *69*, 2983–2994.
Li, Y., W. Han, T. Shinoda, C. Wang, R.-C. Lien, J. N. Moum, and J.-W. Wang (2013), Effects of the diurnal cycle in solar radiation on the tropical Indian Ocean mixed layer variability during wintertime Madden-Julian oscillation, *J. Geophys. Res. Oceans*, *118*, 4945–4964, doi:10.1002/jgrc.20395.
Liebmann, B., H. H. Hendon, and J. D. Glick (1994), The relationship between tropical cyclones of the Western Pacific and Indian Oceans and the Madden-Julian oscillation, *J. Meteorol. Soc. Jpn.*, *72*, 401–412.
Liess, S., and S. Bengtsson (2004), The intraseasonal oscillation in ECHAM4. Part II: Sensitivity studies, *Clim. Dyn.*, *22*, 671–688.
Liess, S., L. Bengtsson, and K. Arpe (2004), The intraseasonal oscillation in ECHAM4. Part I: Coupled to a comprehensive ocean model, *Clim. Dyn.*, *22*, 671–688.

Lin, H., G. Brunet, and J. Derome (2009), An observed connection between the North Atlantic Oscillation and the Madden-Julian oscillation, *J. Clim.*, *22*, 364–380.
Lin, J. L., et al. (2006), Tropical intraseasonal variability in 14 IPCC AR4 climate models. Part I: Convective signals, *J. Clim.*, *19*, 2665–2690.
Lin, X., and R. H. Johnson (1996), Heating, moistening and rainfall over the Western Pacific Warm Pool during TOGA COARE, *J. Atmos. Sci.*, *53*, 3367–3383.
Lindzen, R. S., and S. Nigam (1987), On the role of the sea surface temperature gradients in forcing low-level winds and convergence in the Tropics, *J. Atmos. Sci.*, *44*, 2440–2458.
Ling, J., C. Zhang, and P. Bechtold (2013), Large-scale distinctions between MJO and non-MJO convective initiation over the tropical Indian Ocean, *J. Atmos. Sci.*, *70*, 2696–2712.
Liu, F., and B. Wang (2012), A conceptual model for self-sustained active-break Indian summer monsoon, *Geophys. Res. Lett.*, *39*, L2014, doi:10.1029/2012GL053663.
Liu, F., and B. Wang (2013), An air-sea coupled skeleton model for the Madden-Julian oscillation, *J. Atmos. Sci.*, *70*, 3147–3156.
Liu, P., M. Satoh, B. Wang, H. Fudeyasu, T. Nasuno, T. Li, H. Miura, H. Taniguchi, H. Masunaga, X. Fu, and H. Annamalai (2009), An MJO simulated by the NICAM at 14- and 7-km resolutions, *Mon. Weather Rev.*, *137*, 3254–3268.
Lloyd, I. D., and G. A. Vecchi (2010), Submonthly Indian Ocean cooling events and their interactions with large-scale conditions, *J. Clim.*, *23*, 700–716.
Lopez, H., B. P. Kirtman, E. Tziperman, and G. Gebbie (2013), Impact of interactive westerly wind bursts on CCSM3, *Dyn. Atmos. Oceans*, *59*, 24–51.
Lorenz, D. J., and D. L. Hartmann (2006), The effect of the MJO on the North American monsoon, *J. Clim.*, *19*, 333–343, doi:10.1175/jcli3684.1.
Lucas, L. E., D. E. Waliser, and R. Murtugudde (2010), Mechanisms governing sea surface temperature anomalies in the eastern tropical Pacific Ocean associated with the Madden-Julian oscillation, *J. Geophys. Res.*, *115*, C05012, doi:10.1029/2009JC005450.
Lukas, R., and E. Lindstrom (1991), The mixed layer of the western equatorial Pacific Ocean, *J. Geophys. Res.*, *96*, 3343–3357.
Lukas, R., S. P. Hayes, and K. Wyrtki (1984), Equatorial sea level response during the 1982–1983 El Niño, *J. Geophys. Res.*, *89*, 10,425–10,430.
Madden, R. A., and P. R. Julian (1971), Detection of a 40–50 day oscillation in the zonal wind in the tropical Pacific, *J. Atmos. Sci.*, *28*, 702–708.
Madden, R. A., and P. R. Julian (1972), Description of global-scale circulation cells in the tropics with a 40–50 day period, *J. Atmos. Sci.*, *29*, 1109–1123.
Madden, R. A., and P. R. Julian (1994), Observations of the 40–50 day tropical oscillation—A review, *Mon. Weather Rev.*, *122*, 814–837.
Madden, R. A., and P. R. Julian (2012), Historical perspective, in *Intraseasonal Variability in the Atmosphere-Ocean Climate System, Springer Praxis Books*, edited by R. A. Madden and P. R. Julian, pp. 1–19, Springer, Berlin.
Madhu, N. V., R. Jyothibabu, P. A. Maheswaran, V. J. Gerson, T. C. Gopalakrishnan, and K. K. C. Nair (2006), Lack of seasonality in phytoplankton standing stock (chlorophyll a) and production in the western Bay of Bengal, *Continental Shelf Res.*, *26*, 1868–1883.
Majda, A. J., and S. N. Stechmann (2009), The skeleton of tropical intraseasonal oscillations, *Proc. Natl. Acad. Sci.*, *106*, 8417–8422.
Majda, A. J., and S. N. Stechmann (2012), Multiscale theories for the MJO, in *Intraseasonal Variability in the Atmosphere-Ocean Climate System (Second Edition), Springer Praxis*, edited by A. J. Majda and S. N. Stechmann, pp. 549–568, Springer, Berlin.
Maloney, E. D. (2009), The moist static energy budget of a composite tropical intraseasonal oscillation in a climate model, *J. Clim.*, *22*, 711–729.
Maloney, E. D., and D. L. Hartmann (2000), Modulation of eastern North Pacific hurricanes by the Madden–Julian oscillation, *J. Clim.*, *13*, 1451–1460.
Maloney, E. D., and J. T. Kiehl (2002), MJO-related SST variations over the tropical Eastern Pacific during Northern Hemisphere summer, *J. Clim.*, *15*, 675–689.
Maloney, E. D., and A. H. Sobel (2004), Surface fluxes and ocean coupling in the tropical intraseasonal oscillation, *J. Clim.*, *17*, 4368–4386.
Maloney, E. D., and A. H. Sobel (2007), Idealized hot spot experiments with a general circulation model, *J. Clim.*, *20*, 908–925.
Mapes, B. E. (2000), Convective inhibition, subgrid-scale triggering energy, and stratiform instability in a toy tropical wave model, *J. Atmos. Sci.*, *57*, 1515–1535.
Marshall, A. G., O. Alves, and H. H. Hendon (2008), An enhanced moisture convergence–evaporation mechanism for MJO air-sea interaction, *J. Atmos. Sci.*, *65*, 970–986.
Marshall, A. G., H. H. Hendon, T. H. Durant, and M. A. Hemer (2015), Madden Julian Oscillation impacts on global ocean surface waves, *Ocean Model.*, doi:10.1016/j.ocemod.2015.06.002.
Matsuno, T. (1966), Quasigeostrophic motions in the equatorial area, *J. Meteorol. Soc. Jpn.*, *44*, 25–43.
Matthews, A. J. (2008), Primary and successive events in the Madden-Julian oscillation, *Q. J. R. Meteorol. Soc.*, *134*, 439–453.
Matthews, A. J., and M. P. Meredith (2004), Variability of Antarctic circumpolar transport and the Southern Annular Mode associated with the Madden-Julian oscillation, *Geophys. Res. Lett.*, *31*, L24312, doi:10.1029/2004GL021666.
Matthews, A. J., P. Singhruck, and K. J. Heywood (2010), Ocean temperature and salinity components of the Madden-Julian oscillation observed by Argo floats, *Clim. Dyn.*, *35*, 1149–1168.
Matthews, A. J., D. B. Baranowski, K. J. Keywood, P. J. Flatau, and S. Schimdtko (2014), The surface diurnal warm layer in the Indian Ocean during CINDY/DYNAMO, *J. Clim.*, *27*, 9101–9122.
McClain, C. R., G. C. Feldman, and S. B. Hooker (2004), An overview of the SeaWiFS project and strategies for producing a climate research quality global ocean bio-optical time series, *Deep Sea Res.*, *51*, 5–42.
McPhaden, M. J. (2002), Mixed layer temperature balance on intraseasonal timescales in the equatorial Pacific Ocean, *J. Clim.*, *15*, 2632–2647.
McPhaden, M. J. (2004), Evolution of the 2002/03 El Niño, *Bull. Am. Meteorol. Soc.*, *85*, 677–695.
McPhaden, M. J., et al. (1998), The Tropical Ocean-Global Atmosphere observing system: A decade of progress, *J. Geophys. Res.*, *103*(C7), 14,169–14,240, doi:10.1029/97JC02906.
McPhaden, M. J., et al. (2009), The global tropical moored buoy array, in *Proceedings of OceanObs'09: Sustained Ocean Observations and Information for Society,* vol. 2, pp. 459–480, ESA Publication WPP-306, Venice, Italy, doi:10.5270/OceanObs09.cwp.61.
McPhaden, M. J., and G. R. Foltz (2013), Intraseasonal variations in the surface layer heat balance of the central equatorial Indian Ocean: The importance of zonal advection and vertical mixing, *Geophys. Res. Lett.*, *40*, 2737–2741, doi:10.1002/grl.50536.
Melville, W. K. (1996), The role of surface-wave breaking in air-sea interaction, *Annu. Rev. Fluid Mech.*, *28*, 279–321.
Mignot, J., C. de Boyer Montégut, A. Lazar, and S. Cravatte (2007), Control of salinity on the mixed layer depth in the world ocean: 2. Tropical areas, *J. Geophys. Res.*, *112*, C10010, doi:10.1029/2006JC003954.
Miura, H., M. Satoh, T. Nasuno, A. T. Noda, and K. Oouchi (2007), A Madden-Julian oscillation event realistically simulated by a global cloud-resolving model, *Science*, *318*, 1763–1765.

Miyakawa, T., M. Satoh, H. Miura, H. Tomita, H. Yashiro, A. T. Noda, Y. Yamada, C. Kodama, M. Kimoto, and K. Yoneyama (2014), Madden-Julian oscillation prediction skill of a new-generation global model demonstrated using a supercomputer, *Nat. Commun.*, *5*, 3769, doi:10.1038/ncomms4769.

Moum, J. N., et al. (2013), Air-sea interactions from westerly wind bursts during the November 2011 MJO in the Indian Ocean, *Bull. Am. Meteorol. Soc.*, *95*, 1185–1199, doi:10.1175/bams-d-12-00225.1.

Murtugudde, R. G., S. R. Signorini, J. R. Christian, A. J. Busalacchi, C. R. McCalin, and J. Picaut (1999), Ocean color variability of the tropical Indo-Pacific basin observed by SeaWiFS during 1997–1998, *J. Geophys. Res.*, *104*, 18,351–18,366.

Myers, D. S., and D. E. Waliser (2003), Three-dimensional water vapor and cloud variations associated with the Madden-Julian oscillation during Northern Hemisphere winter, *J. Clim.*, *16*, 929–950.

Neale, R., and J. Slingo (2003), The Maritime Continent and its role in the global climate: A GCM study, *J. Clim.*, *16*, 834–848.

Neale, R., J. H. Richter, and M. Jochum (2008), The impact of convection on ENSO: From a delayed oscillator to a series of events, *J. Clim.*, *21*, 5904–5924.

Neelin, J. D. (1989), On the interpretation of the Gill model, *J. Atmosc. Sci.*, *46*, 2466–2468.

Neelin, J. D., I. M. Held, and K. H. Cook (1987), Evaporation-wind feedback and low-frequency variability in the tropical atmosphere, *J. Atmos. Sci.*, *44*, 2341–2348.

Newman, M., P. D. Sardeshmukh, and C. Penland (2009), How important is air-sea coupling in ENSO and MJO evolution?, *J. Clim.*, *22*, 2958–2977.

Onogi, K., et al. (2007), The JRA-25 reanalysis, *J. Meteorol. Soc. Jpn.*, *85*, 369–432, doi:10.2151/jmsj.85.369.

Parsons, D. B., K. Yoneyama, and J.-L. Redelsperger (2000), The evolution of the tropical western Pacific atmosphere-ocean system following the arrival of a dry intrusion, *Q. J. R. Meteorol. Soc.*, *126*, 517–548.

Paulson, C. A., and J. J. Simpson (1977), Irradiance measurements in the upper ocean, *J. Phys. Oceanogr.*, *7*, 952–956.

Peatman, S. C., A. J. Matthews, and D. P. Stevens (2014), Propagation of the Madden-Julian oscillation through the Maritime Continent and scale interaction with the diurnal cycle of precipitation, *Q. J. R. Meteorol. Soc.*, *140*, 814–825.

Peatman, S. C., A. J. Matthews, and D. P. Stevens (2015), Propagation of the Madden-Julian oscillation and scale interaction with the diurnal cycle in a high-resolution GCM, *Clim. Dyn.*, doi:10.1007/s00382-015-2513-5.

Pegion, K., and B.-P. Kirtman (2008a), The impact of air-sea interactions on the predictability of the tropical intraseasonal oscillation, *J. Clim.*, *21*, 5870–5886.

Pegion, K., and B. P. Kirtman (2008b), The impact of air-sea interactions on the simulation of tropical intraseasonal variability, *J. Clim.*, *21*(24), 6616–6635, doi:10.1175/2008jcli2180.1.

Perez, C. L., A. M. Moore, J. Zavala-Garay, and R. Kleeman (2005), A comparison of the influence of additive and multiplicative stochastic forcing on a coupled model of ENSO, *J. Clim.*, *18*, 5066–5085.

Piquat, J., M. Ioaulalen, C. Menkes, T. Delcroix, and M. J. McPhaden (1996), Mechanism of the zonal displacements of the Pacific warm pool: Implications for ENSO, *Science*, *274*, 1486–1489.

Pohl, B., and A. J. Matthews (2007), Observed changes in the lifetime and amplitude of the Madden-Julian oscillation associated with interannual ENSO sea surface temperature anomalies, *J. Clim.*, *20*, 2659–2674.

Ragueneau, O., et al. (2000), A review of the Si cycle in the modern ocean: Recent progress and missing gaps in the application of biogenic opal as a paleoproductivity proxy, *Global Planet. Change*, *26*, 317–365, doi:10.1016/s0921-8181(00)00052-7.

Rajendran, K., and A. Kitoh (2006), Modulation of tropical intraseasonal oscillations by atmosphere-ocean coupling, *J. Clim.*, *19*, 366–391.

Ramage, C. S. (1975), Preliminary discussion of the meteorology of the 1972–73 El Niño, *Bull. Am. Meteorol. Soc.*, *56*, 234–242.

Ramanathan, V., et al. (2001), Indian Ocean Experiment: An integrated analysis of the climate forcing and effects of the great Indo-Asian haze, *J. Geophys. Res.*, *106*, 28,371–28,398, doi:10.1029/2001JD900133.

Randall, D. A., Harshvardhan, and D. A. Dazlich (1991), Diurnal variability of the hydrologic cycle in a general circulation model, *J. Atmos. Sci.*, *48*, 40–62.

Raymond, D. J. (2001), A new model of the Madden-Julian oscillation, *J. Atmos. Sci.*, *58*, 2807–2819.

Raymond, D. J., and Z. Fuchs (2009), Moisture modes and the Madden-Julian oscillation, *J. Clim.*, *22*, 3031–3046.

Rebmann, C., O. Kolle, B. Heinesch, R. Queck, A. Ibrom, and M. Aubinet (2012), Data acquisition and flux calculations, in *Eddy Covariance, Springer Atmos. Sci.*, pp. 59–83, Springer, Netherlands.

Resplandy, L., J. Vialard, M. Lévy, O. Aumont, and Y. Dandonneau (2009), Seasonal and intraseasonal biogeochemical variability in the thermocline ridge of the southern tropical Indian Ocean, *J. Geophys. Res.*, *114*, C07024, doi:10.1029/2008JC005246.

Reynolds, R. W., and T. M. Smith (1994), Improved global sea surface temperature analyses using optimum interpolation, *J. Clim.*, *7*, 929–948.

Rienecker, M. M., et al. (2011), MERRA: NASA's Modern-Era Retrospective Analysis for Research and Applications, *J. Clim.*, *24*, 3624–3648, doi:10.1175/jcli-d-11-00015.1.

Riley, E., B. E. Mapes, and S. N. Tulich (2011), Clouds associated with the Madden-Julian oscillation: A new perspective, *J. Atmos. Sci*, *68*, 3032–3051.

Riley Dellaripa, E., and E. D. Maloney (2015), Analysis of MJO wind-flux feedbacks in the Indian Ocean using RAMA observations, *J. Meteorol. Soc. Jpn.*, doi:10.2151/jmsj.2015-021.

Roberts, J., C. A. Clayson, F. R. Robertson, and D. L. Jackson (2010), Predicting near-surface atmospheric variables from Special Sensor Microwave/Imager using neural networks with a first-guess approach, *J. Geophys. Res.*, *115*, D13099, doi:10.1029/2009JD013099.

Robertson, E. (2012), Biophysical coupling in the ocean mixed layer, PhD thesis, Department of Meteorology, Univ. of Reading.

Roemmich, D., M. Morris, W. R. Young, and J. R. Donguy (1994), Fresh equatorial jets, *J. Phys. Oceanogr.*, *24*(3), 540–558, doi:10.1175/1520-0485(1994)024<0540:fej>2.0.co;2.

Roemmich, D., G. C. Johnson, S. Riser, R. Davis, J. Gilson, W. B. Owens, S. L. Garzoli, C. Schmid, and M. Ignaszewski (2009), The Argo Program: Observing the global ocean with profiling floats, *Oceanography*, *22*(2), 34–43.

Ruppert, J. H., and R. H. Johnson (2015), Diurnally modulated cumulus moistening in the preonset stage of the Madden-Julian oscillation during DYNAMO, *J. Atmos. Sci.*, *72*, 1622–1647.

Saha, S., et al. (2006), The NCEP Climate Forecast System, *J. Clim.*, *19*, 3483–3517, doi:10.1175/jcli3812.1.

Saji, N. H., B. N. Goswami, P. N. Vinayachandran, and T. Yamagata (1999), A dipole mode in the tropical Indian Ocean, *Nature*, *401*, 360–363.

Saji, N. H., S.-P. Xie, and C.-Y. Tam (2006), Satellite observations of intense intraseasonal cooling events in the tropical south Indian Ocean, *Geophys. Res. Lett.*, *33*, L14704, doi:10.1029/2006GL026525.

Saxen, T. R., and S. A. Rutldge (1998), Surface fluxes and boundary layer recovery in TOGA COARE: Sensitivity to convective organization, *J. Atmos. Sci.*, *55*, 2763–2781.

Schiller, A., and J. S. Godfrey (2005), A diagnostic model of the diurnal cycle of sea surface temperature for use in coupled ocean-atmosphere models, *J. Geophys. Res.*, *110*, C11014, doi:10.1029/2005JC002975.
Schiller, A., S. E. Wijffels, J. Sprintall, R. Molcard, and P. R. Oke (2010), Pathways of intraseasonal variability in the Indonesian Throughflow region, *Dyn. Atmos. Oceans*, *50*, 174–200.
Schott, F. A., S.-P. Xie, and J. P. McCreary (2009), Indian ocean circulation and climate variability, *J. Geophys. Res.*, *47*, RG1002, doi:10.1029/2007RG000245.
Schulz, J., P. Schluessel, and H. Grassl (1993), Water vapour in the atmospheric boundary layer over oceans from SSM/I measurements, *Int. J. Remote Sens.*, *14*, 2773–2789, doi:10.1080/01431169308904308.
Schulz, J., J. Meywerk, and S. Ewald (1997), Evaluation of satellite-derived latent heat fluxes, *J. Clim.*, *10*, 2782–2795.
Seiki, A., M. Katsumata, T. Horii, T. Hasegawa, K. J. Richards, K. Yoneyama, and R. Shirooka (2013), Abrupt cooling associated with the oceanic Rossby wave and lateral advection during CINDY2011, *J. Geophys. Res. Oceans*, *118*, 5523–5535, doi:10.1002/jgrc.20381.
Sengupta, D., R. Senan, B. N. Goswami, and J. Vialard (2007), Intraseasonal variability of equatorial Indian Ocean zonal currents, *J. Clim.*, *20*, 3036–3055.
Seo, H., A. C. Subramanian, A. J. Miller, and N. R. Cavanaugh (2014), Coupled impacts of the diurnal cycle of sea surface temperature on the Madden-Julian oscillation, *J. Clim.*, *27*, 8422–8443.
Seo, K.-H., and W. Wang (2010), The Madden-Julian oscillation simulated in the NCEP Climate Forecast System model: The importance of stratiform heating, *J. Clim.*, *23*, 4770–4793.
Seo, K.-H., J.-K. E. Schemm, W. Wang, and A. Kumar (2007), The boreal summer intraseasonal oscillation simulations in the NCEP Climate Forecast System: The effect of sea surface temperature, *Mon. Weather Rev.*, *135*, 1807–1827.
Seo, K.-H., W. Wang, J. Gottschalck, Q. Zhang, J.-K. E. Schemm, W. R. Higgins, and A. Kumar (2009), Evaluation of MJO forecast skill from several statistical and dynamical forecast models, *J. Clim.*, *22*, 2372–2388.
Shelly, A., P. Xavier, D. Copsey, T. Johns, J. M. Rodriguez, S. Milton, and N. P. Klingaman (2014), Coupled versus uncoupled hindcast simulations of the Madden-Julian oscillation in the Year of Tropical Convection, *Geophys. Res. Lett.*, *41*, 5670–5677, doi:10.1002/2013GL059062.
Shinoda, T. (2005), Impact of diurnal cycle of solar radiation on intraseasonal SST variability in the western equatorial Pacific, *J. Clim.*, *18*, 2628–2636.
Shinoda, T., and W. Han (2005), Influence of the Indian Ocean Dipole on Atmospheric Subseasonal Variability, *J. Clim.*, *18*, 3891–3909.
Shinoda, T., and H. H. Hendon (1998), Mixed layer modeling of intraseasonal variability in the tropical western Pacific and Indian Oceans, *J. Clim.*, *11*, 2668–2685.
Shinoda, T., H. H. Hendon, and J. Glick (1998), Intraseaonal variability of surface fluxes and sea surface temperature in the tropical western Pacific and Indian Oceans, *J. Clim.*, *11*, 1685–1702.
Shinoda, T., T. G. Jensen, M. Flatau, and S. Chen (2013a), Surface wind and upper-ocean variability associated with the Madden-Julian oscillation simulated by the Coupled Ocean–Atmosphere Mesoscale Prediction System, *Mon. Weather Rev.*, *141*, 2290–2307.
Shinoda, T., T. G. Jenson, M. Flatau, S. Chen, W. Han, and C. Wang (2013b), Large-scale oceanic variability associated with the Madden-Julian oscillation during the CINDY/DYNAMO field campaign from satellite observations, *Remote Sens.*, *5*, 2072–2092.
Siegel, D. A., J. C. Ohlmann, L. Washburn, R. R. Bidigare, C. T. Nosse, E. Fields, and Y. Zhou (1995), Solar radiation, phytoplankton pigments and the radiant heating of the equatorial Pacific warm pool, *J. Geophys. Res.*, *100*, 4885–4891.
Slingo, J. M., et al. (1996), Intraseasonal oscillations in 15 atmospheric general circulation models: Results from an AMIP diagnostics subproject, *Clim. Dyn.*, *12*, 325–357.
Slingo, J. M., P. M. Inness, and K. R. Sperber (2005), Modeling intraseasonal variability, in *Intraseasonal Variability in the Atmosphere-Ocean Climate System, Springer Praxis Books*, edited by J. M. Slingo, P. M. Inness, and K. R. Sperber, pp. 361–387, Springer, Berlin.
Sobel, A. H., and H. Gildor (2003), A simple time-dependent model of SST hot spots, *J. Clim.*, *16*, 3978–3992.
Sobel, A. H., and E. D. Maloney (2013), Moisture modes and eastward propagation of the MJO, *J. Atmos. Sci.*, *70*, 187–192.
Sobel, A. H., E. D. Maloney, G. Bellon, and D. M. Frierson (2010), Surface fluxes and tropical intraseasonal variability: A reassessment, *J. Adv. Model. Earth Sys.*, *2*, 2, doi:10.3894/JAMES.2010.2.2.
Soloviev, A., and R. Lukas (1997), Sharp frontal interfaces in the near-surface layer of the ocean in the western equatorial Pacific warm pool, *J. Phys. Oceanogr.*, *27*, 999–1017.
Soloviev, A., and R. Lukas (2010), Effects of bubbles and sea spray on air-sea exchange in hurricane conditions, *Boundary Layer Meteorol.*, *136*, 365–376, doi:10.1007/s10546-010-9505-0.
Soloviev, A. V., S. Matt, and A. Fujimura (2015), Three-dimensional dynamics of freshwater lenses in the ocean's surface layer, *Oceanography*, *28*, 142–149.
Sperber, K. R. (2003), Propagation and the vertical structure of the Madden-Julian oscillation, *Mon. Weather Rev.*, *131*, 3018–3037.
Sperber, K. R. (2004), Madden-Julian variability in NCAR CAM2.0 and CCSM2.0, *Clim. Dyn.*, *23*, 259–278.
Sperber, K. R., S. Gualdi, S. Legutke, and V. Gayler (2005), The Madden-Julian oscillation in ECHAM4 coupled and uncoupled general circulation models, *Clim. Dyn.*, *25*, 117–140.
Sperber, K. R., J. M. Slingo, and P. M. Inness (2012), Modeling intraseasonal variability, in *Intraseasonal Variability in the Atmosphere-Ocean Climate System, Springer Praxis*, edited by K. R. Sperber, J. M. Slingo, and P. M. Inness, pp. 399–423, Springer, Berlin.
Sprintall, J., and M. Tomczak (1992), Evidence of the barrier layer in the surface layer of the tropics, *J. Geophys. Res.*, *97*, 7305–7316.
Sprintall, J., S. E. Wijffels, R. Molcard, and I. Jaya (2009), Direct estimates of the Indonesian Throughflow entering the Indian Ocean: 2004–2006, *J. Geophys. Res.*, *114*, C07001, doi:10.1029/2008JC005257.
Sprintall, J., S. E. Wijffels, R. Molcard, and I. Jaya (2010), Direct evidence of the South Java Current system in Ombai Strait, *Dyn. Atmos. Oceans*, *50*, 140–156.
Sprintall, J., A. L. Gordon, A. Koch-Larrouy, T. Lee, J. T. Potemra, K. Pujiana, and S. E. Wijffels (2014), The Indonesian seas and their role in the coupled ocean-climate system, *Nat. Geosci.*, *7*, 487–492.
Stan, C., M. Khairoutdinov, C. A. DeMott, V. Krishnamurthy, D. M. Straus, D. A. Randall, J. L. Kinter, and J. Shukla (2010), An ocean-atmosphere climate simulation with an embedded cloud resolving model, *Geophys. Res. Lett.*, *37*, L01702, doi:10.1029/2009GL040822.
Stephens, G. L., et al. (2002), The CloudSat mission and the A-TRAIN, *Bull. Am. Meteorol. Soc.*, *83*, 1771–1790.
Stopa, J. E., K. F. Cheung, H. L. Tolman, and A. Chawla (2013), Patterns and cycles in the Climate Forecast System Reanalysis wind and wave data, *Ocean Model.*, *70*, 207–220.
Straub, K. H. (2013), MJO initiation in the real-time multivariate MJO Index, *J. Clim.*, *26*, 1130–1151.
Strutton, P. G., F. P. Chavez, and J. Geophys. Res. (2000), Primary productivity in the equatorial Pacific during the 1997–1998 El Niño, *105*, 26,089–26,101.
Subramanian, A. C., M. Jochum, A. J. Miller, R. Murtugudde, R. Neale, and D. E. Waliser (2011), The Madden-Julian oscillation in CCSM4, *J. Clim.*, *24*, 6261–6282.

Sui, C.-H., K.-M. Lau, Y. N. Takayabu, and D. A. Short (1997), Diurnal variations in tropical oceanic cumulus convection during TOGA COARE, *J. Atmos. Sci.*, *54*, 639–655.
Talley, L. D., G. L. Pickard, W. J. Emery, and J. H. Swift (2011), *Descriptive Physical Oceanography: An Introduction*, 6th ed., Academic Press, Boston, Mass.
Tam, C.-Y., and N.-C. Lau (2005), Modulation of the Madden-Julian oscillation by ENSO: Inferences from observations and GCM simulations, *J. Meteorol. Soc. Jpn.*, *83*, 727–743.
Thayer-Calder, K., and D. A. Randall (2009), The role of convective moistening in the Madden-Julian oscillation, *J. Atmos. Sci.*, *66*, 3297–3312.
Tokioka, T., K. Yamazaki, A. Kitoh, and T. Ose (1988), The equatorial 30–60 day oscillation and the Arakawa-Schubert penetrative cumulus parameterization, *J. Meteorol. Soc. Jpn.*, *66*, 883–901.
Tseng, W.-L., B.-J. Tsuang, N. S. Keenlyside, H.-H. Hsu, and C.-Y. Tu (2015), Resolving the upper-ocean warm layer improves the simulation of the Madden-Julian oscillation, *Clim. Dyn.*, *44*, 1487–1503.
Uppala, S. M., et al. (2005), The ERA-40 re-analysis, *Q. J. R. Meteorol. Soc.*, *131*, 2961–3012.
Vecchi, G. A., and D. E. Harrison (2000), Tropical Pacific sea surface temperature anomalies, El Niño, and equatorial westerly wind events, *J. Clim.*, *13*, 1814–1830.
Veron, F., W. K. Melville, and L. Lenain (2008), Wave-coherent air-sea heat flux, *J. Phys. Oceanogr.*, *38*(4), 788–802, doi:10.1175/2007jpo3682.1.
Vialard, J., G. R. Foltz, M. J. McPhaden, J.-P. Duvel, and C. de Boyer Montégut (2008), Strong Indian Ocean sea surface temperature signals associated with the Madden-Julian oscillation in late 2007 and early 2008, *Geophys. Res. Lett.*, *35*, L19608, doi:10.1029/2008GL035238.
Vialard, J., et al. (2009), Cirene: Air-sea interactions in the Seychelles-Chagos thermocline ridge region, *Bull. Am. Meteorol. Soc.*, *90*, 45–61.
Vialard, J., K. Drushka, H. Bellenger, M. Lengaigne, S. Pous, and J. P. Duvel (2012), Understanding Madden-Julian-induced sea surface temperature variations in the North Western Australian Basin, *Clim. Dyn.*, *41*(11–12), 3203–3218, doi:10.1007/s00382-012-1541-7.
Vinayachandran, P. N., and N. H. Saji (2008), Mechanisms of South Indian Ocean intraseasonal cooling, *Geophys. Res. Lett.*, *35*, L23607, doi:10.1029/2008GL035733.
Vitart, F., and F. Molteni (2010), Simulation of the Madden-Julian oscillation and its teleconnections in the ECMWF forecast system, *Q. J. R. Meteorol. Soc.*, *136*, 842–855.
Vitart, F., J. Woolnough, M. A. Balmaseda, and A. M. Tompkins (2007), Monthly forecast of the Madden-Julian oscillation using a coupled GCM, *Mon. Weather Rev.*, *135*, 2700–2715.
Waliser, D. E., K. M. Lau, and J. H. Kim (1999), The influence of coupled sea-surface temperatures on the Madden-Julian oscillation: A model perturbation experiment, *J. Atmos. Sci.*, *56*, 333–358.
Waliser, D. E., et al. (2003), AGCM simulations of intraseasonal monsoon variability associated with the Asian summer monsoon, *Clim. Dyn.*, *21*, 423–446.
Waliser, D. E., R. Murtugudde, P. Strutton, and J.-L. Li (2005), Subseasonal organization of ocean chlorophyll: Prospects for prediction based on the Madden-Julian oscillation, *Geophys. Res. Lett.*, *32*, L23602, doi:10.1029/2005GL024300.
Waliser, D. E., et al. (2012), The "year" of tropical convection (May 2008–April 2010): Climate variability and weather highlights, *Bull. Am. Meteorol. Soc.*, *93*, 1189–1218.
Wang, B. (1988a), Comments on "An air-sea interaction model of intraseasonal variability in the tropics", *J. Atmos. Sci.*, *45*, 3521–3525.
Wang, B. (1988b), Dynamics of tropical low-frequency waves: An analysis of the moist Kelvin wave, *J. Atmos. Sci.*, *45*, 2051–2065.
Wang, B. (2012), Theories, in *Intraseasonal Variability in the Atmosphere-Ocean Climate System (Second Edition), Springer Praxis*, edited by B. Wang, pp. 335–398, Springer, Berlin.
Wang, B., and H. Rui (1990), Dynamics of the coupled moist Kelvin-Rossby wave on an equatorial beta-plane, *J. Atmos. Sci.*, *47*, 397–413.
Wang, B., and H. Rui (1994), Convective interaction with boundary-layer dynamics in the development of a tropical intraseasonal system, *J. Atmos. Sci.*, *51*, 1386–1400.
Wang, B., and X. Xie (1998), Coupled modes of the warm pool climate system. Part I: The role of air-sea interaction in maintaining Madden-Julian oscillations, *J. Clim.*, *8*, 2116–2135.
Wang, W., and M. E. Schlesinger (1999), The dependence on convective parameterization of the tropical intraseasonal oscillation simulated by the UIUC 11-layer atmospheric GCM, *J. Clim.*, *12*, 1423–1457.
Wang, W., and K.-H. Seo (2009), The Madden-Julian oscillation in NCEP coupled model simulation, *Terr. Atmos. Ocean. Sci.*, *20*, 713–725.
Wanninkhof, R., W. E. Asher, D. T. Ho, C. Sweeney, and W. R. McGillis (2009), Advances in quantifying air-sea gas exchange and environmental forcing, *Annu. Rev. Mar. Sci.*, *1*, 213–244.
Watterson, I. G. (2002), The sensitivity of subannual and intraseasonal tropical variability to model ocean mixed layer depth, *J. Geophys. Res.*, *107*(D2), 4020, doi:10.1029/2001JD000671.
Watterson, I. G., and J. Syktus (2007), The influence of air-sea interaction on the Madden-Julian oscillation: The role of the seasonal mean state, *Clim. Dyn.*, *28*, 703–722.
Weare, B. C. (2006), Centered composite analysis of variations associated with the Madden-Julian oscillation, *J. Clim.*, *19*, 1834–1849.
Webber, B. G. M., A. J. Matthews, and K. J. Heywood (2010), A dynamical ocean feedback mechanism for the Madden-Julian oscillation, *Q. J. R. Meteorol. Soc.*, *136*, 740–754.
Webber, B. G. M., A. J. Matthews, K. J. Heywood, and D. P. Stevens (2012), Ocean Rossby waves as a triggering mechanism for primary Madden-Julian events, *Q. J. R. Meteorol. Soc.*, *138*, 514–527.
Webster, P. J., and R. Lukas (1992), TOGA COARE: The Coupled Ocean-Atmosphere Response Experiment, *Bull. Am. Meteorol. Soc.*, *73*, 1377–1416.
Webster, P. J., C. A. Clayson, and J. A. Curry (1996), Clouds, radiation, and the diurnal cycle of sea surface temperature in the tropical Western Pacific, *J. Clim.*, *9*, 1712–1730.
Webster, P. J., et al. (2002), The JASMINE pilot study, *Bull. Am. Meteorol. Soc.*, *83*, 1603–1630.
Weller, R. A., and S. P. Anderson (1996), Surface meteorology and air-sea fluxes in the western equatorial Pacific warm pool during the TOGA Coupled Ocean-Atmosphere Response Experiment, *J. Clim.*, *9*, 1959–1990.
Weng, S.-P., and J.-Y. Yu (2010), A CGCM study on the northward propagation of tropical intraseasonal oscillation over the Asian summer monsoon regions, *Terr. Atmos. Ocean. Sci.*, *21*, 299–312.
Wentz, F. J., C. Gentemann, D. Smith, and D. Chelton (2000), Satellite measurements of sea surface temperature through clouds, *Science*, *288*, 847–850.
Wheeler, M. C., and H. H. Hendon (2004), An all-season real-time multivariate MJO index: Development and index for monitoring and prediction, *Mon. Weather Rev.*, *132*, 1917–1932.
Wijesekera, H. W., C. A. Paulson, and A. Huyer (1999), The effect of rainfall on the surface layer during a westerly wind burst in the western equatorial Pacific, *J. Phys. Oceanogr.*, *29*, 612–632.

Wilson, E. A., A. L. Gordon, and D. Kim (2013), Observations of the Madden Julian oscillation during Indian Ocean dipole events, *J. Geophys. Res. Atmos.*, *118*, 2588–2599, doi:10.1002/jgrd.50241.
Woolnough, S. J., J. M. Slingo, and B. J. Hoskins (2000), The relationship between convection and sea surface temperatures on intraseasonal timescales, *J. Clim.*, *13*, 2086–2104.
Woolnough, S. J., J. M. Slingo, and B. J. Hoskins (2001), The organization of tropical convection by intraseasonal sea surface temperature anomalies, *Q. J. R. Meteorol. Soc.*, *127*, 887–907.
Woolnough, S. J., F. Vitart, and M. A. Balmaseda (2007), The role of the ocean in the Madden-Julian oscillation: Implications for MJO prediction, *Q. J. R. Meteorol. Soc.*, *133*, 117–128.
Wu, Z. (2003), A shallow CISK, deep equilibrium mechanism for the interaction between convection and large-scale circulations in the tropics, *J. Atmos. Sci.*, *60*, 377–392.
Wyrtki, K. (1973), An equatorial jet in the Indian Ocean, *J. Clim.*, *181*, 262–264.
Wyrtki, K. (1975), El Niño—The dynamic response of the equatorial Pacific Ocean to atmospheric forcing, *J. Phys. Oceanogr.*, *5*, 572–584.
Xavier, P. K., et al. (2015), Vertical structure and physical processes of the Madden-Julian oscillation: Biases and uncertainties at short range, *J. Geophys. Res. Atmos.*, *120*, 4749–4763, doi:10.1002/2014JD022718.
Xie, S.-P. (2003), Summer upwelling in the South China Sea and its role in regional climate variations, *J. Geophys. Res.*, *108*, C3261, doi:10.1029/2003JC001867.
Xie, S.-P., H. Xu, W. S. Kessler, and M. Nonaka (2005), Air-sea interaction over the Eastern Pacific warm pool: Gap winds, thermocline dome, and atmospheric convection, *J. Clim.*, *18*, 5–20, doi:10.1175/jcli-3249.1.
Yanai, M., S. Esbensen, and J.-H. Chu (1973), Determination of bulk properties of tropical cloud clusters from large-scale heat and moisture budgets, *J. Atmos. Sci.*, *30*, 611–627.
Yang, G.-Y., and J. Slingo (2001), The diurnal cycle in the tropics, *Mon. Weather Rev.*, *129*, 784–801.
Yasunari, T. (1979), Cloudiness fluctuations associated with the Northern Hemisphere summer monsoon, *J. Meteorol. Soc. Jpn*, *57*, 227–242.
Yokoi, S., M. Katsumata, and K. Yoneyama (2014), Variability in surface meteorology and air-sea fluxes due to cumulus convective systems observed during CINDY/DYNAMO, *J. Geophys. Res. Atmos.*, *119*, 2064–2078, doi:10.1002/2013JD020621.
Yoneyama, K., et al. (2008), MISMO field experiment in the equatorial Indian Ocean, *Bull. Am. Meteorol. Soc.*, *89*, 1889–1903.
Yoneyama, K., C. Zhang, and C. N. Long (2013), Tracking pulses of the Madden-Julian oscillation, *Bull. Am. Meteorol. Soc.*, *94*, 1871–1891.
Yoshida, K. (1959), A theory of the Cromwell current (the equatorial undercurrent) and of the equatorial upwelling—An interpretation in a similarity to a coastal circulation, *J. Oceanograph. Soc. Jpn.*, *15*, 159–170.
Yu, L., X. Jin, and R. A. Weller (2008), Multidecade global flux datasets from the Objectively Analyzed Air-sea Fluxes (OAFlux) Project: Latent and sensible heat fluxes, ocean evaporation, and related surface meteorological variables, OAFlux Project Tech. Rep. OA-2008-01, Woods Hole Oceanographic Institution, Woods Hole, Mass.
Yu, W., W. Han, E. D. Maloney, D. Gochis, and S.-P. Xie (2011), Observations of eastward propagation of atmospheric intraseasonal oscillations from the Pacific to the Atlantic, *J. Geophys. Res.*, *116*, D02101, doi:10.1029/2010JD014336.
Zebiak, S. E. (1986), Atmospheric convergence feedback in a simple mode for El Niño, *Mon. Weather Rev.*, *114*, 1263–1271.
Zeng, X., and R. E. Dickinson (1998), Impact of diurnally-varying skin temperature on surface fluxes over the tropical Pacific, *Geophys. Res. Lett.*, *25*, 1411–1414.
Zhang, C. (1996), Atmospheric intraseasonal variability at the surface in the tropical western Pacific Ocean, *J. Atmos. Sci.*, *53*, 739–758.
Zhang, C. (1997), Intraseasonal variability of the upper-ocean thermal structure observed at 0° and 165°E, *J. Clim.*, *10*, 3077–3092.
Zhang, C. (2005), Madden-Julian oscillation, *Rev. Geophys.*, *43*, RG2003, doi:10.1029/2004RG000158.
Zhang, C. (2013), Madden-Julian oscillation: Bridging weather and climate, *Bull. Am. Meteorol. Soc.*, *94*, 1849–1870.
Zhang, C., and S. P. Anderson (2003), Sensitivity of intraseasonal perturbations in SST to the structure of the MJO, *J. Atmos. Sci.*, *60*, 2196–2207.
Zhang, C., and J. Gottschalck (2002), SST anomalies of ENSO and the Madden-Julian oscillation, *J. Clim.*, *15*, 2429–2445.
Zhang, C., and M. J. McPhaden (2000), Intraseasonal surface cooling in the equatorial western Pacific, *J. Clim.*, *13*, 2261–2276.
Zhang, C., M. Dong, S. Gualdi, H. H. Hendon, E. D. Maloney, A. Marshall, K. R. Sperber, and W. Wang (2006), Simulations of the Madden-Julian oscillation in four pairs of coupled and uncoupled global models, *Clim. Dyn.*, *27*, 573–592.
Zhang, C., J. Gottschalck, E. D. Maloney, M. W. Moncrieff, F. Vitart, D. E. Waliser, B. Wang, and M. C. Wheeler (2013), Cracking the MJO nut, *Geophys. Res. Lett.*, *40*, 1223–1230, doi:10.1002/grl.50244.
Zhang, G. J., and M. Mu (2005), Simulation of the Madden-Julian oscillation in the NCAR CCM3 using a revised Zhang-McFarlane convective parameterization scheme, *J. Clim.*, *18*, 4046–4064.
Zhang, G. J., and X. Song (2009), Interaction of deep and shallow convection is key to Madden-Julian oscillation simulation, *Geophys. Res. Lett.*, *36*, L09708, doi:10.1029/2009GL037340.
Zhang, L., B. Wang, and Q. Zeng (2009), Impact of the Madden-Julian oscillation on summer rainfall in southeast China, *J. Clim.*, *22*, 201–216, doi:10.1175/2008jcli1959.1.
Zheng, Y., D. E. Waliser, W. F. Stern, and C. Jones (2004), The role of coupled sea surface temperatures in the simulation of the tropical intraseasonal oscillation, *J. Clim.*, *17*, 4109–4134.
Zhou, L., R. B. Neale, M. Jochum, and R. Murtugudde (2012), Improved Madden-Julian oscillations with improved physics: The impact of modified convection parameterizations, *J. Clim.*, *25*, 1116–1136.
Zhou, S., and A. J. Miller (2005), The interaction of the Madden-Julian oscillation and the Arctic Oscillation, *J. Clim.*, *18*, 143–159, doi:10.1175/jcli3251.1.